

COMPUTATIONAL AND EXPERIMENTAL INVESTIGATION INTO THE ROLE  
OF CALCIUM IN STRIATAL PLASTICITY

by

Rebekah Evans  
A Dissertation  
Submitted to the  
Graduate Faculty  
of  
George Mason University  
in Partial Fulfillment of  
The Requirements for the Degree  
of  
Doctor of Philosophy  
Neuroscience

Committee:

Kim L. Blackwell

Dr. Kim Blackwell, Dissertation Director

Ted Abel

Dr. Ted Abel, Committee Member

Ted Dumas

Dr. Ted Dumas, Committee Member

Dan Cox

Dr. Dan Cox, Committee Member

James Olds

Dr. James Olds, Director, Krasnow Institute  
for Advanced Studies

Richard Diecchio

Dr. Richard Diecchio, Interim Dean,  
Associate Dean for Student and Academic  
Affairs, College of Science

Peggy Agouris

Dr. Peggy Agouris, Interim Dean, College  
of Science

Date: 11/22/13

Fall Semester 2013  
George Mason University  
Fairfax, VA

Computational and Experimental Investigation into the Role of Calcium in Striatal  
Plasticity

A Dissertation submitted in partial fulfillment of the requirements for the degree of  
Doctor of Philosophy at George Mason University

by

Rebekah Evans  
Master of Education  
George Mason University, 2006

Director: Dr. Kim Blackwell, Professor  
Department of Neuroscience

Fall Semester 2013  
George Mason University  
Fairfax, VA



This work is licensed under a [creative commons attribution-noncommercial 3.0 unported license](https://creativecommons.org/licenses/by-nc/3.0/).

## **DEDICATION**

This dissertation is dedicated to my grandpa, Dwight Johnson, who was one of the most curious people in my life.

## ACKNOWLEDGEMENTS

I would like to thank Kim Avrama Blackwell for being an amazing mentor and getting my best out of me. Thanks to my committee for allowing me to spend time in each of their labs learning many of the techniques I used in this dissertation or will use in the future: Genotyping from Ted Abel and Ted Dumas's lab, *in situ* hybridization from Ted Dumas's lab, and histology from Dan Cox's lab. I would like to thank Jim Olds and Giorgio Ascoli for supplementary mentorship and for advice on my academic career. I would also like to thank the online science community which inspired me during the toughest part of this work. The Krasnow Institute at George Mason University has been a supportive and nurturing place to conduct my research. Without the Presidential Scholarship, Dissertation Completion Grant, and the availability of graduate student health insurance, the completion of this dissertation would have been unbearably stressful if not impossible. In addition thanks to NINDS for providing me with a NRSA F31 grant to work on these projects.

## TABLE OF CONTENTS

	Page
List of Tables .....	x
List of Figures .....	xi
List of Abbreviations and Symbols.....	xiii
Abstract .....	xv
Chapter One: Calcium Amplitude, Duration, or Location? .....	1
Abstract .....	1
Introduction .....	1
Amplitude.....	3
The <i>two threshold</i> hypothesis .....	3
Experimental evidence .....	3
Computational models.....	6
Problems with the <i>two threshold</i> amplitude hypothesis .....	7
Duration.....	9
The <i>low and slow, high and fast</i> hypothesis .....	9
Experimental evidence .....	9
Computational models.....	11
Problems with the <i>low and slow, high and fast</i> duration hypothesis.....	12
Location.....	13
The <i>microdomain/nanodomain</i> hypothesis .....	13
Experimental evidence .....	14
Computational models.....	17
Problems with the <i>microdomain/nanodomain</i> location hypothesis.....	18
Conclusion.....	19
Contributions .....	19
Chapter Two: Striatal Cellular Models.....	20
Definition .....	20

Cell classes in the striatum .....	20
Simple MSN Models.....	22
Complex MSN Models.....	22
Interneuron Models .....	24
Conclusion.....	26
Contributions .....	26
Chapter Three: The effects of NMDA subunit composition on calcium influx and spike timing-dependent plasticity in striatal medium spiny neurons .....	28
Abstract .....	28
Introduction .....	29
Results .....	31
Validation of model medium spiny projection neuron .....	31
STDP protocol type modulates calcium influx through NMDAR .....	34
GluN2 subunit composition modulates calcium elevation due to NMDAR .....	38
Spines on distal dendrites show reduced sensitivity to AP timing .....	45
Differences between thalamo-striatal and cortico-striatal synapses.....	48
Discussion .....	50
Striatal STDP protocols and NMDAR-mediated calcium.....	52
Distance from the soma and STDP.....	52
Cortico-striatal and thalamo-striatal synapses .....	53
GluN2 subunits and their effects on synaptic plasticity .....	53
Implications for learning, behavior, and pathology.....	55
Methods.....	57
Electrophysiology for Model Tuning .....	57
Electrophysiology for plasticity experiments .....	58
Spike timing-dependent plasticity induction protocols .....	59
Medium spiny projection neuron model.....	60
Ionic Channels .....	61
Synaptic Channels .....	62
Contributions.....	64
Chapter Four: Dynamic modulation of spike-timing dependent calcium influx during cortico-striatal upstates .....	65
Abstract .....	65

Introduction .....	66
Methods.....	68
General MSN model.....	68
Ionic channels.....	71
Calcium channels.....	74
Calcium diffusion, buffers, and pumps. ....	74
Synaptic channels.....	75
Synaptic inputs and spike timing.....	78
Voltage clamp of calcium currents.....	80
Simulation and analysis.....	81
Results .....	82
Part 1: Mechanisms underlying the calcium sensitivity to AP timing during the upstate.....	82
Intrinsic physiology and calcium dynamics in the MSN model match published data .....	82
Two mechanisms can account for the relationship between calcium and AP timing	83
The calcium-AP relationship depends on input shape and distance from the soma..	88
CDI replicates the effect of NMDA receptor blockade on the relationship between calcium and AP timing .....	90
Part 2: Effect of neuromodulation and implications for in vivo plasticity.....	93
Modulation of intrinsic, but not synaptic excitability alters calcium relationship with AP timing.....	94
Fast and slow calcium binding partners are differentially influenced by AP timing and AP number.....	96
AP timing during the upstate interacts with spike timing dependent plasticity protocols .....	99
Discussion .....	101
Is CDI or NaSI more likely?.....	101
Three testable predictions.....	102
Implications for plasticity .....	105
Conclusion.....	107
Contributions.....	108
Chapter Five: Regional and age-dependent variability in calcium dependent inactivation of calcium channels in the striatum .....	109

Abstract .....	109
Introduction .....	109
Methods.....	111
Electrophysiology .....	111
Drugs and Drug Application.....	113
Data Analysis.....	113
Results .....	114
Isolating CDI in HVA channels.....	114
CDI increases with age, but is modulated by striatal region. ....	115
L-type calcium channels contribute to the jump in medial CDI that occurs at eye opening. ....	117
PKA phosphorylation and calcineurin dephosphorylation do not affect total inactivation .....	122
Discussion .....	123
Region and age dependent variation in amplitude and CDI.....	123
The significance of eye opening.....	124
VGCC types and CDI.....	125
Conclusion.....	127
Contributions.....	127
Chapter Six: Spatial specificity of intracellular signalling molecules is crucial for striatal synaptic plasticity.....	128
Abstract .....	128
Introduction .....	129
Methods.....	130
Brain slice preparation.....	130
Whole Cell recording.....	131
White matter stimulation. ....	132
Data analysis.....	132
Drug information. ....	133
Results .....	133
Medium Spiny Neuron characteristics .....	133
HFS induced LTP is NMDA and PKA dependent. ....	136
Spatial specificity of PKA activity is crucial for striatal LTP .....	137

Post-synaptic PKA activity and anchoring is necessary for striatal LTP .....	139
Discussion .....	141
Contributions.....	144
Chapter Seven: Summary and Extended Applications .....	145
Introduction .....	145
Background and context.....	145
Computational approaches .....	146
Experimental approaches .....	148
Conclusion.....	152
References.....	153

## LIST OF TABLES

Table	Page
Table 1 Computational Models of striatal neurons.....	26
Table 2 Steady state and tau equations for ionic channels.....	33
Table 3 Maximal conductance and permeability for ionic channels. ....	34
Table 4 NMDA subunit parameters.....	39
Table 5 Cortico-striatal and thalamo-striatal parameters.....	49
Table 6 Steady state equations.....	71
Table 7 Tau equations for inward currents. ....	72
Table 8 Maximal conductance and permeability for ionic channels. ....	73
Table 9 Calcium buffer parameters.....	75
Table 10 conductances and time constants for synaptic channels. ....	75
Table 11 Input gradients used to create upstates. ....	80

## LIST OF FIGURES

Figure	Page
Figure 1 Calcium Amplitude Hypothesis .....	3
Figure 2 Calcium Duration Hypothesis .....	9
Figure 3 Three iterations of the calcium location hypothesis.....	14
Figure 4 Model cell shows MSN characteristics. ....	32
Figure 5 STDP protocol type changes calcium influx through NMDAR.....	35
Figure 6 Added variability to spike time in model MSN.....	37
Figure 7 Characteristics of GluN2 containing NMDARs.....	39
Figure 8 Calcium curves for different GluN2 subunit containing NMDARs.....	40
Figure 9 GluN2B broadens the STDP curve. A-B. Inhibition of GluN2B restricts the time window of tLTP induction. ....	44
Figure 10 Distance from soma reduces dependence on AP timing. ....	46
Figure 11 The cortico-striatal and thalamo-striatal synapses onto MSNs have different synaptic characteristics. ....	50
Figure 12 Computational model comparison with electrophysiological data. ....	69
Figure 13 Intrinsic calcium signaling in the model matches published data. ....	70
Figure 14 Input pattern affects calcium dependence on AP timing.....	79
Figure 15 Two basic mechanisms can account for the relationship between calcium elevation and AP timing during the upstate: reduced AP backpropagation (NaSI) or reduced calcium response (CDI).....	85
Figure 16 Robustness tests.....	87
Figure 17 Distance from soma affects calcium dependence on AP timing. ....	89
Figure 18 Dependence on NMDA receptors during flat and graded inputs. ....	92
Figure 19 A change in intrinsic excitability alters calcium relationship with AP timing. ....	95
Figure 20 Preference for calcium binding partners differs with AP timing and AP number. ....	97
Figure 21 STDP can occur during an upstate. ....	100
Figure 22 Striatal CDI depends on age and region. ....	115
Figure 23 L type calcium channels contribute to the increase in CDI that occurs at eye opening.....	117
Figure 24 Proportion of current carried by L-type calcium channels is not altered by region at eye opening. ....	119
Figure 25 Blocking L type channels increases VDI. ....	121
Figure 26 PKA phosphorylation and calcineurin dephosphorylation do not affect total inactivation medially at eye opening. ....	123
Figure 27 Characterization of medium spiny neurons.....	134

Figure 28 HFS induces PKA and NMDA dependent LTP in cortico-striatal synapses.	135
Figure 29 Blocking PKA from anchoring to AKAPs prevents LTP. ....	138
Figure 30 Post-synaptic PKA activity and PKA anchoring is necessary for striatal LTP. .....	140
Figure 31 No plasticity in AKAP 150 knock out strain.....	150
Figure 32 Theta burst LTP using whole cell preparation .....	151

## LIST OF ABBREVIATIONS AND SYMBOLS

$\alpha$ -Amino-3-hydroxy-5-methyl-4-isoxazolepropionic acid .....	AMPA
Acetylcholinergic .....	ACh
Action potential.....	AP
After hyperpolarization.....	AHP
AMPA receptor.....	AMPA
AMPA subunit .....	GluA
A kinase anchoring protein .....	AKAP
Artificial cerebrospinal fluid.....	aCSF
Big conductance potassium channel .....	BK
Calcineurin.....	CaN/PP2B
Calcium dependent inactivation.....	CDI
Calmodulin.....	CaM
Calmodulin kinase II.....	CaMKII
CaM C lobe.....	CaMC
CaM N lobe.....	CaMN
cAMP activated protein kinase .....	PKA
current-frequency.....	IF
current-voltage .....	IV
cyclic adenosine monophosphate.....	cAMP
Delayed rectifying potassium channel .....	Kdr
Dorsolateral striatum.....	DM
Dorsomedial striatum.....	DL
Excitatory post-synaptic current .....	EPSC
Excitatory post-synaptic potential.....	EPSP
Fast potassium A channel .....	KaF
Fast sodium channel.....	NaF
Fast spiking interneuron.....	FSI
Gamma-aminobutyric acid.....	GABA
High frequency stimulation.....	HFS
High voltage activated .....	HVA
Inhibitory post-synaptic potential .....	IPSP
Inwardly rectifying potassium channel .....	Kir
Long term depression.....	LTD
Long term potentiation.....	LTP
Low frequency stimulation .....	LFS
Low voltage activated.....	LVA

Medium spiny neuron .....	MSN
Micro.....	$\mu$
Neuropeptide Y.....	NPY
N-methyl-D-aspartate .....	NMDA
NMDA receptor .....	NMDAR
NMDA subunit.....	GluN
Nucleus Accumbens.....	N. Acc.
Phosphodiesterase .....	PDE
Post synaptic density.....	PSD
Protein phosphatase 2 A.....	PP2A
Resistant persistent potassium channel.....	Krp
Slow inactivating sodium channel .....	NaSI
Slow potassium A channel.....	KaS
Small conductance potassium channel.....	SK
Spike timing dependent plasticity.....	STDP
Steady State.....	SS
Striatal enriched protein phosphatase .....	STEP
Timing dependent LTP .....	tLTP
Timing interval.....	$\Delta t$
Voltage dependent inactivation.....	VDI
Voltage gated calcium channel .....	VGCC

## **ABSTRACT**

### **COMPUTATIONAL AND EXPERIMENTAL INVESTIGATION INTO THE ROLE OF CALCIUM IN STRIATAL PLASTICITY**

Rebekah Evans, Ph.D.

George Mason University, 2013

Dissertation Director: Dr. Dr. Kim Blackwell

This dissertation presents a detailed computational model of a striatal medium spiny neuron and uses it to investigate post-synaptic calcium dynamics during carefully timed plasticity protocols. We measure the calcium through the NMDA receptor and use it as a predictor of long term potentiation (LTP) during spike timing dependent plasticity (STDP) protocols. We show that same timing intervals that result in high calcium elevations also result in LTP. The kinetics of the calcium influx through the NMDA receptor is altered by the GluN2 subunit it contains. Therefore, we modeled all for GluN2 subunits (GluN2A,B,C, and D) and ran simulations comparing the calcium peaks during a range of timing intervals. Simulations show that the available subunit controls the timing intervals that result in high calcium elevations in the model, and that induce LTP in slice experiments. We extend this work by including a sophisticated model of calcium diffusion, buffering, and pump extrusion. This more physiological model was used to simulate the cortico-striatal upstates that are seen in medium spiny neurons during sleep.

There is a relationship between the amplitude of the calcium elevation in the dendrite and the timing of a single action potential during the upstate. We use this updated model to predict that calcium dependent inactivation (CDI) governs this relationship between calcium and action potential timing. Using voltage clamp experiments, we confirm that CDI does occur in striatal neurons. We further find that CDI changes with age and striatal region. Specifically, these experiments show that there is an increase in CDI at eye opening in the medial striatum. We also determine that L type calcium channels contribute to this increase in CDI. This dissertation presents the most sophisticated model of a medium spiny neuron to date, and presents the first experiments characterizing CDI in striatal neurons.

## CHAPTER ONE: CALCIUM AMPLITUDE, DURATION, OR LOCATION?

### **Abstract**

Calcium plays a role in long term plasticity by triggering post-synaptic signaling pathways. Calcium is necessary for both the strengthening (LTP) and weakening (LTD) of synapses. Since these are opposing processes, several hypotheses have been made to explain how calcium can trigger LTP in some situations and LTD in others. These hypotheses fall broadly into three categories, based on the *amplitude* of calcium concentration, the *duration* of the calcium elevation, and the *location* of the calcium influx. Here we review the experimental evidence for and against each of these hypotheses and review recent computational models based on each.

### **Introduction**

The relationship between calcium and plasticity is a complicated one. In many cell types, the strengthening of neuronal connections (long term potentiation, LTP) and the weakening of neuronal connection (long term depression, LTD) both require some degree of intracellular calcium (Artola and Singer 1993; Cummings et al. 1996; Fino et al. 2010). But LTP and LTD are opposing processes with opposing results. How can calcium cause strengthening in one situation and weakening in another?

Since the importance of calcium in plasticity was first discovered, extensive experimental and computational studies have been conducted to investigate which characteristics of the calcium signal determine the direction of plasticity. While there are

many hypotheses on the subject, most of them fall into three categories: *Amplitude*, *Duration*, and *Location*. These categories refer to which aspects of the spatio-temporal calcium signal control which specific proteins calcium binds to. The hypotheses claiming that calcium *amplitude* determine the direction of plasticity were the first to emerge (Lisman 1989; Artola and Singer 1993). This hypothesis usually takes the form of a two-threshold hypothesis where a moderate calcium elevation is necessary for LTD but an even higher calcium elevation is necessary for LTP. The *duration* hypothesis predicts that the time course of calcium elevation in conjunction with the amplitude determines the direction of plasticity. Usually this hypothesis asserts that a lower, slower calcium signal results in LTD, while a higher, faster calcium transient results in LTP. Finally, the *location* hypothesis states that the specific site of calcium entry determines which direction of plasticity by controlling which calcium binding proteins are in close proximity to the calcium influx.

In this chapter, I review the experiments supporting and refuting each theory, as well as the computational models utilizing each hypothesis to develop plasticity and learning rules. I also discuss the possible interactions between these three hypotheses, and detail the important questions which remain unanswered. Finally, I argue that with new experimental techniques and sophisticated computational algorithms, it is time to take a new look at the *location* hypothesis.

## Amplitude

### The *two threshold hypothesis*

The calcium *amplitude* hypothesis states that the peak calcium determines the direction of plasticity. Specifically, a low but still significant calcium elevation results in LTD, while a higher calcium elevation results in LTP (Figure 1).

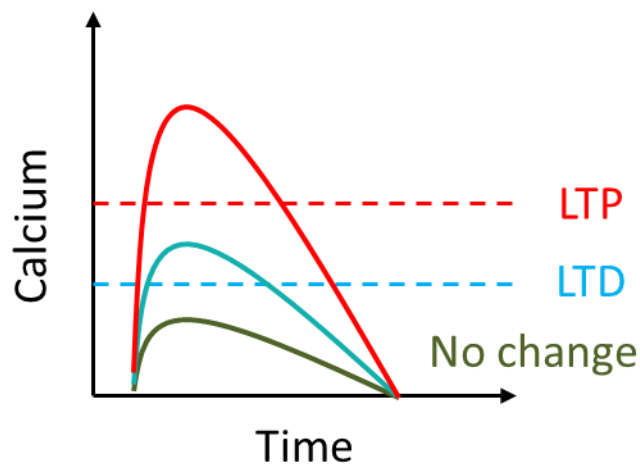


**Figure 1 Calcium Amplitude Hypothesis**

Peak calcium must cross one threshold to induce LTD, and another, higher threshold to induce LTP.

### Experimental evidence

There are several key experiments that suggest calcium amplitude determines the direction of synaptic plasticity. It is well established that in many brain areas high frequency stimulations (HFS) cause LTP, while low frequency stimulations (LFS) cause LTD (reviewed in Stanton, 1996). It has been postulated that the direction of plasticity depends on frequency because of the difference in calcium amplitude evoked by HFS and

LFS. Specifically, HFS which induces LTP, evokes a large amplitude calcium signal, while LFS induces LTD and evokes a small amplitude calcium signal.

A more direct experimental study was conducted by Hansel et al., (1996) in which frequency-based stimulation patterns known to induce LTP and LTD were applied to a cell filled with the calcium sensitive dye Fura-2. Hansel et al. (1996) found that the calcium peak was highest during the LTP protocol, but was also significant during the LTD protocol. This experiment shows that the stimulation pattern that induces LTP correlates with higher calcium amplitudes than the stimulation pattern that induces LTD (Hansel et al. ,1996, Figure 1). While this experiment does not show a causal relationship between calcium amplitude and plasticity, it supports the two threshold hypothesis.

It is clear that calcium is required for both directions of plasticity, as intracellular calcium chelators such as BAPTA and EGTA can prevent both LTP and LTD (reviewed in Artola and Singer, 1993). However, at low concentrations, these chelators selectively block LTP, but not LTD. Specifically, one group varied the concentration of EGTA and compared the same induction paradigm. They found that high concentrations (20mM) prevented both LTP and LTD, while a medium concentration of EGTA (10mM) resulted in LTD and a low concentration (<1mM) resulted in LTP (Cho et al. 2001). These results would support the amplitude hypothesis if a high chelator concentration prevents the peak calcium amplitude from crossing both the LTD and the LTP thresholds, a medium concentration prevents it from crossing only the LTP threshold, and a low concentration allows the LTP threshold to be crossed. An early study showed that lowering the extracellular calcium concentration turned LTP into LTD when the same stimulation

frequency was applied (Mulkey and Malenka 1992). This supports the amplitude hypothesis because the same channels would be opened in both stimulation conditions, but the calcium through the channels would be decreased due to the lower extracellular concentration. Finally another study used glutamate iontophoresis to directly compare calcium amplitude with plasticity (Cormier et al., 2001). The authors measured the calcium signal via an intracellular calcium sensitive dye (fura-2) while simultaneously measuring the slope of the excitatory post-synaptic potential (EPSP). A temporary application of glutamate caused a strong calcium transient and induced plasticity. When the authors compared the amplitude of the calcium transient to the subsequent plasticity, they were able to determine specific calcium concentrations needed to induce LTD (180-500nM) and LTP (>500nM).

The calcium amplitude hypothesis not only explains plasticity outcomes from frequency-based induction protocols, but it can also explain the direction of plasticity due to Spike Timing Dependent Plasticity (STDP) protocols. In classical STDP protocols, the timing of the post-synaptic action potential relative to the pre-synaptic stimulation predicts the direction of plasticity. When the action potential is before the pre-synaptic stimulation (post-pre), LTD is induced, but when the action potential comes after (pre-post), LTP is induced (reviewed in Bi and Poo, 2001). This form of plasticity can also be explained through the calcium amplitude hypothesis. During a post-pre stimulation (known to induce LTD), calcium is higher than either pre or post stimulation alone. However, during the pre-post stimulation (known to induce LTP), calcium is even higher

than during the post-pre stimulation (Koester and Sakmann 1998). Once again LTP correlates with higher calcium and LTD correlates with lower calcium.

### **Computational models**

Biophysical computational models have shown that both frequency-based and STDP-based plasticity rules can be predicted by calcium amplitude. In several computational models, high stimulation frequencies (which also induce LTP) evoke strong increases in calcium, while low frequencies (which induce LTD) evoke more moderate increases. Using a biophysical model, Holmes and Levy (1990) showed that calcium amplitude in the spine head was fourfold higher in response to a 200Hz stimulation than a 10Hz stimulation, and that this frequency-dependent difference was increased with the addition of specific intracellular calcium dynamics such as the saturation of calcium buffers.

Similarly, other computational models show that pre-post STDP pairings (which induce LTP) result in higher calcium amplitudes than post-pre STDP pairings (which induce LTD). Assuming that the main source of calcium in the dendrites is the NMDA receptor, Shouval et al. (2002) created a plasticity-predictive model based on calcium amplitude. Using this model, the authors were able to match both a frequency based (0.5-20Hz) and a spike timing (STDP) based plasticity curve (Shouval et al., 2002, figure 3). Another simplified model implements calcium based stochastic transitions between high and low synaptic states (Bush and Jin 2012). The authors tune their model to match hippocampal STDP experiments and show that it also replicates the plasticity that occurs from a variety of stimulation paradigms. Our own simulations in a biophysical model of a

striatal medium spiny neuron show that the LTP part of the STDP curve can be predicted by the amplitude of the NMDA receptor-mediated calcium, and that manipulation of the NMDA GluN2 subunit changes the shape of the experimental STDP curve as well as the corresponding calcium amplitudes (Evans et al. 2012).

### **Problems with the *two threshold amplitude hypothesis***

That calcium amplitude would differentially cause LTP and LTD seems both reasonable and useful at first glance, but several questions remain unanswered by this hypothesis. Because it is a two-threshold hypothesis, it is not clear whether passing the LTP threshold prevents LTD, or simply overwhelms it. In other words, does high calcium turn off the calcium-triggered LTD mechanisms? Or do those mechanisms persist, hidden by the stronger LTP mechanisms? Experimental evidence demonstrating that LTP is enhanced by drugs that normally block LTD would support this simultaneous induction of LTP and LTD, but it also seems inefficient for the cell to expend the energy to induce both LTP and LTD at the same time if one is going to win-out in the end. A mechanistic explanation is needed to fully understand how amplitude differences alone could turn off LTD mechanisms while activating LTP mechanisms.

Another question is that of balance and saturation. If a synapse is strengthened, the calcium influx into that spine is also going to be enhanced (Sterratt et al. 2012). If the strength of the synapses depends only on calcium amplitude, then a strong synapse would only continue to get stronger. A possible resolution to this problem would be if the spine head corresponding to the strengthened synapse had grown larger. The larger the volume

for calcium to fill, the stronger the signal would have to be for the calcium to reach the same concentration as it could in a smaller spine head.

In addition to these questions, several serious problems arise when considering a calcium amplitude explanation of plasticity. The most obvious comes from the computational models of calcium-based STDP. Shouval et al., (2002) show an STDP curve with two windows for LTD. The first window is in the post-pre timing range and matches up with experimental data, but the second window is in the pre-post range between about 70 and 120ms time difference between the pre-synaptic stimulation and the post-synaptic action potential. This is a problem because the experimental data does not support this shape for the STDP curve. Most experiments demonstrating STDP show no LTD at all during pre-post intervals (Bi and Poo 1998; Pawlak and Kerr 2008).

The most direct evidence against the amplitude hypothesis comes from an experimental study. Nevian and Sakmann (2006) found that calcium amplitude can predict LTP and LTD at extreme concentrations, but that there is a middle range where calcium amplitude does not predict the direction of plasticity. They show that two separate induction protocols can have the same measured calcium amplitude, but induce opposite directions of plasticity. Amplitude may provide a reasonable explanation of plasticity in certain cases, but there is strong evidence that it is not always a sufficient predictor.

## Duration

### The *low and slow, high and fast* hypothesis

The calcium *duration* hypothesis is not an alternative to the *amplitude* one, but rather it adds additional criteria. It states that the kinetics of the calcium influx in conjunction with differences in peak calcium strongly influences the direction of plasticity. Specifically it is thought that a *high and fast* calcium signal will trigger LTP, while a *low and slow* calcium signal will trigger LTD (Figure 2).

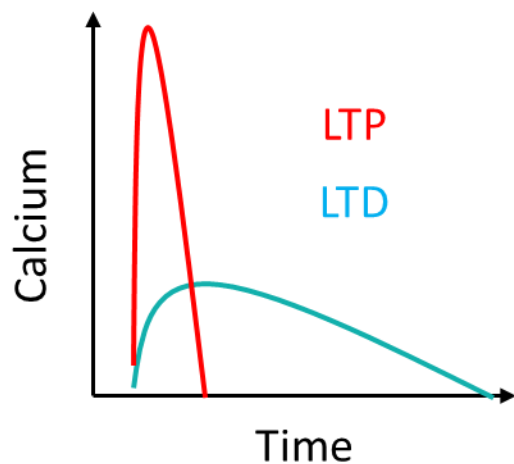


**Figure 2 Calcium Duration Hypothesis**

A low, slow calcium elevation results in LTD, while a high and fast calcium elevation results in LTP.

## Experimental evidence

Several studies support the idea that calcium kinetics determine plasticity. One study shows that the photolytic uncaging of intracellular calcium in hippocampal slices can induce either LTP or LTD. This study found that the direction of plasticity was not governed by the strength of the calcium uncaging, indicating that there is not amplitude

threshold difference between the two processes (Neveu and Zucker 1996). However, the calcium uncaging method used in this study only allows for moderate calcium increases (Yang, Tang, and Zucker 1999), allowing for the possibility that the calcium increases causing both LTP and LTD are similar to ‘middle range’ described in Nevian and Sakmann (2006) in which the calcium amplitude did not consistently predict the direction of plasticity.

In a subsequent study, the same group used a newer calcium uncaging method that allows for more precise temporal control of calcium elevation and higher calcium peaks (Yang, Tang, and Zucker 1999). Precisely controlling the duration of the calcium elevations, Yang et al. (1999) found that a high and fast elevation of calcium produced LTP, while a low and slow elevation in calcium produced LTD (Yang et al., 1999, figure 2). These experiments show that the duration of the calcium elevation along with the peak amplitude determine the direction of plasticity.

The amount of time that calcium stays elevated is important, but a more recent study has shown that the ‘velocity’ of the initial calcium rise is a strong predictor of plasticity (Aihara et al. 2007). The authors tested three calcium measurements (velocity, peak, and integration) during STDP protocols in hippocampal slices and found that the velocity of the calcium signal (the initial rise time) correlates most strongly with the direction and magnitude of synaptic plasticity (Aihara et al. 2007). Peak and Integration correlated with the direction of plasticity somewhat, but the velocity was the strongest predictor.

It is extremely difficult to experimentally manipulate the time course of calcium elevation. It is even difficult to measure the duration of influx because calcium reporters must bind and unbind the calcium molecules, consequently altering the calcium kinetics. Because of this difficulty, computational models are particularly useful in investigating the effects of calcium duration, because it provides the ability to precisely control the total quantity of calcium influx.

### **Computational models**

Several computational models evaluate the consequences of different durations of calcium influx. These models simulate calcium binding to different downstream molecules (kinases and phosphatases) which are known to activate either LTP or LTD. The proportion of calcium binding to ‘LTP’ molecules compared to the calcium binding to ‘LTD’ molecules can predict which stimulation patterns will produce which direction of plasticity.

An early computational model showed that high frequency stimulation more effectively activates calmodulin than low frequency stimulation (Gamble and Koch 1987). More recently Li et al. (2012) used a biophysical modeling approach to compare the activation of CaMKII (an LTP facilitating molecule) and calcineurin (CaN or PP2B, a LTD facilitating molecule). The authors held the total number of calcium ions constant while changing input frequencies and found that higher frequencies (higher amplitude, shorter durations) more efficiently activated CaMKII, while lower frequencies (lower amplitude, longer durations) facilitated phosphatase activation. By graphing the ratio of kinase to phosphatase activity, Li et al. defines a frequency curve with the ratio favoring

LTD between 1-3 Hz, and LTP between 10-200Hz (Li et al., 2012, figure 6B). However, the authors show that this frequency curve is modulated by the amplitude of calcium. When the total number of calcium ions was increased, CaMKII became sensitive to lower frequencies, shifting the frequency-curve to the left. When the number of calcium ions was decreased, the frequency curve was shifted toward higher frequencies (Li et al., 2012, figure 7).

Using the CaMKII/PP2A biophysical compartment model from Pi and Lisman (2008), Carlson and Giordano (2011) demonstrate the importance of calcium kinetics in LTP and LTD. They show that the amplitude and the duration work together to predict the direction of plasticity. Specifically they show that above a certain calcium amplitude threshold, LTP is induced, while below that threshold, LTD is induced only when the duration of the calcium elevation is greater than 45ms (Carlson and Giordano 2011, figure 2). They also show that this addition of calcium kinetics solves the main problem of the calcium amplitude hypothesis. Their simulations predict the STDP curves seen in experiments (Bi and Poo 1998) where there is no secondary LTD dip at long interval pre-post pairings (Carlson and Giordano 2011, figure 6).

### **Problems with the *low and slow, high and fast duration hypothesis***

The experimental and computational studies supporting the duration hypothesis show that the effects of calcium *duration* are modified by calcium *amplitude*. In each case, *duration* is not the only factor predicting LTP or LTD. What these studies show, however, is that duration is often a critical characteristic of the calcium signal and in some situations can predict the direction of plasticity. Experiments directly manipulating

the kinetics of calcium channels are needed to clarify the role of duration in calcium signaling.

## **Location**

### **The *microdomain/nanodomain* hypothesis**

The calcium *location* hypothesis states that the specific location of the calcium influx is what predicts its binding partners and therefore the direction of plasticity which the influx will trigger. The location for calcium influx required for LTP and LTD can be as far apart as spine and dendrite (microdomains), or as close together as the PSD and adjacent membrane (nanodomains). Because imaging studies have so far not been able to reveal nanodomains, the experimental evidence often shows that different channels or receptors are coupled to LTP and LTD. An example from the striatum would be that calcium influx from the L-type calcium channels is required for LTD, while calcium influx through NMDA receptors is required for LTP (Fino et al. 2010). Another example would be that calcium influx in the spine results in LTP, while calcium influx on the dendritic shaft results in LTD. Finally, an even more specific example would be that calcium influx at the synapse on a spine causes a different direction of plasticity than calcium influx at non-synaptic sites on the spine head or neck (Figure 3).

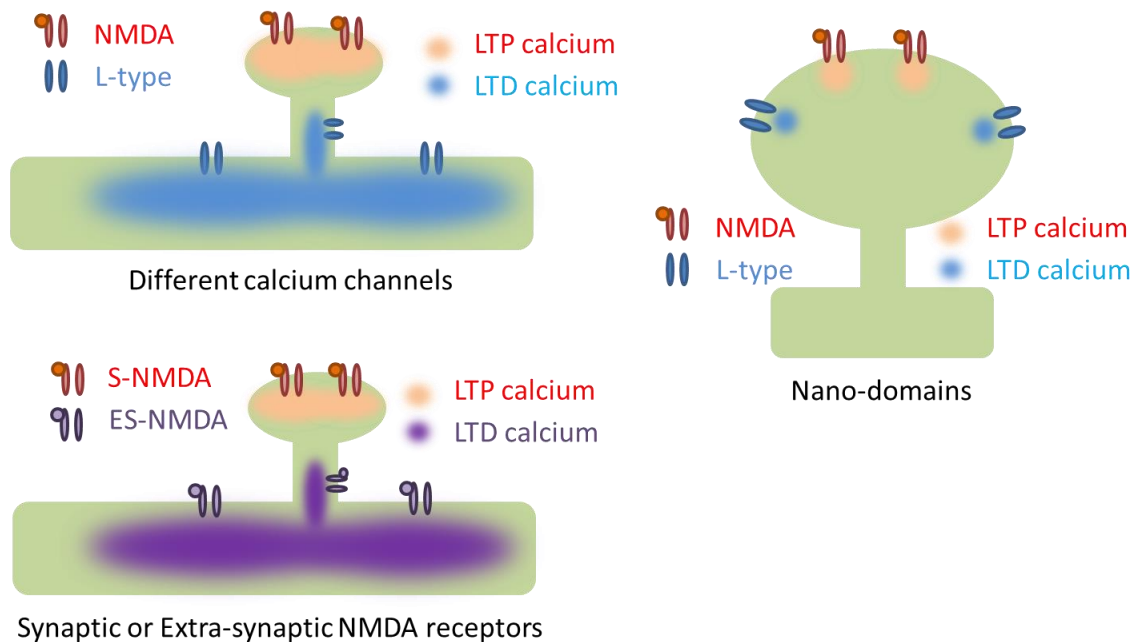


**Figure 3 Three iterations of the calcium location hypothesis.** Calcium channel specificity, synaptic (S) vs. extra-synaptic (ES) NMDA receptors, and the nano-domain hypothesis.

### Experimental evidence

Most broadly, calcium location can be determined by channel specificity. That is, if a specific calcium channel is necessary for LTP or LTD, it may be because that channel allows calcium into a specific location. In the striatum, several studies have shown that NMDA receptors are specifically necessary for LTP, while other calcium sources such as L-type calcium channels are necessary for LTD (Fino et al. 2010; Shindou et al., 2011). It has been proposed that the NMDA/L-type ratio may determine the direction of plasticity (Paille et al. 2013). While it is tempting to think that channel specificity means location specificity, each channel has its own kinetics and therefore affects the *duration* of calcium influx as well as the location. It has even been suggested that if NMDA receptors

are blocked, very strong activation of L-type calcium channels can allow in a high enough *amplitude* of calcium to facilitate LTP (Grover and Teyler 1990).

Another location hypothesis is that calcium influx into the spine acts differently than calcium influx into the dendritic shafts. One way of exploring this question is to compare the calcium through the synaptic NMDA receptors at the spine head to the calcium through the extrasynaptic NMDA receptors on the spine neck and dendritic shafts. One study shows that even though traditionally NMDA receptors are thought to contribute to hippocampal LTP, selectively activating the extrasynaptic NMDA receptors causes LTD (Liu et al., 2013). In striatal cultures, stimulating synaptic NMDA receptors or extrasynaptic NMDA receptors cause opposite effects. Specifically activating synaptic NMDA receptors increases phosphorylated CREB, while activating extrasynaptic NMDA receptors decreases it. The effects of NMDA receptor location go even further. It determines whether cell survival or cell death pathways are activated (Hardingham and Bading 2010). It is not yet known why calcium through extrasynaptic NMDA receptors trigger one set of mechanisms while calcium through synaptic NMDA receptors trigger an opposing set. A likely reason for this is that there is a difference in proteins anchored to each type of NMDA receptor.

The location hypothesis can take the form of a *nanodomain* hypothesis. In this case, the location of the calcium source within a dendritic spine could be important. Yasuda et al. (2003) shows that a specific calcium triggered event only occurs when L-type calcium channels are stimulated, but not when NMDA receptors are. Specifically, they find that while the L-type calcium channel does not noticeably contribute to the

calcium elevation in a spine, it is essential for the depression of R-type calcium channels due to back propagating action potentials (Yasuda et al., 2003). The authors conclude that distinct calcium pools within a spine activate distinct downstream molecules.

Calcium nanodomains have also been suggested through the use of fast and slow calcium buffers. BAPTA binds calcium quickly, while EGTA binds it more slowly. Therefore BAPTA will constrain the spatial specificity of calcium much more than EGTA will (Naraghi and Neher 1997). Isaacson and Murphy (2001) show that NMDA receptors are in close proximity to the big conductance calcium-activated potassium channel (BK) in olfactory bulb granule cells. They show that BAPTA prevents the activation of BK by NMDA receptors, while EGTA does not, suggesting a nano-scale calcium domain (Isaacson and Murphy 2001). Bloodgood and Sabatini (2007) show that local calcium influx through R type calcium channels selectively activates the small conductance calcium-activated potassium channel (SK) in the spines of hippocampal neurons. When R-type calcium channels were blocked, calcium in the spine head was actually increased, but the effect of SK channel blockers was occluded, suggesting that the local calcium through R-type channels selectively activated the SK channel via a calcium microdomain (Bloodgood and Sabatini 2007). Similarly, the calcium dependent inactivation (CDI) of L type calcium channels is not sensitive to either BAPTA or EGTA, while the CDI of N and R type calcium channels is absent in the presence of EGTA. This result lead Liang et al. to conclude that N and R type calcium channels are sensitive to global changes in calcium, while L type calcium channels respond to local calcium elevation (Liang et al. 2003).

### **Computational models**

Several computational models explore the role of calcium microdomains in plasticity. Mihalas (2011) created a minimalistic model that co-localized specific calcium binding molecules with specific calcium sources. In the Mihalas model, CaMKII was located near NMDA receptors, PP2B (calcineurin) was located near VGCCs, and phosphodiesterases (PDEs) were located either near NMDA receptors (to mimic spines in cortical slices) or IP3 receptors (to mimic spines in hippocampal cultures). Mihalas found that this model replicated the standard STDP curve and was able to account for the difference seen in STDP-like triplets in cortical slices compared to hippocampal cultures. Pre-post-pre triplets cause LTD and post-pre-post triplets cause LTP when PDEs are located near IP3 receptors, while the opposite occurs when PDEs are located near NMDA receptors.

Using MCell (Bartol et al. 1991), Keller et al. (2008) simulated a spine with spatial detail. Voltage gated calcium channels (VGCCs) were added uniformly to the spine, while the NMDA receptors were concentrated at the post-synaptic density (PSD). Under these conditions pre-post stimulations and post-pre stimulations created different spatial profiles for the calcium concentration. The pre-post stimulation caused a steep gradient with the densest calcium in the PSD and the lowest calcium at the base of the spine, while post-pre stimulation resulted in a weaker gradient (Keller et al., 2008, figure 6). These results indicate that STDP stimulation patterns would cause different spatial profiles of calcium concentration in the spine. These differing calcium gradients could determine which downstream molecules calcium binds to, and consequently which plasticity mechanisms are set into motion.

Using the cellular dynamics simulator (CDS) (Byrne et al., 2010), Kubota and Waxham (2010) test whether the two lobes of calmodulin could be sensitive to calcium microdomains with the spine. They found that the fast binding N lobe of calmodulin was much more sensitive to calcium channel location than the slow binding C lobe, and that saturated calmodulin N lobe itself forms a distinct gradient within the spine. Because calcium binding to N or C lobes of calmodulin differentially activates CaMKII (Forest et al. 2008), this may be a mechanism by which calcium location affects plasticity.

### **Problems with the *microdomain/nanodomain* location hypothesis**

The main difficulty with the calcium location hypothesis is the difficulty in testing it. The experimental evidence presented in this review shows that calcium can specifically act on the micro and nano scale, but it does not show that this action directs plasticity. The experiments showing that VGCCs are essential for LTD and NMDA receptors are essential for LTP do not necessarily mean that the location of these specific calcium sources is important. This result could be because VGCCs have different kinetics than NMDA receptors and therefore support the *duration* hypothesis. Testing whether calcium at the PSD is required for LTP while calcium on the extrasynaptic side of the spine head is necessary for LTD will require advances in calcium uncaging and imaging.

New techniques like array tomography (Micheva et al. 2010), SBEM (Briggman, Helmstaedter, and Denk 2011), and STORM (Xu, Zhong, and Zhuang 2013) now permit unprecedented levels of specificity in defining location of calcium channels on spine heads necks and dendritic shafts. New advances in calcium imaging such as LOTOS (Chen et al. 2012) and GCaMP6 (Chen et al. 2013) create the ability to

image single spines *in vivo*. Similarly, new sophisticated computational modeling software such as NeuroRD (Oliveira et al. 2010), Smoldyn (Andrews et al. 2010), and VCell (Cowan et al. 2012) allow for the simulation of realistic calcium gradients in computational models (reviewed in Blackwell, 2013). The location hypothesis of calcium-dependent plasticity should be re-examined in light of these new tools.

## **Conclusion**

The question of *amplitude*, *duration*, and *location* is not as simple as it sounds. Some of the data that seems to support one hypothesis could actually be interpreted as supporting another. For example, the calcium buffering data supporting the *amplitude* hypothesis could be interpreted as supporting the *location* hypothesis, given that different concentrations of EGTA or BAPTA would restrict the diffusion of calcium away from its source (Naraghi and Neher 1997) as suggested in Mihalas (2011). Further confusing the *duration* and *location* hypotheses, Kubota and Waxham found that the calcium kinetics (specifically the speed of calcium influx) could determine the size of the calcium microdomain even when the total number of calcium molecules was kept constant (Kubota and Waxham 2010). While new techniques will allow for a more complete analysis of the *location* hypothesis, it is still likely that a full understanding of the role of calcium in plasticity will require a combination of all three of these hypotheses.

## **Contributions**

Wrote chapter: Rebekah C. Evans

Edited chapter: Kim T. Blackwell

Publication status: *In preparation*

## CHAPTER TWO: STRIATAL CELLULAR MODELS

### **Definition**

The [striatum](#) is the main output structure of the Basal Ganglia, and is implicated in [habit learning](#), [addiction](#), and neuropathologies such as [Parkinson's Disease](#) and [Huntington's Disease](#). Parkinson's Disease is a motor dysfunction caused by degeneration of dopaminergic neurons that project strongly to the striatum. Huntington's disease is another motor dysfunction caused by degeneration of a subset of the neurons in the striatum. Experiments in both humans and animals have demonstrated that normal habit learning involves the striatum, and in particular changes in striatal neural activity are observed consequent to cortical glutamatergic activity (in response to environmental stimuli or motor activity) and dopamine release in response to reward.

### **Cell classes in the striatum**

The projection neurons of the striatum are the medium spiny neurons (MSNs) which make up the majority (90-95%) of the neurons. MSNs are further subdivided into two classes: those with dopamine D1 receptors, which co-release substance P and dynorphin, and those with dopamine D2 receptors, which co-release mu-opioids. Three other classes of interneurons have been extensively studied: the GABAergic fast spiking interneurons (FSIs) which are connected by gap junctions, the GABAergic neuropeptide Y positive (NPY) interneurons which also produce nitrous oxide, and the acetylcholinergic (ACh) interneurons, also called the tonically active neuron because of its spontaneous

and regular firing pattern. More recently it has been possible to characterize a set of tyrosine hydroxylase expressing neurons using transgenic expression systems. These neurons exhibit four different firing patterns, but their role in striatal circuits remains to be elucidated. The GABAergic interneurons are in a position to modulate the timing and pattern of firing of the projection neurons of the striatum. In addition, their interconnections via both chemical and electrical synapses may play a role in synchronization. The acetylcholinergic neurons modulate dopamine release from the substantia nigra, and modulate striatal neuron properties through pre- and post-synaptic metabotropic receptors.

One of the compelling questions about striatal function is the role of the D1 versus D2 MSNs. The prevalent theory regarding Parkinson's disease is that dopamine increases excitability of D1 MSNs and decreases excitability of D2 MSNs. This leads to overactivity of the D2 MSNs which tend to inhibit motor movement. Thus, some striatal models have been developed to evaluate which characteristics of MSNs can explain the difference between D1 and D2 neurons and the effect of dopamine. Both neuron classes exhibit a characteristic bi-modal membrane potential distribution during anesthesia and sleep, known as up-states and down-states. Though the significance of this activity is still unclear, several models have investigated which neuron mechanisms underlie this activity. Both normal habit learning and the overly strong habit learning of drug addiction likely involve synaptic plasticity of the MSNs, thus several models have investigated the control of calcium concentration during synaptic and neuronal activity, which are essential for synaptic plasticity.

### **Simple MSN Models**

Some models contain only a subset of cellular components and attempt to reproduce a specific cellular phenomenon. The purpose of these types of models is to explain cellular behavior using the smallest possible subset of mechanisms. This has the dual advantage of minimizing the number of free parameters and also demonstrating that specific channels/interactions are required. It has the disadvantage of being unable to demonstrate possible alternative mechanisms which might explain the data just as well. An example of this approach is Gruber et al. (2003) which uses two potassium channels and one calcium channel to test whether the known effects of dopamine on these channels affects membrane bi-stability. Another model (Koos et al. 2004) represents the complete morphology, but contains no voltage-dependent channels. This model shows that morphological characteristics, such as electrotonic distance, can account for the difference in amplitude of inhibitory post-synaptic potentials (IPSPs) produced by FSIs compared to MSNs.

### **Complex MSN Models**

Another class of striatal models includes the complex models. These contain a large number of cellular features, and attempt to reproduce many characteristics of voltage and/or calcium waveforms. The advantage of this approach is being able to isolate specific channels or morphological characteristics within the context of many cellular characteristics to demonstrate the necessity or sufficiency of a mechanism in replicating an experimental finding. These models can often be re-used to explain new data with minimal change. The disadvantage of this approach is having numerous free parameters, and the complexity can sometimes hinder the ability to illuminate concepts.

The first complete MSN model (Wolf et al. 2005) used the [NEURON simulation software](#) to model a neuron from the ventral striatum (also called the nucleus accumbens). It contains two sodium channels, six potassium channels, and six calcium channels, as well as synaptic channels (NMDA, AMPA, GABA). This model replicates many of the characteristics of MSNs such as the long delay to action potential at rheobase and the low frequency of spiking. The model was used to test the effects of the NMDA/AMPA ratio on entrainment to oscillation (Wolf et al. 2005) and later to test the effects of dopamine modulation on synaptic integration (Moyer et al. 2007). The inwardly rectifying potassium current (Kir) was re-tuned (Steephen and Manchanda 2009) and implemented in this model to investigate the role of inactivating Kir in MSN excitability. This model was adapted by Spiga et al. (2010), who added morphology based on a digital reconstruction of an MSN and tested the effects of spine loss and AMPA current reduction on AP frequency during simulated upstates.

Several other complex models of dorsal striatal MSNs have been developed. A NEURON model MSN by (Gertler et al. 2008) has one sodium channel, one calcium channel, five potassium channels and synaptic channels (AMPA). The model was used to test the contribution of morphological differences between D1 and D2 MSNs in describing their different electrophysiological characteristics. This model was adapted by (Plotkin et al. 2011) to test the ability of distal dendrites to evoke sustained somatic depolarizations. A similar model, by the same group (Day et al. 2008) was used to investigate the back propagation of the action potential into MSN dendrites.

Another NEURON model MSN by Flores-Barrera et al. (2009) has one sodium channel, two calcium channels, and five potassium channels as well as synaptic channels (NMDA,AMPA, GABA). This model is used to test whether GABAergic input, which is depolarizing below its reversal potential (roughly -60mV), plays a role in maintaining the depolarization of an MSN during a cortico-striatal upstate.

The most recent model (Evans et al. 2012) uses the [GENESIS simulation software](#) to model a dorsal striatum MSN containing one sodium channel, six potassium channels, five calcium channels, and four different NMDA receptor types as well as AMPA receptors. This model is used to test whether the NMDA receptor subtypes, based on the four GluN2 subunits, differentially affect the calcium influx into spines during closely-timed pairings of pre and post-synaptic activity (spike timing dependent plasticity protocols).

### **Interneuron Models**

Most striatal models focus on the spiny projection neurons, but there are several models of striatal interneurons.

The first complete model of a fast spiking interneuron (FSI) (Hellgren Kotaleski et al. 2006) contains three potassium channels, one sodium channel and synaptic channels (AMPA, GABA). This model replicated the observed spike latency and high firing frequency of striatal FSIs. This model was used to investigate how upstate firing of FSIs is controlled by transient potassium currents and the contribution of these channels to enhancing signal detection. This model was further used to construct a network model

(Hjorth et al. 2009) that investigated the contribution of gap junctions in FSI sensitivity to coincident input from the cortex.

Several simple models of acetylcholinergic neurons (ACh) have been developed. The goal of most of these models is to explain mechanisms underlying the rhythmic firing and burst firing observed in these neurons. Two models demonstrate two different set of currents which can explain membrane potential oscillations in these models. The first model (Wilson 2005) demonstrates that Kir, HCN (Hyperpolarization-activated and cyclic nucleotide-gated channel) and leak conductance in a single compartment could explain membrane potential oscillations in the voltage range of -80 to -60 mV. A second model investigates yet a different mechanism responsible for a slower time course of oscillations. This model (Wilson and Goldberg 2006) is implemented in [XPPAUT](#) and is also a single compartment. It contains an L type calcium channel, high voltage activated potassium channel, leak current, a calcium dependent potassium current, and calcium concentration calculated using a single time constant of decay. Simulations investigated why the slow afterhyperpolarization (sAHP) is activated by long depolarizations (even of small amplitude) but not activated by brief ones. Another model of ACh neurons (Goldberg et al. 2009) was used to investigate the role of calcium channel colocalization in mediating slow and fast after hyperpolarizations. This model had a single electrical compartment that was subdivided into multiple concentric calcium compartments coupled by diffusion. Several calcium binding proteins enabled the model to demonstrate that the transient calcium influx produced by an action potential preferentially binds to SK channels, whereas the lower but more prolonged calcium influx produced by

subthreshold depolarization preferentially binds to the slower, higher affinity binding proteins.

## Conclusion

There are several models of striatal neurons that contain cellular detail. These models vary in complexity, morphology, and active channels. Each model is configured to test a specific aspect of striatal physiology as efficiently and accurately as possible, and therefore both the simple and the complex models are valuable. With the increasing power of computers and tools for parameter optimization, the accuracy and efficiency of complex models is likely to increase.

## Contributions

Wrote chapter: Rebekah C. Evans, Sriram Damodaran, Kim T. Blackwell

Edited chapter: Rebekah C. Evans, Sriram Damodaran, Kim T. Blackwell

Citation and Publication status:

Evans RC, Damodaran S, Blackwell KT (2013) Striatal models: Cellular Detail, *Encyclopedia of Computational Neuroscience. SpringerReference*. Eds. Dieter Jaeger and Ranu Jung. (*invited, in revisions*)

**Table 1 Computational Models of striatal neurons.**

<b>Citation</b>	<b>Cell type</b>	<b>Simple/complex</b>	<b>Software</b>	<b>Available modelDB</b>
Gruber et al. 2003	MSN	Simple	NEURON	Yes
Moyer et al. 2007; Wolf et al. 2005	MSN, N. Acc.	Complex	NEURON	Yes
Steephen and Manchanda	MSN, N. Acc.	Complex	NEURON	Yes

2009				
Spiga et al. 2010	MSN, N. Acc.	Complex	NEURON	Yes
Koos et al. 2004	MSN	Simple	NEURON	No
Gertler et al. 2008	MSN	Complex	NEURON	No
Day et al. 2008	MSN	Complex	NEURON	No
Flores-Barrera et al. 2009	MSN	Complex	NEURON	No
Evans et al. 2012	MSN	Complex	Genesis	Yes
Hellgren Kotaleski et al. 2006	FSI	Complex	Genesis	Yes
Wilson 2005	ACh	Simple	XPPAUT	No
Wilson and Goldberg 2006	ACh	Simple	XPPAUT	No
Goldberg et al. 2009	ACh	Simple	XPPAUT	No

## **CHAPTER THREE: THE EFFECTS OF NMDA SUBUNIT COMPOSITION ON CALCIUM INFLUX AND SPIKE TIMING-DEPENDENT PLASTICITY IN STRIATAL MEDIUM SPINY NEURONS**

### **Abstract**

Calcium through NMDA receptors (NMDARs) is necessary for the long-term potentiation (LTP) of synaptic strength; however, NMDARs differ in several properties that can influence the amount of calcium influx into the spine. These properties, such as sensitivity to magnesium block and conductance decay kinetics, change the receptor's response to spike timing dependent plasticity (STDP) protocols, and thereby shape synaptic integration and information processing. This study investigates the role of GluN2 subunit differences on spine calcium concentration during several STDP protocols in a model of a striatal medium spiny projection neuron (MSPN). The multi-compartment, multi-channel model exhibits firing frequency, spike width, and latency to first spike similar to current clamp data from mouse dorsal striatum MSPN. We find that NMDAR-mediated calcium is dependent on GluN2 subunit type, action potential timing, duration of somatic depolarization, and number of action potentials. Furthermore, the model demonstrates that in MSPNs, GluN2A and GluN2B control which STDP intervals allow for substantial calcium elevation in spines. The model predicts that blocking GluN2B subunits would modulate the range of intervals that cause long term potentiation. We confirmed this prediction experimentally, demonstrating that blocking GluN2B in the striatum, narrows the range of STDP intervals that cause long term

potentiation. This ability of the GluN2 subunit to modulate the shape of the STDP curve could underlie the role that GluN2 subunits play in learning and development.

## **Introduction**

The striatum is the main input structure of the basal ganglia, which is necessary for proper motor function and habit formation. The medium spiny projection neurons (MSNs), which comprise ~95% of striatal neurons, undergo changes in synaptic strength during the learning of a motor task (Yin et al. 2009). This synaptic plasticity is thought to be the cellular basis of motor learning and habit formation, and it is disrupted in animal models of Parkinson's Disease (Paillé et al. 2010) and Huntington's Disease (Kung et al. 2007).

One of the critical mechanisms for inducing synaptic plasticity in neurons is calcium elevation in the spine. The sources of calcium are quite diverse, and depend on brain region and direction of plasticity. In particular, LTD often requires release of calcium from intracellular stores (Bender et al. 2006) or voltage dependent calcium channels (Bender et al. 2006; Shindou et al. 2011). In contrast, the source of spine calcium that contributes to long-term potentiation (LTP) is the NMDA receptor (NMDAR) in the hippocampus (Murphy et al. 1997), cortex (Artola and Singer 1987), and striatum (Calabresi et al. 1992).

Because NMDARs permit calcium influx in response to the coincidence of pre-synaptic glutamate release and post-synaptic depolarization, they are well situated to modulate spike timing dependent plasticity (STDP). In STDP protocols, an action potential (AP) is caused by depolarizing the soma of a neuron and is paired in time with a

pre-synaptic stimulation. NMDAR subunits differ in several properties that may be critical for timing-dependent synaptic plasticity. They contain various combinations of GluN1, 2, and 3 subunits which can change their maximal conductance, current decay time, and sensitivity to magnesium block (Paoletti 2011). While the GluN1 splice variant contributes to the kinetic properties of the NMDAR, the four GluN2 subunits (A, B, C, and D) determines them when the GluN1 splice variant is kept the same (Paoletti 2011). The specific differences determined by the GluN2 subunit, maximal conductance, decay time, and sensitivity to magnesium block, would affect the dependence of the NMDARs on AP timing. By controlling the kinetic properties of the NMDAR, the GluN2 subunit may determine how much calcium enters the spine during STDP pairings. Because calcium through the NMDAR plays an essential role in striatal timing-dependent long term potentiation (tLTP) (Fino et al. 2010; Pawlak and Kerr 2008; Fino et al. 2011) we hypothesized that changes in GluN2 subunit would affect the potentiation due to STDP protocols in the striatum.

The MSNs of the striatum contain both GluN2A and GluN2B subunits in abundance (Chapman et al. 2003), and it has been suggested that GluN2D subunits may be present in low concentrations (Logan et al. 2007). In animal models of Parkinson's disease, the NMDAR subunit composition is altered in the striatum (Paillé et al. 2010) and subunit-specific NMDAR antagonists have been shown to alleviate Parkinson's like symptoms (Nash and Brotchie 2002). However, the intracellular consequences of such altered NMDAR subunit composition has not yet been made clear. In this study, we investigate the effects of altering NMDAR subunit composition on tLTP in the striatum.

Using a multi-compartmental model of a MSN, we examine NMDAR-mediated calcium influx through receptors containing different GluN2 subunits and under different STDP conditions. We find that calcium elevation depends on the available GluN2 subunit, the relative timing of the AP, the duration of somatic depolarization, and the number of consecutive APs. More significantly, model predictions about the effect of GluN2 subunit on the shape of the STDP curve are confirmed experimentally.

## **Results**

### **Validation of model medium spiny projection neuron**

To evaluate the role of the GluN2 subunit in STDP, we used a model of a dorsal striatal MSN, which was modified from a nucleus accumbens neuron model (Wolf et al. 2005; Moyer et al. 2007).

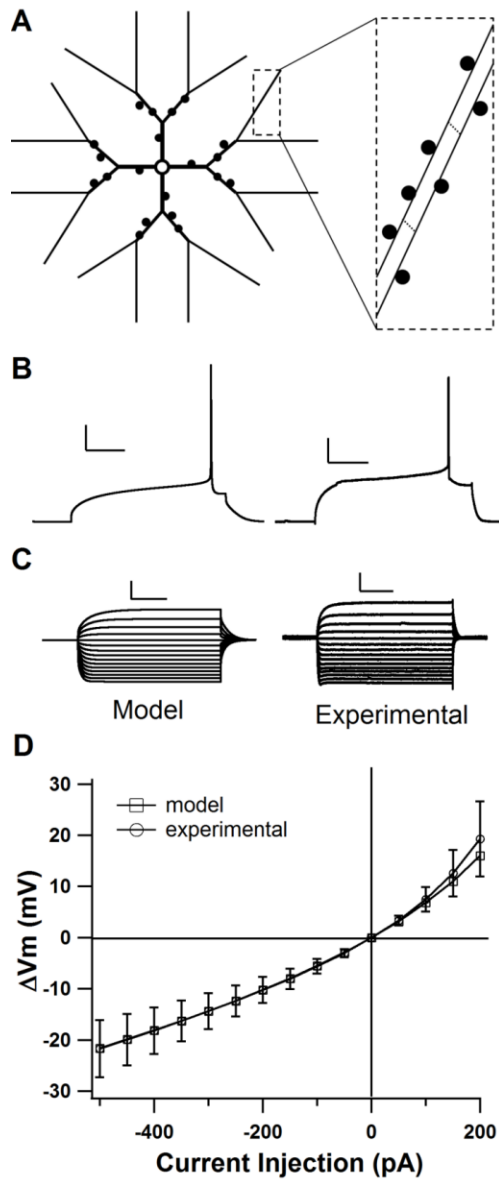


**Figure 4 Model cell shows MSN characteristics.**

A. Morphology of model MSN (not to scale). Inset: tertiary dendrites have 11 segments each  $35\mu\text{m}$  in length. B. Comparison traces demonstrating latency to first AP in the model MSN and an experimental whole-cell recording of a mouse MSN. Both traces are a voltage response to current injection of  $280\text{pA}$ . Scale bars:  $20\text{mV}$  vertical, and  $100\text{ms}$  horizontal. C. Comparison current-voltage relationships ( $-500\text{pA}$  to  $200\text{pA}$ ) for the model MSN and an experimental recording demonstrating inward rectification. Scale bars:  $10\text{mV}$  vertical, and  $100\text{ms}$  horizontal. D. current-voltage relationship for computational model compared with mean current-voltage relationship from 25 MSNs of the mouse dorsal striatum. (see also Supplemental Methods) Error bars  $\pm\text{SD}$ .

The model of the dorsal striatum MSN had the same general morphology as the nucleus accumbens model (Figure 4A), with explicit spines that include synaptic glutamate receptors (AMPA and NMDA) and voltage dependent calcium channels. Kinetics and maximal conductances of voltage dependent channels (See Table 2 and Table 3) were tuned to match the characteristics of neurons in the dorsal striatum, such as long latency to first spike during somatic depolarization (Figure 4B), AP width of ~1ms, and distinct inward rectification (Figure 4C). When a series of hyperpolarizing and depolarizing current incrementing by 50pA from -500pA to 200pA is applied to this model, the resulting current-voltage relationship matches very closely to the average current-voltage relationship of 25 MSNs from the mouse dorsal striatum undergoing the same current series (Figure 4D and see supplemental methods). This model did not contain GABAergic synapses and represents experimental conditions in which GABAergic channels are blocked (Pawlak and Kerr 2008; Shen et al. 2008; Fino et al. 2010).

**Table 2 Steady state and tau equations for ionic channels.**

V=voltage, scale= value by which time constants were scaled during tuning, [Ca] = calcium concentration, EC50 = half activation for calcium dependence, F=Faraday constant , R=Ideal Gas constant. Equations: sigmoid = rate/(1 + (exp((V- vhalf)/slope))), exp = exp((V-vhalf)/slope), SK\_eqn = (([Ca]/EC50)^5.4)/(1+([Ca]/EC50)^5.4), BK\_eqn1 = (B\*[Ca])/([Ca]+K\*(exp((2VDF)/(RT))), BK\_eqn2 = B/(1+[Ca]/(K\*(exp((2VDF)/(RT))))

Channel Name	m or h	Steady State	tau	scale	$\alpha$ or $\beta$	Vhalf (mV)	Slope (mV)	Rate
NaF	m	sigmoid	tab	1.2	-	-25	-9.2	1
	h	sigmoid	tab	1.2	-	-62	6	1
Kir	m	sigmoid	tab	0.5	-	-102	13	1
KaF	m	$\alpha/(\alpha+\beta)$	$1/(\alpha+\beta)$	1.5	$\alpha$ (sigmoid)	4	-17	$1.5 \text{ ms}^{-1}$
					$\beta$ (sigmoid)	10	9	$0.6 \text{ ms}^{-1}$
	h	$\alpha/(\alpha+\beta)$	$1/(\alpha+\beta)$	0.67	$\alpha$ (sigmoid)	-121	22	$105 \text{ s}^{-1}$
					$\beta$ (sigmoid)	-55	-11	$65 \text{ s}^{-1}$
KaS	m	$\alpha/(\alpha+\beta)$	$1/(\alpha+\beta)$	2.5	$\alpha$ (sigmoid)	50	-20	$250 \text{ s}^{-1}$
					$\beta$ (sigmoid)	-90	35	$50 \text{ s}^{-1}$

	h	$\alpha/(\alpha+\beta)$	$1/(\alpha+\beta)$	2.5	$\alpha$ (sigmoid)	-95	16	$2.5 \text{ s}^{-1}$
					$\beta$ (sigmoid)	50	-70	$2 \text{ s}^{-1}$
Kdr	m	$1/(1+a)$	$0.05*b/(1-a) \text{ s}$	0.5	a (exp)	-13	9.09	-
					b (exp)	-13	12.5	-
BK	m	$\alpha/(\alpha+\beta)$	$1/(\alpha+\beta)$	1	$\alpha$ (BK_eqn1)	D=-0.84, K=0.003, B=480s <sup>-1</sup>		
					$\beta$ (BK_eqn2)	D=-1, K=0.009, B=280s <sup>-1</sup>		
SK	m	SK_eqn	4e-3	1	-	EC50=0.57μM		

**Table 3 Maximal conductance and permeability for ionic channels.**

Gbar= maximal conductance S/M<sup>2</sup>=Siemens per meter squared; Pbar = maximal calcium permeability. Prox dend = proximal dendrites; mid dend = middle dendrites; dist dend = distal dendrites.

<b>Gbar (S/M<sup>2</sup>)</b>	<b>soma</b>	<b>prox dend</b>	<b>mid dend</b>	<b>dist dend</b>	<b>spine</b>
NaF	90,000	2,730	2,730	975	0
KaF	765.24	765.24	168.21	112.14	0
KaS	360.1	38.93	38.93	38.93	0
Kir	8	8	8	8	0
KDR	6.04	6.04	6.04	6.04	0
SK	2	2	2	2	0
BK	10	10	10	10	0
Pbar					
CaL1.3	1.59E-07	1.59E-07	1.59E-07	1.59E-07	4.25E-07
CaT	8.81E-09	8.81E-09	8.81E-09	8.81E-09	2.35E-08
CaR	9.75E-07	9.75E-07	9.75E-07	9.75E-07	1.30E-06
CaN	3.75E-07	3.75E-07	3.75E-07	3.75E-07	0
CaL1.2	1.26E-07	1.26E-07	1.26E-07	1.26E-07	3.35E-07

### **STDP protocol type modulates calcium influx through NMDAR**

Because NMDAR channel opening requires both glutamate to activate the channel and membrane depolarization to relieve the voltage-dependent magnesium block, the occurrence of a somatic AP close in time to glutamatergic stimulation can drastically increase the calcium elevation due to the NMDAR. Previous studies have shown that different somatic depolarization patterns back-propagate into the dendrites with varying

strength (Saudargiene et al. 2004; Carter and Sabatini 2004; Zhou et al. 2005).

Consequently, STDP protocols that have been used on striatal cells vary in AP number and length of somatic depolarization.

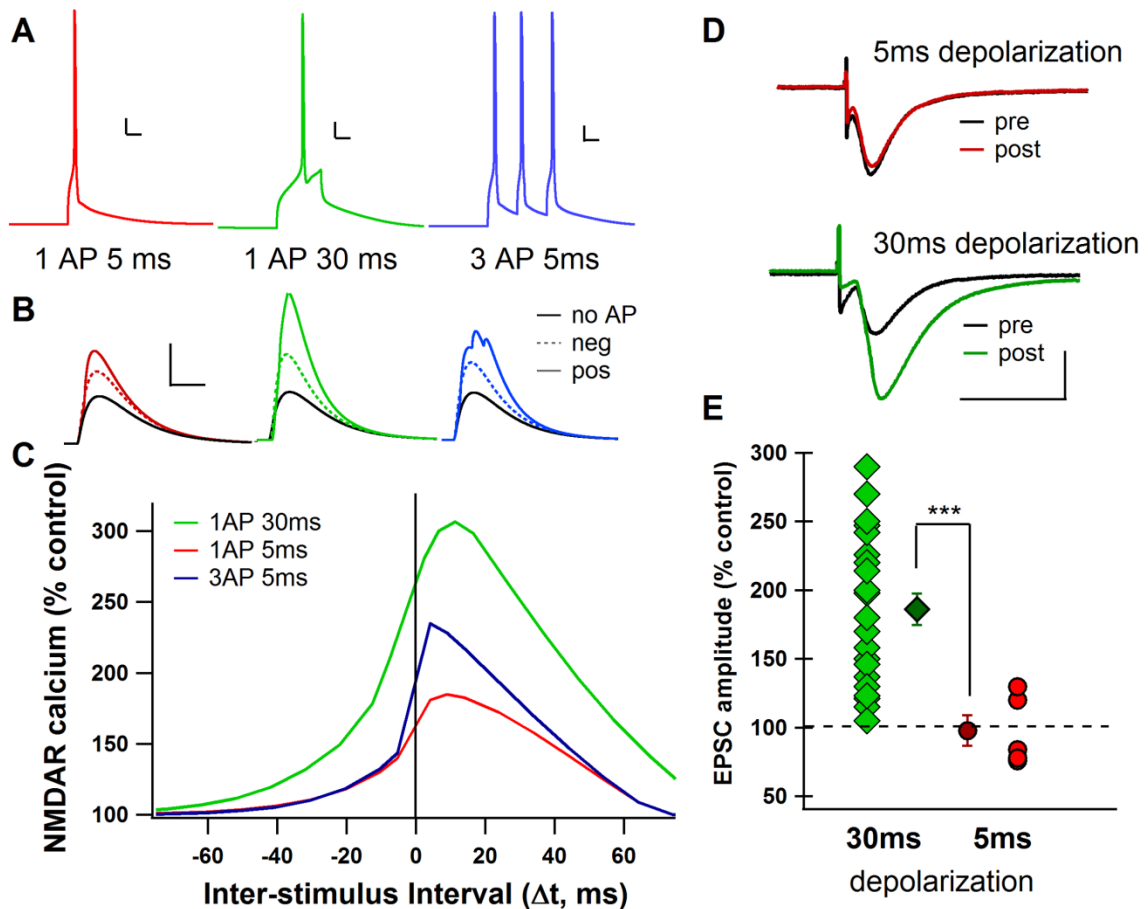


**Figure 5 STDP protocol type changes calcium influx through NMDAR.**

A. Model traces showing each STDP protocol. Scale bars: 10mV vertical, 10ms horizontal. B. NMDAR-mediated calcium during positive (solid color line) and negative (dotted color line)  $\Delta t$  compared to calcium through NMDA during synaptic stimulation only (No AP, solid black line). Scale bars:  $2\mu\text{M}$   $[\text{Ca}^{2+}]$  vertical, 50ms horizontal. C. Model calcium curves showing change in peak NMDAR calcium as a percentage of control (synapse stimulation with no AP). Spines stimulated are  $40\mu\text{m}$  from the soma. D. Example single experiments showing tLTP in response to 30ms depolarization STDP, but not to 5ms depolarization STDP. pre = average of baseline EPSCs prior to STDP; post = average of EPSCs around 60 minutes after STDP. Scale bars: 100pA vertical, 20ms horizontal. E. All experimental data points approximately 60 minutes after STDP protocol application as % of baseline. 5ms depolarization STDP failed to induce significant tLTP when compared to 30ms depolarization STDP. (\*\*\*) =  $p < 0.0001$ .

To investigate the influence that different protocols have on the NMDAR-mediated calcium elevation in the spine, simulations were performed for each STDP protocol that has been used in the striatum: a 30ms depolarization to 1 AP (Fino et al.2005; Fino et al. 2010), a 5ms depolarization to 1 AP (Pawlak and Kerr 2008), and an AP triplet at a frequency of 50Hz (Pawlak and Kerr 2008; Shen et al. 2008) (Figure 5A). Each simulation involved the stimulation of two adjacent spines on the secondary dendrite of the model cell and a somatic depolarization to AP initiation, with the two events separated by a specific temporal interval ( $\Delta t$ ). For each STDP protocol, the peak calcium elevation due to the NMDAR in a single spine was recorded for both positive and negative  $\Delta t$  and was compared to the peak NMDAR-mediated calcium elevation due to control stimulation with no somatic AP (Figure 5B). When repeated over a range of  $\Delta t$ , simulations reveal that a 30ms depolarization to 1 AP significantly increased the NMDAR-mediated calcium in the spine when it occurred +2 to +20 ms after pre-synaptic stimulation (~250% increase), while a 5ms depolarization to AP caused much reduced elevations in NMDAR-mediated calcium at these intervals (~175% increase). The NMDAR-mediated calcium elevation observed with negative  $\Delta t$  was reduced compared to positive  $\Delta t$  for all three protocols, consistent with the experimental observation that in the presence of GABA inhibitors, negative  $\Delta t$  does not produce tLTP (Fino et al. 2010). Because in reality, the AP does not always occur at the exact same time within the depolarization, STDP simulations were repeated with added random synaptic input to cause noise and jitter to the timing of the AP within the 30ms depolarization. Simulations were repeated 6 times using different input frequencies and random seed values. The

averages of these simulations overlay the control conditions, demonstrating that this model and protocol are robust to noise (Figure 6).

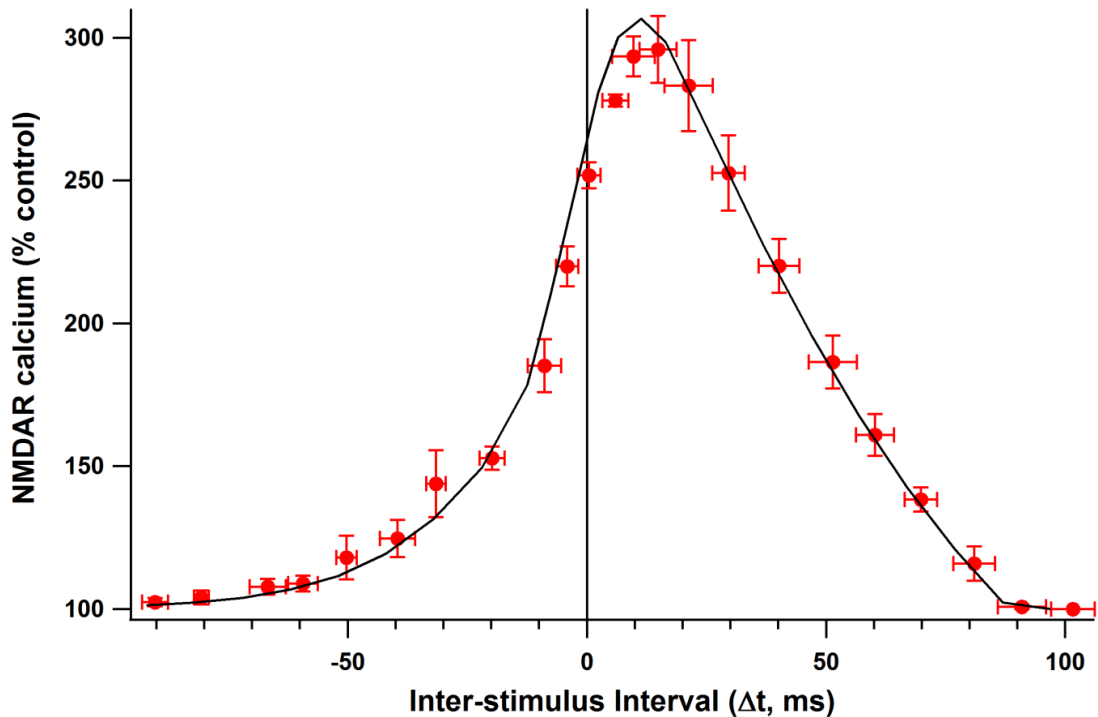


**Figure 6 Added variability to spike time in model MSN.**

Adding low level synaptic input to spines added jitter to the spike time during the 30ms STDP protocol, but did not alter the shape of the STDP curve. Red circles are the means of 6 jitter trials averaged with the control trial for a total  $n=7$ . Black line is control trial (same trace as green line in figure 2C). Error bars  $\pm$ SD.

Because calcium through the NMDAR is essential for tLTP (Fino et al. 2010; Fino et al. 2011), the model predicts that the 30ms depolarization protocol, which causes a strong increase in NMDAR-mediated calcium, will more readily induce tLTP than the 5ms depolarization protocol which causes a weak increase in NMDAR-mediated calcium. This model prediction was confirmed experimentally with whole-cell patch-clamp recordings in rat striatal slices. STDP experiments show that using  $\Delta t$  of +5 to

+30ms, robust tLTP is induced with the 30ms depolarization protocol, but tLTP is not induced with the 5ms depolarization protocol (Figure 5D &E). Indeed, with the 30ms depolarization protocol, the mean EPSC amplitude value, recorded 60 minutes after the induction protocol, was  $186.0 \pm 11.6\%$ , ( $\Delta t = +18.6 \pm 1.5$  ms,  $n=22$ ), a value significantly different ( $p < 0.01$ ) from baseline (Figure 5E). However, 5 ms postsynaptic suprathreshold depolarizations paired with presynaptic stimulations ( $\Delta t = +10.3 \pm 0.4$ ms,  $n=5$ ) were not able to induce significant plasticity. The mean EPSC amplitude recorded 60 minutes after the induction protocol ( $97.5 \pm 11.0\%$ ) did not significantly differ from baseline (Figure 5E).

#### **GluN2 subunit composition modulates calcium elevation due to NMDAR**

The type of GluN2 subunit (A, B, C, and D) strongly determines the maximal conductance, decay time, and sensitivity to magnesium block for the NMDAR (Paoletti 2011). Therefore, differences in GluN2 subunit are predicted to modulate synaptic plasticity by controlling the calcium influx through the NMDAR. To evaluate this hypothesis, simulations were repeated using the 30 ms depolarization STDP protocol that caused tLTP for four types of NMDAR each representing a receptor containing two GluN1 subunits and two GluN2 subunits of the same type (either A, B, C, or D). The current decay time, maximal conductance, and magnesium block parameters of these NMDARs were adjusted to reflect experimental measurements (Monyer et al. 1994; Vicini et al. 1998) (Table 4, Figure 7A & B).

**Table 4 NMDA subunit parameters.**

S=Siemens, s=seconds. "Mg<sup>2+</sup> block" is parameter A used in equation 1

	GluN2A	GluN2B	GluN2C	GluN2D
<b>Gmax (S)</b>	0.94e-9	0.94e-9	0.325e-9	0.119e-9
<b>Tau decay (s)</b>	25e-3	150e-3	125e-3	850e-3
<b>Mg<sup>2+</sup> block</b>	3.57	3.57	25	40

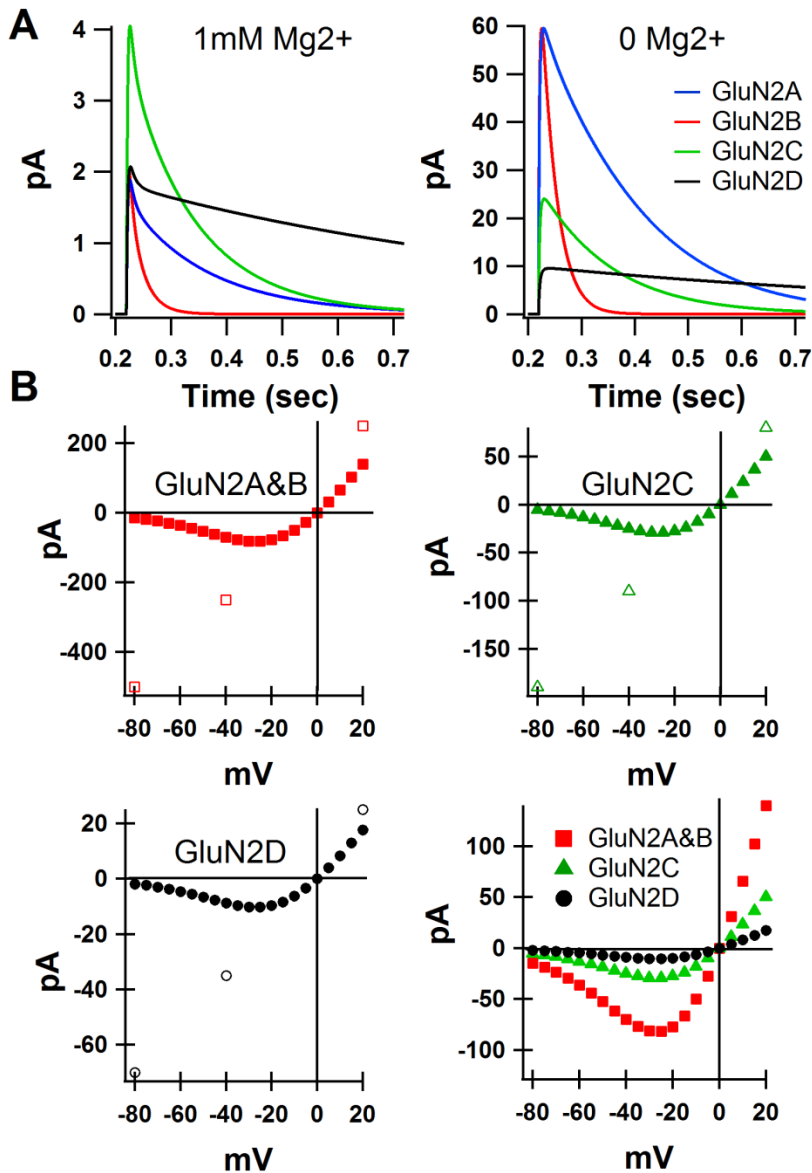


**Figure 7 Characteristics of GluN2 containing NMDARs.**

A. Model NMDAR current in response to synaptic stimulation in a magnesium-containing (left) and a magnesium-free (right) condition for each GluN2 subunit-containing receptor. B. Current-Voltage relationships for each GluN2 subunit-

containing NMDAR in the magnesium-free condition (open symbols) and the magnesium-containing condition (filled symbols). Fourth panel shows subunit-specific current-voltage curves overlaid for the magnesium-containing condition only.

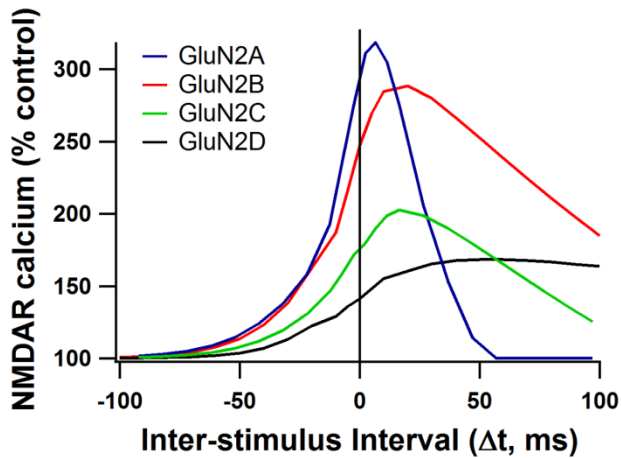


**Figure 8 Calcium curves for different GluN2 subunit containing NMDARs.**

Dependence of NMDAR-mediated calcium on AP timing is different for each GluN2 subunit. Normalized peak NMDAR calcium is plotted for each AP timing interval ( $\Delta t$ ) using the 30ms STDP protocol. Spines stimulated are 40  $\mu\text{m}$  from the soma.

Calcium elevation due to NMDAR was evaluated for each GluN2 subunit condition over all  $\Delta t$  (from -100 to +100ms). The resulting calcium curves (Figure 8) show clear differences in shape depending on GluN2 subunit. GluN2A and GluN2B conditions show the highest normalized calcium peaks, reaching greater than 250% of control, while GluN2C demonstrates a much reduced increase in calcium due to AP timing, just reaching 200% at the narrowest intervals. Similarly, GluN2D exhibits reduced calcium peaks and shows very little change in calcium concentration based on the AP timing (Figure 8). These simulations suggest that tLTP would be readily induced

in GluN2A and GluN2B-containing synapses, but would not be as easily induced in GluN2C and GluN2D-containing synapses.

Although GluN2A and GluN2B-containing receptors both reach calcium peaks greater than 250%, the shapes of the calcium curves are strikingly different. Because of the faster decay time of GluN2A, the range of  $\Delta t$  that causes strong calcium elevation is much narrower than for the more slowly decaying GluN2B-containing receptors. Calcium elevation due to influx through GluN2A only reaches levels  $>250\%$  for narrow  $\Delta t$ . However, the GluN2B-containing receptors maintain elevations in calcium  $>250\%$  even at wide  $\Delta t$  (Figure 8).

Because the predicted intervals that allow significant amounts of calcium through NMDARs differ between GluN2A and GluN2B and because striatal MSNs contain both GluN2B and GluN2A subunits (Ding et al. 2008), the model predicts that blocking the GluN2B subunit in an MSN would narrow the range of  $\Delta t$  that produces tLTP. To test this prediction, STDP experiments were conducted in either normal aCSF, or in the presence of 10  $\mu\text{M}$  Ifenprodil, a potent and selective GluN2B antagonist. In the control condition,  $\Delta t$  between +5ms and +30ms elicits tLTP ( $186.0 \pm 11.6\%$ ,  $n=22$ ) (Figure 9A-D). This  $\Delta t$  range includes both narrow timing intervals ( $5\text{ms} < \Delta t < 12\text{ms}$ ), and wide timing intervals ( $12\text{ms} < \Delta t < 30\text{ms}$ ). Under control aCSF conditions, the tLTP induced using narrow  $\Delta t$  ( $207 \pm 26\%$ ,  $n=5$ ) does not significantly differ from the tLTP induced using wide  $\Delta t$  ( $179.9 \pm 13.4\%$ ,  $n=17$ ) ( $P=0.72$ ). In contrast, when GluN2B-containing NMDARs are blocked with Ifenprodil, tLTP at intervals wider than +12ms is abolished ( $97.7 \pm 6\%$ ,  $n=7$ ), while tLTP between +5ms and +12ms was maintained ( $142 \pm 12\%$ ,  $n=12$ ). This

difference between wide and narrow timing intervals is significant for the Ifenprodil condition ( $p < 0.05$ ; Figure 9D). These results demonstrate that GluN2 subunits not only control *whether* potentiation occurs, as previous studies have shown (Li et al. 2009; Zhang et al. 2009; Banerjee et al. 2009), but also that they *hone* plasticity, making it sensitive to wider or narrower time intervals between pre-synaptic neurotransmitter release and post-synaptic firing.

To reflect these experiments in the model cell, control aCSF simulations were run using a combined GluN2A and B decay time constant (25% GluN2B, 75% GluN2A). To mimic the effects of Ifenprodil in blocking the GluN2B containing receptors, the NMDA response had 75% of the amplitude of the control simulations and a decay time constant of the GluN2A subunit. For both cases the calcium response was normalized by the control aCSF no AP condition.

The calcium curves generated by the model MSN reflect the experimental STDP curves. When GluN2A and GluN2B are present, calcium elevation due to NMDAR stays above 250% of control for both narrow ( $2\text{ms} < \Delta t < 12\text{ms}$ ) and wide ( $12\text{ms} < \Delta t < 30\text{ms}$ )  $\Delta t$ , whereas when GluN2A is present alone, calcium elevation due to NMDAR drops below 250% of control for wide timing intervals (Figure 9E&F). Interestingly, when GluN2A and GluN2B are present, the interval at which NMDAR-mediated calcium drops below 250% in the model (+40ms  $\Delta t$ ) is the same interval that no longer gives tLTP in the experiments (Figure 9C &E).

During the narrow timing intervals ( $5\text{ms} < \Delta t < 12\text{ms}$ ), Ifenprodil significantly reduced the amount of tLTP induced for the experiments, and reduced the NMDAR

mediated calcium in the model simulations. This result is not surprising considering that the synapses in the Ifenprodil condition have fewer total NMDARs available than those in the control condition.

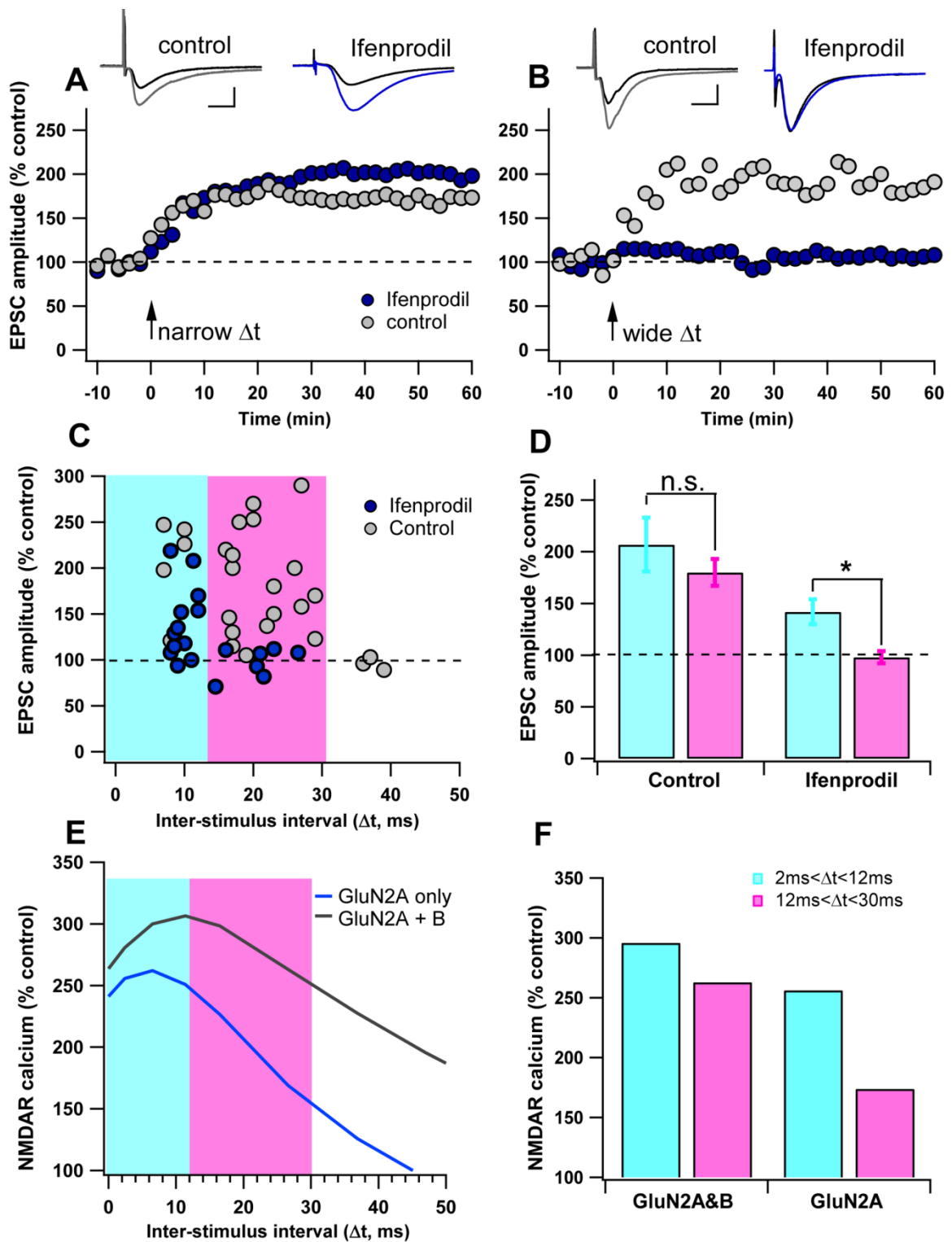


**Figure 9** GluN2B broadens the STDP curve. A-B. Inhibition of GluN2B restricts the time window of tLTP induction.

Representative experiments illustrate the time course of synaptic efficacy changes induced by pre-post pairings in control aCSF and in the presence of ifenprodil (10  $\mu$ M). Insets: averaged EPSCs before (black) or after (grey: control);

blue: ifenprodil treatment) STDP. Scale bars 100pA vertical, 10ms horizontal. A. Example experiments showing tLTP induced by narrow AP timing intervals ( $0 < \Delta t < 12$ ms) in control and ifenprodil conditions. B. Example experiments showing tLTP is induced by wide AP timing intervals ( $12 < \Delta t < 30$ ms) in control conditions, but not induced when GluN2B containing NMDARs were blocked by Ifenprodil. Black arrow indicates the STDP protocol induction. C. Summary of Experimental data: Spike-timing dependent changes in synaptic efficacy estimated 60 minutes after STDP induction in control and Ifenprodil conditions. Blue shading highlights  $\Delta t$  shorter than 12ms; pink shading highlights  $\Delta t$  between 12ms and 30ms. D. Bar graph of long-term synaptic efficacy changes shows that the GluN2B inhibition affects the range of  $\Delta t$  that permits tLTP induction. (\* =  $p < 0.05$ , n.s. = not significant) E. Peak NMDAR calcium curves from the model MSN for positive  $\Delta t$ . To represent the selective experimental blockade of GluN2B receptors, both curves are normalized to the GluN2A+B no AP condition. F. Bar graph showing average NMDA calcium elevation for narrow intervals (+2ms to +12ms) and wide intervals (+13ms to +30ms) for each NMDAR condition (GluN2A+B and GluN2A alone).

### **Spines on distal dendrites show reduced sensitivity to AP timing**

Previous studies in other neuronal types have shown that distance from the soma alters the strength (Froemke et al. 2005) and direction of STDP (Sjöström and Häusser 2006). Because the AP decays as it back-propagates in MSNs (Day et al. 2008), we hypothesized that the timing dependence seen in secondary dendrites of these neurons would shift with distance from the soma. To investigate these interactions, we evaluated the peak calcium elevation during the 30ms depolarization STDP protocol while stimulating spines located on the third segment of the tertiary dendrite, 150 $\mu$ m away from the soma, compared to the secondary dendrites at 40  $\mu$ m. Because a smaller branch diameter increases the input resistance at the tertiary dendrite, stimulating two adjacent tertiary spines resulted in a larger post-synaptic potential (PSP) than stimulating the two adjacent secondary spines, when seen at the spine head (Figures 5A & B). However, the greater electrotonic distance for the tertiary stimulation causes the same stimulation to be smaller when seen at the soma (Figure 10A&C). As predicted by cable theory (Rall 1969), the depolarization seen in the spine due to the back propagating AP is smaller in the tertiary dendrites than in the secondary dendrites (Figure 10D).

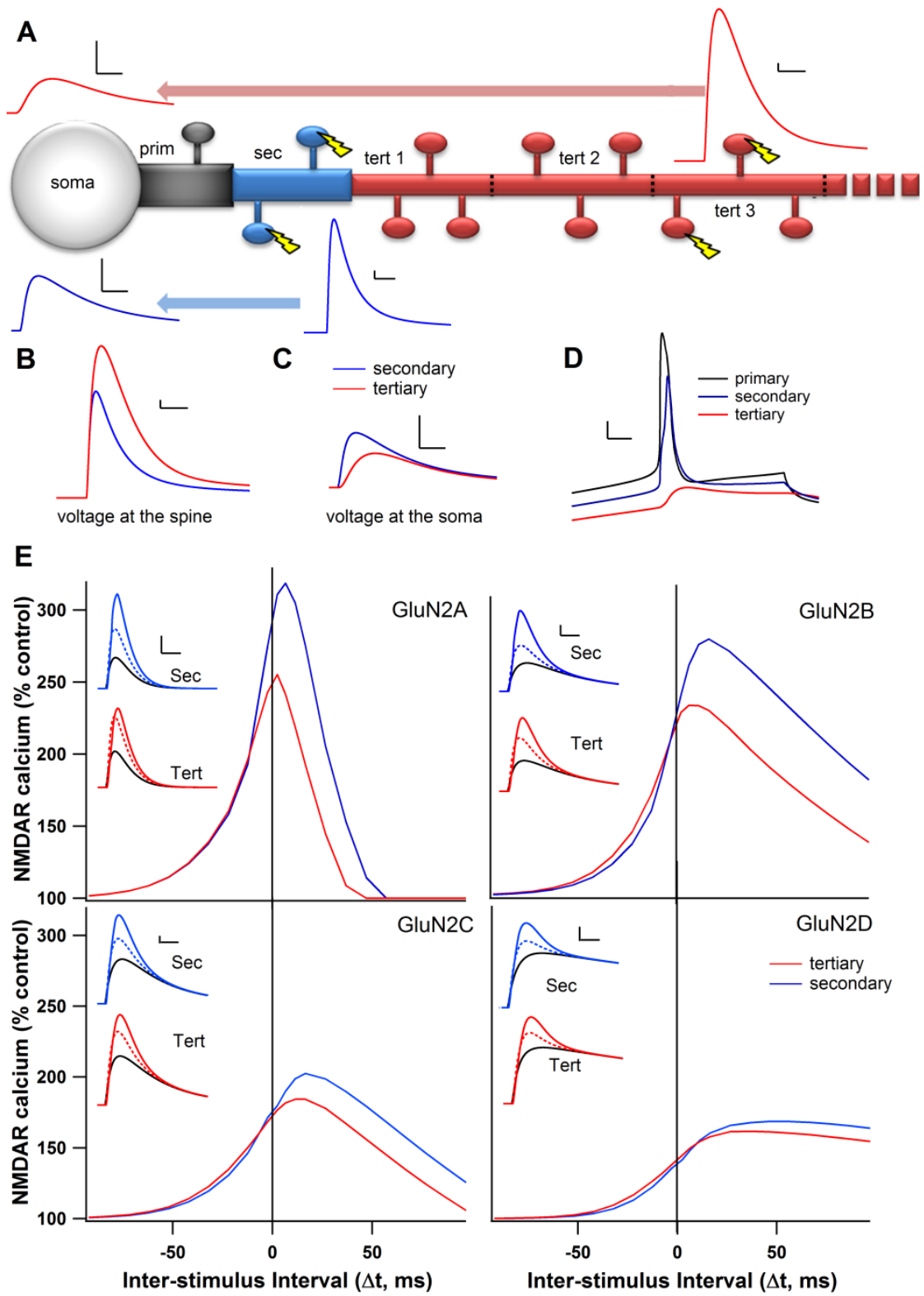


Figure 10 Distance from soma reduces dependence on AP timing.

A. Illustration of dendritic branch, showing the decay of the EPSP traveling from either the tertiary (red) or secondary (blue) dendritic spines. In all panels “tertiary” refers to the third segment of the tertiary dendrite (tert 3). Scale bars 0.5mV vertical, 10ms horizontal. B. Overlaid tertiary and secondary EPSPs as seen at the spine. Scale bars: 0.5mV vertical, 10ms horizontal. C. Overlay of tertiary and secondary EPSPs for the same stimulations in B as seen at the soma. Scale bars: 0.5mV, 10ms D. Spine depolarizations resulting from the back-propagating AP for the primary, secondary, and tertiary dendrites. Scale bars: 10mV vertical, 5ms horizontal. E. Peak NMDAR calcium curves for each GluN2 subunit on the tertiary dendrite and the secondary dendrite. Insets: NMDAR-mediated calcium traces for secondary (top) and tertiary (bottom) dendrites for positive ( $\Delta t=+11$ ms, solid color), negative ( $\Delta t=-12$ ms, dotted color) and no AP control conditions (solid black). Scale bars 1 $\mu$ M, vertical, 10ms horizontal.

A reduced sensitivity to AP timing for positive  $\Delta t$  is observed under every GluN2 subunit condition (Figure 10E), due to both the decrement in back-propagating AP, which decreases the amplitude of the NMDAR-mediated calcium elevation, and the larger PSP, which decreases the need for depolarization by the AP. In contrast, virtually no change in calcium elevation or timing dependence appears for negative  $\Delta t$  (Figure 10E). The most drastic decreases in NMDAR-mediated calcium elevation occurs in the subunit conditions most sensitive to the magnesium block, i.e. GluN2A and GluN2B, while the GluN2C and GluN2D subunit conditions showed a smaller decrease in NMDAR-mediated calcium elevation due to distance. Because there is no change for negative  $\Delta t$  and a decrease in peak calcium for positive  $\Delta t$ , the difference between positive and negative  $\Delta t$  is strongly reduced when synapses are on the tertiary dendrite. For example, when GluN2A is stimulated on the tertiary spine, positive  $\Delta t$  causes nearly the same elevation in calcium as negative  $\Delta t$  (Figure 10E inset). Under these distal dendrite conditions, positive  $\Delta t$  is unlikely to produce tLTP, and the dependence on AP timing is drastically reduced.

### **Differences between thalamo-striatal and cortico-striatal synapses**

The MSNs of the striatum receive inputs from almost all areas of the cortex (Smith and Bolam 1990) and from the thalamus (Takada et al. 1985). Using a slice preparation which preserves both cortico-striatal and cortico-thalamic fibers (Smeal et al. 2007), Ding et al. (Ding et al. 2008) and Smeal et al. (2008) have characterized the two major glutamatergic inputs to the striatum in mouse and rat respectively. Ding et al. found that thalamo-striatal synapses had a lower NMDAR/AMPA ratio than cortico-striatal synapses in the mouse, while Smeal et al. found the opposite, that the NMDAR/AMPA ratio was higher for thalamo-striatal synapses in the rat. Measuring the decay time constant, Smeal et al. found that thalamo-striatal synapses had lower GluN2B/NMDAR ratios than cortico-striatal synapses, while using bath application of Ifenprodil Ding et al. found the opposite, that thalamo-striatal synapses had a higher GluN2B/NMDAR ratio. Smeal et al. also found that the thalamo-striatal synapses were electrotonically more distant from the soma than the cortico-striatal synapses, Ding et al. did not measure this (Table 5). To investigate the implications of differences in the NMDAR/AMPA ratio, the GluN2B/NMDAR ratio, and the electrotonic distance from the soma, we modeled synapses with specific cortico-striatal characteristics and specific thalamo-striatal characteristics. Because the two studies report contrasting results (Ding et al. 2008; Smeal et al. 2008), we ran separate simulations using each set of data.

**Table 5 Cortico-striatal and thalamo-striatal parameters.**

Ctx=cortico-striatal synapses; Th=thalamo-striatal synapses.  $\tau$ =decay time constant for NMDA current. Arrows represent a relative increase or decrease in NMDA/AMPA ratio or GluN2B/NMDA ratio between cortico-striatal and thalamo-striatal synapses for each study.

	<b>NMDAR/AMPA</b>			<b>GluN2B/NMDAR</b>		<b>Distance from soma</b>
<b>Smeal et al., 2008 (from rat)</b>	Ctx	1.52	↓	Ctx $\tau=233\text{ms}$	↑	Ctx more proximal
	Th	2.6	↑	Th $\tau=193\text{ms}$	↓	Th more distal
<b>Ding et al., 2008 (from mouse)</b>	Ctx	2.75	↑	Ctx 0.25	↓	--Not Addressed--
	Th	2.04	↓	Th 0.42	↑	

We found that, based on different electrotonic properties, thalamo-striatal and cortico-striatal synapses differentially affect the NMDAR mediated calcium elevations for positive  $\Delta t$ , but not negative  $\Delta t$ . The distal thalamo-striatal synapses had lower peak calcium, and a weaker dependence on AP timing than did the cortico-striatal synapses for both mouse and rat (Figure 11A). This result suggests that NMDAR-dependent tLTP would be more readily induced in cortico-striatal synapses than in thalamo-striatal. However, this result assumes that thalamo-striatal synapses are more distal than the cortico-striatal as has been experimentally suggested (Smeal et al. 2008). To distinguish the effect of distance from the effect of NMDAR/AMPA and GluN2B/NMDAR ratios, simulations were repeated with thalamo-striatal synapses in the same location (secondary dendrite) as the cortico-striatal synapses. When the synapses were located at the same distance from the soma, the effect of  $\Delta t$  on peak calcium concentration did not differ strongly between thalamo-striatal and cortico-striatal synapses (Figure 11A). Therefore, the lower calcium peaks in the thalamo-striatal simulations are entirely due to its location on the tertiary dendrite. Interestingly, this result was independent of which dataset (Ding et al. or Smeal et al.) was used.

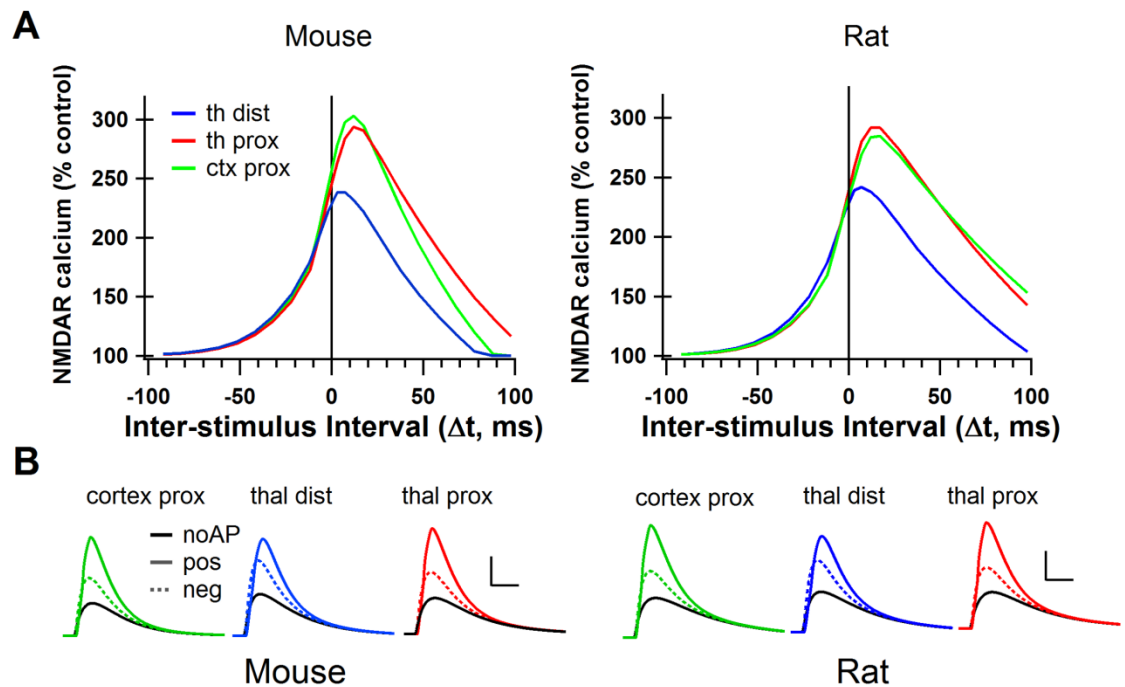


**Figure 11 The cortico-striatal and thalamo-striatal synapses onto MSNs have different synaptic characteristics.** A. Peak NMDAR calcium curves from simulations using cortico-striatal and thalamo-striatal parameters from mouse striatum (Ding et al., 2008) and from rat striatum (Smeal et al., 2008). Cortico-striatal curve for mouse is the same as the green trace in figure 2C. B. NMDAR-mediated calcium for positive ( $\Delta t=+1$  ms, solid color), negative ( $\Delta t=-12$  ms, dotted color) and no AP control conditions (solid black) under cortico-striatal and thalamo-striatal conditions in mouse and rat. Scale bars:  $2\mu\text{M}$   $[\text{Ca}^{2+}]$  vertical, 50ms horizontal. th dist = thalamo-striatal synapses stimulated on tertiary dendritic spines, th prox = thalamo-striatal synapses stimulated on secondary dendritic spines. Ctx prox = cortico-striatal synapses stimulated on secondary dendritic spines.

In conclusion, we predict that the cortico-striatal and thalamo-striatal synapses onto an MSN will respond similarly to STDP protocols if they are located a similar distance away from the soma. However, if as Smeal et al. (2008) have shown, the thalamo-striatal synapses are more distal, then we predict it will be more difficult to induce NMDAR dependent tLTP in those synapses than in cortico-striatal synapses.

## Discussion

We developed a multi-compartment, multi-channel model of a striatal medium spiny projection neuron to investigate the relationship between NMDAR mediated

calcium influx and tLTP. We demonstrated that a longer somatic depolarization to action potential produced a larger calcium elevation in the model and more readily induced tLTP experimentally than a short depolarization. Also, we showed that the GluN2 subunit altered NMDAR sensitivity to action potential timing, and modified the shape of the STDP curve. The model predicted that synapses containing GluN2B subunits would be sensitive to a wider range of positive  $\Delta t$  than synapses containing only GluN2A subunits. We tested this prediction experimentally and found that blocking GluN2B effectively narrowed the range of  $\Delta t$  that induced tLTP.

The NMDAR is critical for learning and STDP because it admits calcium in response to the coincidence of pre-synaptic activity and post-synaptic depolarization. It is clear that other mechanisms besides calcium are important for long term synaptic plasticity (Hellgren Kotaleski and Blackwell 2010). While there are many mechanisms to increase calcium in the cell, such as voltage sensitive calcium channels, calcium permeable AMPA receptors, and calcium release from internal stores, these mechanisms do not all serve the same function (Higley and Sabatini 2010) and not all sources of calcium contribute to tLTP (Bender et al. 2006; Fino et al. 2010). NMDAR-mediated calcium has consistently been shown to be essential for tLTP in the striatum (Pawlak and Kerr 2008; Shen et al. 2008; Fino et al. 2010), while it is not necessary for tLTD (Fino et al. 2010; Fino et al. 2011; Shindou et al. 2011). Therefore, the NMDAR-mediated calcium elevations recorded from this model are used to predict tLTP, but are not relevant to the development of tLTD.

### **Striatal STDP protocols and NMDAR-mediated calcium**

The addition of an appropriately timed back propagating AP during a 30ms depolarization more than doubled the elevation in spine calcium that occurred in response to synaptic stimulation alone, whereas the 5 ms protocol caused little calcium elevation in the model. Similarly, experiments revealed that the 30 ms depolarization protocol, but not the 5 ms depolarization caused tLTP. In cortex and hippocampus, a 5ms depolarization often is sufficient to induce tLTP (Bender et al. 2006; Fuenzalida et al. 2010); however, MSNs usually do not depolarize and fire an AP within 5ms. Cortico-striatal inputs build up over a longer time-course to cause an upstate and AP (Kerr and Plenz 2004; Calabresi et al. 1990); thus, a 30ms depolarization to AP mimics this more natural time course for these cells. One study was able to induce tLTP in the striatum with a 5ms depolarization to AP, and found the same degree of tLTP with the three AP protocol (Pawlak and Kerr 2008). However, these experiments were conducted in the presence of glycine, a NMDA co-agonist, which could have increased NMDAR sensitivity (Thomson 1989).

### **Distance from the soma and STDP**

In the model, NMDAR-mediated calcium elevations show strong sensitivity to AP timing in proximal dendrites, but this sensitivity as well as the maximum change in calcium is diminished at distal synapses. The decrease in spine calcium with distance from the soma is observed for all STDP protocols and was independent of GluN2 subunit. Given the diminished effect of AP timing in tertiary dendrites, LTP at distal synapses might be achieved through entirely different plasticity mechanisms not requiring a somatic AP. A recent study suggests that a limited number of inputs on distal dendritic branches can induce upstates in MSNs due to the high input resistance of the

branch and non-linearity of the NMDA receptor (Plotkin et al. 2011). Thus, the conjunction of many synaptic inputs may be more important than somatic depolarization for distal synaptic plasticity. However, further work is needed to investigate whether this upstate induction can induce LTP at synapses distal to the soma.

### **Cortico-striatal and thalamo-striatal synapses**

We have used the recently characterized thalamo-striatal and cortico-striatal inputs to MSNs to model synapses of each type. Our results show that regardless of the dataset used (Ding et al. 2008; Smeal et al. 2008), the calcium due to NMDAR activation shows the same timing dependence for thalamo-striatal and cortico-striatal synapses when they are the same distance from the soma. However, if the thalamo-striatal synapses are more distal than the cortico-striatal synapses as suggested experimentally (Smeal et al. 2008), the spine calcium elevation due to NMDAR activation is reduced for thalamic inputs during positive  $\Delta t$ . Since distance is the only factor influencing the differential response to STDP protocols between thalamo-striatal and cortico-striatal synapses, our results predict that any disparity in plasticity expression between these synapses will not be NMDAR related, and will come from other neuromodulatory mechanisms, such as differences in pre-synaptic endocannabinoid receptor expression (Uchigashima et al. 2007).

### **GluN2 subunits and their effects on synaptic plasticity**

Our model shows that GluN2 subunit can influence the way synapses respond to STDP protocols. GluN2A and GluN2B allow for large calcium increases and strong sensitivity to AP timing, while GluN2C and GluN2D cause much smaller calcium

increases that are less sensitive to AP timing. Although the striatum contains mostly GluN2A and GluN2B subunits, our findings predict that neuron types with predominantly GluN2C or GluN2D will not exhibit NMDAR dependent tLTP. In addition, GluN2A, because of its fast decay time, results in a narrowing of the STDP curve by decreasing the  $\Delta t$  that permit sufficient calcium influx. In contrast, GluN2B, because of its slower decay time, serves to broaden the STDP curve. While previous studies have focused on *whether* a particular GluN2 subunit is necessary for plasticity (Li et al. 2009; Zhang et al. 2009; Banerjee et al. 2009), we have shown that the relationship between GluN2 subunit and plasticity is more complex than simply allowing or preventing LTP.

In addition to the basic subunit characteristics modeled here, there are other, less well understood parameters that differ between the four GluN2 subunits. For example, differing amino acid patterns in the C-terminal tail allow differential phosphorylation by kinases and differential binding to scaffolding proteins (Foster et al. 2010). Some of these differences are known to change the calcium permeability of the channel (Skeberdis et al. 2006), and could further influence the receptor's response to STDP. Similarly, the intracellular location of the GluN2 subunits is not well known in the striatum. A few studies have looked at the synaptic versus extrasynaptic location of GluN2A and GluN2B (Gardoni et al. 2006; Milnerwood et al. 2010) in the striatum, but the techniques used were comparative rather than quantitative; thus we cannot be certain that we are not stimulating extrasynaptic NMDARs, but the low frequency stimulation (always 1 Hz or lower) used here is unlikely to cause significant glutamate spillover (Hires et al. 2008). It is possible that NMDA triheteromers (containing both GluN2A and B) are present in the

striatum (Li et al. 2004), but see (Ding et al. 2008). Our experimental protocol does not distinguish between di or triheteromers and therefore we cannot specifically determine whether the effect is due to Ifenprodil's full blockade of GluN2B diheteromers or its weak blockade of GluN2A/B triheteromers (Hatton and Paoletti 2005).

The balance between GluN2A and GluN2B, and thus the shape of the STDP curve may be modulated dynamically. Studies in the hippocampus have demonstrated a widening of the STDP curve in response to dopamine D1 receptor stimulation (Zhang et al. 2009), and  $\beta$ -adrenergic receptor stimulation (Lin et al. 2003). Interestingly, both D1 and  $\beta$ -adrenergic receptors activate the cAMP-dependent protein kinase (PKA) which is essential for striatal LTP (Calabresi et al. 2000). PKA phosphorylation is known to increase the calcium permeability of NMDARs and in particular, those containing GluN2B subunits (Skeberdis et al. 2006). Therefore, PKA activation may widen the STDP curve by increasing the calcium permeability of GluN2B-containing NMDARs.

### **Implications for learning, behavior, and pathology**

The role for NMDAR subunits in neurological disorders has recently been suggested. Studies conducted in rodent models of Parkinson's Disease have shown that dopamine depletion results in the reconfiguration of the NMDARs, specifically in a reduction of GluN2B subunits (Gardoni et al. 2006). Other studies have found that the administration of GluN2B antagonists reduces dyskinesia in animal models of Parkinson's Disease while GluN2A antagonists may increase it (Hallett and Standaert 2004). Similarly, GluN2B containing receptors are selectively potentiated by mutant huntingtin (Li et al. 2003), suggesting abnormal GluN2B subunit activity in Huntington's

Disease. An imbalance of GluN2B containing NMDARs may allow non-specific potentiation that could lead to excessive and uncontrolled movement. Our results contribute to the emerging picture of GluN2 subunit antagonists as treatments for neurological disorders of the striatum by elucidating a possible mechanism for GluN2 subunit alterations to alter striatal plasticity and therefore motor behavior.

Our findings suggest a novel role for the GluN2A NMDAR subunit in striatal synaptic plasticity. Instead of allowing or preventing LTP, this subunit *hones* plasticity, narrowing the STDP curve and allowing for the fine-tuning of neuronal pathway strength. Previous work has shown that the medial striatum undergoes plastic changes during the early, more coarse, phase of skill learning, while the lateral striatum undergoes plasticity during the late, fine-tuning, phase of skill learning (Yin et al. 2009). Interestingly, the lateral striatum contains a higher ratio of GluN2A to GluN2B subunits than the medial striatum (Chapman et al. 2003). A high density of the GluN2A subunit may functionally underlie the fine-tuning phase of skill learning, allowing potentiation of only the most closely-timed connections. While the higher ratio of GluN2B subunits in the medial striatum would be useful for less specific, but possibly faster acquisition of a skill. This role for GluN2A may also underlie the experience-dependent developmental shift from GluN2B to GluN2A in the visual cortex (Yashiro and Philpot 2008), and may be responsible for the increase in spatial learning ability that coincides with the developmental switch from GluN2B to GluN2A at hippocampal synapses (Stoneham et al. 2010).

## **Methods**

### **Electrophysiology for Model Tuning**

Animal handling and procedures were in accordance with the National Institutes of Health animal welfare guidelines and were approved by the George Mason University IACUC committee. C57BL/6 male and female mice (p20-33) were anesthetized with isoflurane and decapitated. Brains were quickly extracted and placed in oxygenated ice-cold slicing solution (in mM: KCL 2.8, Dextrose 10, NaHCO<sub>3</sub> 26.2, NaH<sub>2</sub>PO<sub>4</sub> 1.25, CaCl 0.5, Mg<sub>2</sub>SO<sub>4</sub> 7, Sucrose 210). Hemicoronal slices from both hemispheres were cut 350 $\mu$ m thick using a vibratome (Leica VT 1000S). Slices were immediately placed in an incubation chamber containing artificial cerebrospinal fluid (aCSF) (in mM: NaCl 126, NaH<sub>2</sub>PO<sub>4</sub> 1.25, KCl 2.8, CaCl 2, Mg<sub>2</sub>SO<sub>4</sub> 1, NaHCO<sub>3</sub> 26.2, Dextrose 11) for 30 minutes at 33°C, then removed to room temperature (21-24°C) for at least 90 more minutes before use.

A single hemislice was transferred to a submersion recording chamber (ALA Science) gravity-perfused with oxygenated aCSF containing 50 $\mu$ M picrotoxin. Temperature was maintained at 30-32°C (ALA Science) and was monitored with an external thermister. Whole cell patch clamp recordings were obtained from neurons under visual guidance using infrared differential interference contrast imaging (Zeiss Axioskop2 FS plus). Pipettes were pulled from borosilicate glass on a laser pipette puller (Sutter P-2000) and fire-polished (Narishige MF-830) to a resistance of 3-7 M $\Omega$ . Pipettes were filled with a potassium based internal solution (in mM: K-gluconate 132, KCl 10, NaCl 8, HEPES 10, Mg-ATP 3.56, Na-GTP 0.38, EGTA 0.1, Biocytin 0.77) for all recordings. Intracellular signals were collected in current clamp and filtered at 3kHz

using an Axon2B amplifier (Axon instruments), and sampled at 10-20 kHz using an ITC-16 (Instrutech) and Pulse v8.80 (HEKA Elektronik). Series resistance (6-30M $\Omega$ ) was manually compensated.

### **Electrophysiology for plasticity experiments**

All experiments were performed in accordance with local animal welfare committee (Center for Interdisciplinary Research in Biology and College de France and EU guidelines (directive 86/609/EEC). Every precaution was taken to minimize stress and the number of animals used in each series of experiments.

Animals, OFA rats (Charles River, L'Arbresle, France) (postnatal days 17-25) were sacrificed by decapitation and brains were immediately removed. Patch-clamp recordings of MSNs were performed in horizontal brain slices (330  $\mu$ m) from OFA rats. These horizontal slices included the somatosensory cortical area and the corresponding cortico-striatal projection field (Fino et al. 2005) and were prepared with a vibrating blade microtome (VT1000S and VT1200S, Leica Microsystems, Nussloch, Germany). Patch-clamp whole-cell recordings were performed in the somatosensory area of the dorsal striatum and made as previously described (Fino et al. 2005; Fino et al. 2010). Briefly, borosilicate glass pipettes of 5-7 M $\Omega$  resistance contained (mM): 105 K-gluconate, 30 KCl, 10 HEPES, 10 phosphocreatine, 4 ATP-Mg, 0.3 GTP-Na, 0.3 EGTA (adjusted to pH 7.35 with KOH). The composition of the extracellular solution was (mM): 125 NaCl, 2.5 KCl, 25 glucose, 25 NaHCO<sub>3</sub>, 1.25 NaH<sub>2</sub>PO<sub>4</sub>, 2 CaCl<sub>2</sub>, 1 MgCl<sub>2</sub>, 10  $\mu$ M pyruvic acid bubbled with 95% O<sub>2</sub> and 5% CO<sub>2</sub>. Picrotoxin (50  $\mu$ M) (Sigma, Saint Quentin, France) was dissolved in ethanol and then added in the external solution for a

final ethanol concentration of 0.01%. All recordings were performed at 34°C using a temperature control system (Biopetechs ΔTC3, Butler, PA, USA and Bath-controller, Luigs&Neumann, Ratingen, Germany) and slices were continuously superfused at 2-3 ml/min with the extracellular solution. Individual neurons were identified using infrared-differential interference contrast microscopy with CCD camera (Hamamatsu C2400-07; Hamamatsu, Japan). Signals were amplified using EPC10-2 amplifiers (HEKA Elektronik, Lambrecht, Germany). Current-clamp recordings were filtered at 2.5 kHz and sampled at 5 kHz, and voltage-clamp recordings were filtered at 5 kHz and sampled at 10 kHz using the program Patchmaster v2x32 (HEKA Elektronik). The series resistance was compensated at 75-80%.

### **Spike timing-dependent plasticity induction protocols**

Electrical stimulation of the cerebral cortex was performed with a bipolar electrode (Phymep, Paris, France) placed in the layer 5 of the somatosensory cortex (Fino et al. 2005). Electrical stimulations were monophasic at constant current (Stimulator WPI, Stevenage, UK or ISO-Flex stimulator controlled by a Master-8, A. M. P. I., Jerusalem, Israel). Currents were adjusted in order to evoke striatal excitatory postsynaptic currents (EPSCs) ranging in amplitude from 50 to 200pA. Repetitive control stimuli were applied at 0.1 Hz, a frequency for which neither short- nor long-term synaptic efficacy changes in EPSC amplitudes were induced (Fino et al. 2005).

STDP protocols consisted in pairings of pre- and post-synaptic stimulations with the two events separated by a specific temporal interval ( $\Delta t$ ) repeated 100 times at 1 Hz. Pre-synaptic stimulations correspond to cortical stimulations and the post-synaptic

stimulation to an AP evoked by a direct application of a depolarizing current step (5 or 30 ms duration) in the MSN. Neurons were recorded for 10 minutes during baseline and for at least 60 minutes after the cellular conditioning protocol; long-term synaptic efficacy changes were measured after approximately 60 minutes. Series resistance was monitored and calculated from the response to a hyperpolarizing potential (-5 mV) step during each sweep throughout the experiments and a variation above 20% led to the rejection of the experiment. Repetitive control stimuli were applied at a frequency of 0.1 Hz for 60 minutes. Drugs were applied in the bath, after recording 10 minutes of baseline and 10 minutes before cellular conditioning protocol, and were present continuously until the end of the recording. Ifenprodil was dissolved in water at 15 mM and then added to extracellular solution for a final concentration of 10 $\mu$ M (Tocris, Ellisville, MO, USA).

Off-line analysis was performed using Igor-Pro 6.0.3 (Wavemetrics, Lake Oswego, OR, USA). All results are expressed as mean $\pm$ SEM and statistical significance was assessed using the Student's t-test or the non-parametric Wilcoxon signed-rank test when appropriate at the significance level ( $p$ ) indicated. Statistical analysis was performed using Prism 5.0 software (San Diego, CA, USA).

### **Medium spiny projection neuron model**

A dorsal striatum MSN model cell was created based on the nucleus accumbens neuron model by Wolf et al. (2005). The Wolf model was translated from NEURON into Genesis simulation software, and channel concentrations and kinetics were adjusted to closely match those of a mature (> 3 weeks old) MSN in the mouse dorsal striatum (see supplemental methods). The MSN morphology is the same as in Wolf et al. (Wolf et al.

2005), but with the addition of individual spine compartments on the primary dendrites to the third segment of the tertiary dendrites (Figure 4A). Primary dendrites are 20  $\mu\text{m}$  long, secondary dendrites 24  $\mu\text{m}$ , and each of the 11 tertiary segments is 36  $\mu\text{m}$  long. For all simulations, two adjacent spines were stimulated (on the third segment of the tertiary dendrite, or on the secondary dendrite), and the NMDAR-mediated calcium was recorded from one of the two spines. This model is available on Model DB:

<http://senselab.med.yale.edu/modeldb/>

### **Ionic Channels**

All channel kinetics (Table 2) were taken from published data, using dorsal striatum MSNs when possible. The  $\text{Na}^+$  kinetics were obtained from dissociated dorsal striatum MSNs in the guinea pig (Ogata and Tatebayashi 1990). The fast A-type potassium channel (Kv4.2) data was obtained from slice dorsal striatum MSNs in rat (Tkatch et al. 2000). The slow A-type potassium channel (Kv1.2) data was obtained from dissociated and slice dorsal striatum MSNs in rat (Shen et al. 2004). The inwardly rectifying potassium channel (Kir) kinetics were extracted from the computational studies of Wolf et al. (2005) and Steephen and Manchanda (2009). The KDr channel was from Migliore et al. (1999) The BK channel (Berkefeld et al. 2006) and SK channel (Maylie et al. 2004) were activated by a specific pool of calcium from the N and R type calcium channels, but not the T or L type calcium channels (Wolf et al. 2005; Vilchis et al. 2000). L (Cav1.2 and Cav1.3), N, R, and T type voltage sensitive calcium channels are the same as Wolf et al. (2005) and were added to the soma, and dendritic shafts. L,R, and T-type channels were also added to spines (Carter and Sabatini 2004). MSNs of the dorsal

striatum display different characteristics from those of the ventral striatum (Hopf et al. 2010). Both hand tuning and the simulated annealing parameter optimization routine in Genesis were used to adjust channel maximal conductances (Table 3), and channel activation and inactivation time constants (Table 2, scaling factor). These parameters were adjusted to match spike frequency, spike width, and latency to first spike extracted from current clamp data obtained at 30-32°C from mouse dorsal striatum MSN (Figures 1B-D). The change in channel time constants of NaF, Kdr, and KaF (scale in Table 2) was required to produce the correct spike width as faster time constants produced spikes that were too narrow. In contrast, varying the maximal conductances by  $\pm 10\%$  did not significantly change spike width (data not shown).  $\Delta t$  for both experiments and the model MSN is defined as the time from pre-synaptic stimulation (stimulus artifact in the experimental case) to the peak of the AP.

### **Synaptic Channels**

AMPA and NMDAR channels were added using the “synchan” object in Genesis to all spines in the model. GABA channels were not added to this model, thus all simulations should be interpreted as occurring in the presence of GABA receptor antagonists. The default AMPA maximal conductance is 342 pS, which agrees with data from Carter and Sabatini (2004). Default NMDA maximal conductance was 940 pS to maintain the NMDA/AMPA ratio of 2.75/1 in cortico-striatal terminals (Ding et al. 2008). AMPARs have an activation time constant of 1.1 ms and an inactivation time constant of 5.75 ms (Götz et al. 1997; Wolf et al. 2005). NMDARs have an activation time constant 2.25ms (Chapman et al. 2003), but inactivation depends on subunit.

Magnesium sensitivity to the NMDAR was implemented by using the “Mg\_block” object in Genesis:

$$\frac{A}{A + [\text{Mg}^{2+}] * \exp\left(-\frac{V_m}{B}\right)}$$

In which, parameter B = 1/62, while parameter A depends on subunit (Table 4).

Specific GluN2-subunit containing NMDARs were modeled by adjusting the decay time constant, the maximal conductance, and the sensitivity to magnesium block according to published data (Monyer et al. 1994; Vicini et al. 1998). GluN2 subunits differ in open probability (Chen et al. 1999) and affinity for glutamate (Laurie and Seeburg 1994). These differences, though not modeled explicitly, contribute to the maximal conductance and the decay time which are taken into account in this model. Single decay time constants, averaged from the fast and slow time constants in Vicini et al. (Vicini et al. 1998), were used for each GluN2 subunit (Table 4). Maximal conductances were calculated from the slope of the magnesium-free data (Monyer et al. 1994) The ratio between the maximal conductance of GluN2A+B, C, and D was maintained, but the conductances were universally reduced such that the value for GluN2A + B (the predominate subunits in striatal MSNs) matched cortico-striatal NMDAR/AMPA ratios (Ding et al. 2008). Current-voltage curves for each subunit in

the presence of 1mM magnesium from Monyer et al. (1994) were matched by adjusting parameter “A” in this equation (Table 4, Figure 7).

### **Contributions**

Conceived of project: Rebekah C. Evans, Kim T. Blackwell

Wrote paper: Rebekah C. Evans, Kim T. Blackwell

Edited paper: Rebekah C. Evans, Kim T. Blackwell, Laurent Venance, Jeanette Hellgren Kotaleski

Made computational model: Rebekah C. Evans, Kai Du, Tom Sheehan

Ran Simulations: Rebekah C. Evans

Analyzed simulation data: Rebekah C. Evans, Kim T. Blackwell

Performed Experiments: Yihu Cui, Theresa Morera-Herreras

Analyzed experimental data: Laurent Venance, Yihu Cui, Theresa Morera-Herreras

Citation:

Evans RC, Morera-Herreras T, Cui Y, Du K, Sheehan T, Hellgren Kotaleski J, Venance L, Blackwell, KT. (2012) The Effects of NMDA Subunit Composition on Calcium Influx and Spike Timing-Dependent Plasticity in Striatal Medium Spiny Neurons. *PLoS Comput Biol* 8(4): e1002493

## **CHAPTER FOUR: DYNAMIC MODULATION OF SPIKE-TIMING DEPENDENT CALCIUM INFLUX DURING CORTICO-STRIATAL UPSTATES**

### **Abstract**

The striatum of the basal ganglia demonstrates distinctive upstate and downstate membrane potential oscillations during slow wave sleep and under anesthetics. The upstates generate calcium transients in the dendrites and the amplitude of these calcium transients depends strongly on the timing of the action potential (AP) within the upstate. Calcium is essential for synaptic plasticity in the striatum and these large calcium transients during the upstates may control which synapses undergo plastic changes. To investigate the mechanisms that underlie the relationship between calcium and AP timing, we have developed a realistic biophysical model of a medium spiny neuron (MSN). We have implemented sophisticated calcium dynamics including calcium diffusion, buffering, and pump extrusion which accurately replicates published data. Using this model, we found that either the slow inactivation of dendritic sodium channels (NaSI) or the calcium inactivation of voltage gated calcium channels (CDI) can cause high calcium corresponding to early APs and lower calcium corresponding to later APs. We find that only CDI can account for the experimental observation that sensitivity to AP timing is dependent on NMDA receptors. Additional simulations demonstrate a mechanism by which MSNs can dynamically modulate their sensitivity to AP timing, and show that sensitivity to specifically timed pre and post-synaptic pairings (as in STDP

protocols) is altered by the timing of the pairing within the upstate. These findings have implications for synaptic plasticity *in vivo* during sleep when the upstate-downstate pattern is prominent in the striatum.

## **Introduction**

Medium spiny neurons (MSNs) are the sole projection neurons of the striatum and plasticity changes in these neurons underlie motor learning (Yin et al. 2009). *In vivo*, the MSNs exhibit distinct membrane potential oscillations referred to as upstates and downstates. Although this upstate-downstate activity pattern was observed more than 30 years ago (Wilson and Groves 1981), its function is still unclear. This pattern of activity is displayed in anesthetized animals and occurs during slow wave sleep, but is much less prominent in the awake animal (Mahon et al. 2006). Because this activity pattern occurs most strongly when the animal is anesthetized or sleeping and consequently motionless, its main function is not likely the direct control of motor output. Rather it may be a means to consolidate and reinforce motor skill learning by controlling which specific synapses are strengthened during sleep (Stoetzner et al. 2010) while cells replay previous wakeful sequences (Ribeiro et al. 2004; Lansink et al. 2009).

Large dendritic calcium transients coincide with the cortico-striatal upstates (Kerr and Plenz 2002; 2004), and calcium elevations are necessary for striatal synaptic plasticity *in vitro* (Fino et al. 2010). Therefore, during the upstate the calcium elevation in the dendrite may dictate whether specific synapses are potentiated or depressed. The timing of the action potential (AP) within the upstate strongly determines the amplitude of the corresponding calcium elevation. APs early in the upstate coincide with higher

calcium peaks than APs late in the upstate, resulting in a non-linear, timing-dependent relationship (Kerr and Plenz 2004). However, the intracellular mechanisms responsible for this relationship and the consequences for synaptic plasticity during the upstate are as yet unknown.

*In vitro* experiments have shown that carefully timed pairings of pre and post-synaptic activity can result in spike timing dependent plasticity (STDP) (Fino et al. 2005; Pawlak and Kerr 2008), and computational models have demonstrated that calcium influx strongly predicts plasticity during these protocols (Evans et al. 2012). However, the noisy *in vivo* environment is very different from the quiet *in vitro* slice preparation. Specifically, a rigidly controlled single pairing of pre and post synaptic activity is not likely to occur *in vivo*. Instead, barrages of synaptic activity and an underlying upstate-downstate pattern characterize the *in vivo* situation. In this study, we investigate the calcium influx due to STDP pairings during these *in vivo* like upstates and discuss the consequences for synaptic plasticity.

Using a multi-channel, multi-compartmental biophysical model and a sophisticated model of calcium diffusion, buffering, and pump extrusion, we investigate two possible mechanisms which can control the relationship between calcium and AP timing during the upstate. In the first half of the paper, we determine that one mechanism is more likely, and confirm its plausibility with voltage clamp experiments. In the second half of the paper, we use the model to make several experimentally testable predictions. Specifically, we show that AP timing affects calcium binding to downstream targets

involved in plasticity, and demonstrate a mechanism by which MSNs could dynamically modulate their sensitivity to AP timing in response to neuromodulation.

## **Methods**

### **General MSN model.**

Using GENESIS simulation software, we developed a model MSN with realistic electrophysiological activity (Figure 12) and calcium dynamics (Figure 13) by modifying our previously published dorsal striatum MSN (Evans et al. 2012). The morphology is similar (Figure 12A), but the maximal dendritic length is reduced to 224 $\mu\text{m}$ , and the long tertiary branches slightly taper from 0.8 $\mu\text{m}$  to 0.7 $\mu\text{m}$  in diameter (Figure 12A). These changes are in accordance with reconstructions of MSNs from the NeuroMorpho.org neuronal reconstruction database (Halavi et al. 2008). For simplicity, this model does not contain dendritic spines except where noted for the STDP simulations.

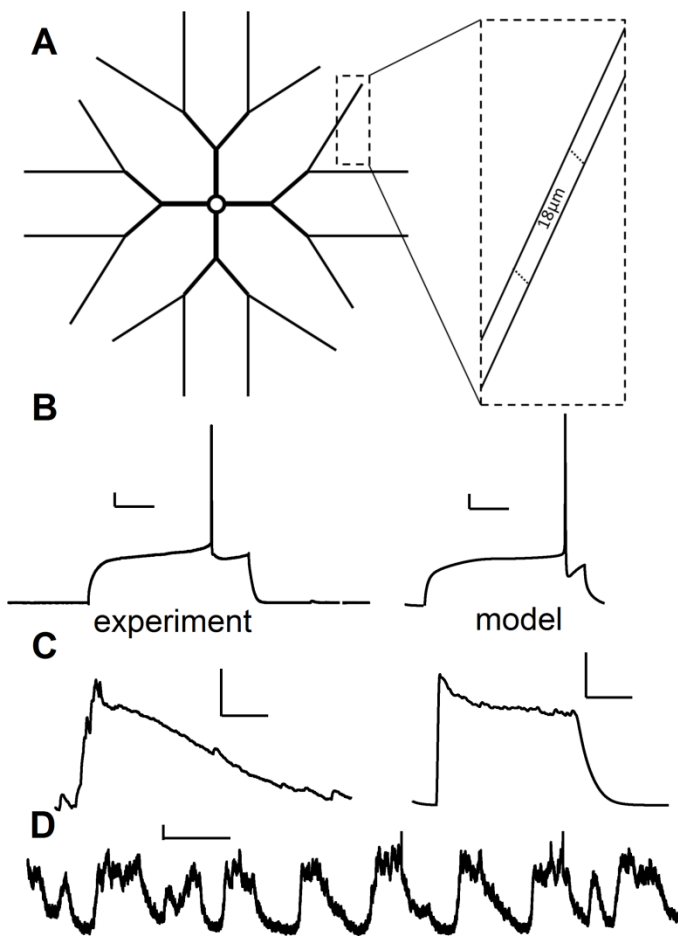


**Figure 12 Computational model comparison with electrophysiological data.**

**A.** Morphology of model MSN, not to scale. Soma is  $16\mu\text{m}$  in diameter, primary dendrites are  $12\mu\text{m}$  long, secondary dendrites are  $14\mu\text{m}$  long, and tertiary dendrites are divided into 11 continuous  $18\mu\text{m}$  long segments. **B.** Experimental and model voltage responses to somatic current injection of  $260\text{pA}$ . Both demonstrate long latency to first action potential. Scale bars vertical:  $10\text{mV}$ , horizontal:  $100\text{ms}$ . **C.** Experimental and model voltage traces showing synaptically evoked upstates. Scale bars vertical:  $10\text{mV}$ , horizontal:  $100\text{ms}$ . Experimental upstate is a spontaneous upstate recorded from organotypic triple co-culture (Blackwell and Plenz, *unpublished*). **D.** *In vivo* upstate traces show variability in upstate shape. Scale bars vertical:  $5\text{mV}$  horizontal:  $1\text{s}$ . Used with permission from John Reynolds.

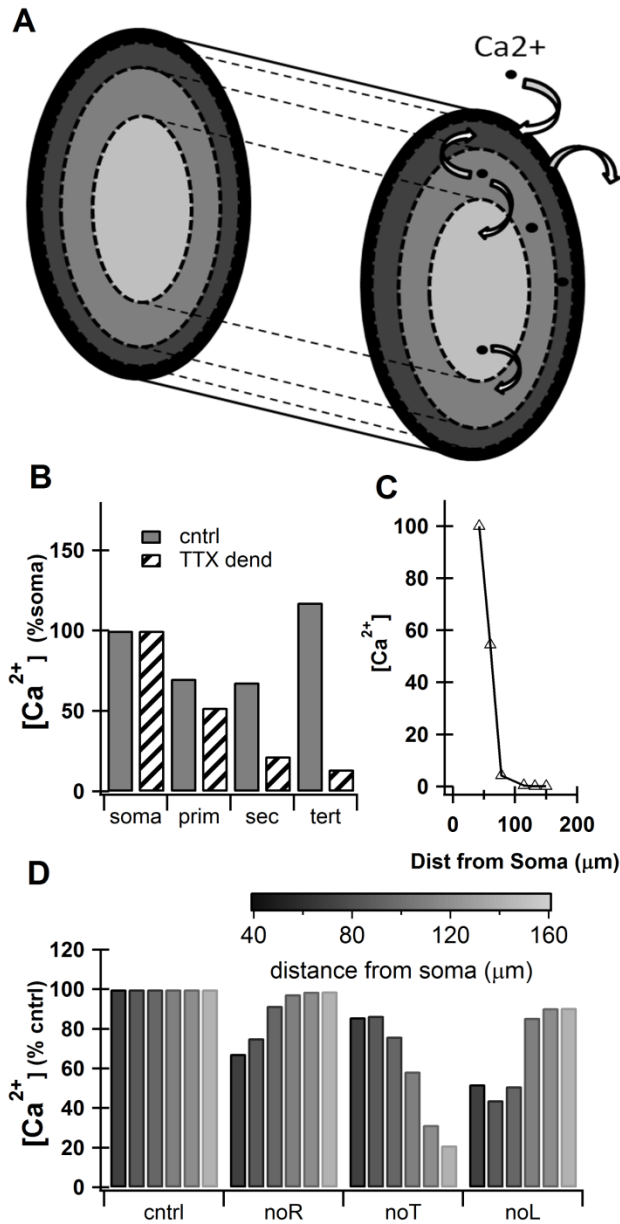


**Figure 13 Intrinsic calcium signaling in the model matches published data.**

A. Schematic drawing of dendritic segment showing diffusion of calcium between shells, extrusion of calcium via pumps, and influx of calcium via VGCCs. B. Model calcium signal (normalized to the signal seen at the soma) strongly responds to a single back propagating AP in proximal dendrites. When sodium channels are removed from the dendrites (TTX dend), calcium decreases with distance from the soma (Similar to Kerr and Plenz 2002 figure 7G). C. Model calcium signal (normalized to tertiary dendrite segment 1, 42μm from soma, in distal dendrites does not strongly respond to backpropagating AP (Similar to D1 neurons in Day et al. 2008 figure 1D). D. The contribution of VGCCs changes with distance from the soma even when the conductances are the same. The relative contribution of R and L type calcium channels is reduced in distal dendrites, while the relative contribution of T type calcium channels is increased (Contributions tuned to be qualitatively similar to Carter and Sabatini 2004 figure 2).

**Ionic channels.**

This model contains one fast sodium channel (Naf) (Ogata and Tatebayashi 1990) and four voltage-gated potassium channels: a fast potassium A current (Kaf, Kv4.2) (Tkatch et al. 2000), a slow potassium A current (Kas, Kv1.2) (Shen et al. 2004), a resistant persistent potassium current (Krp) (Nisenbaum and Wilson 1995), and an inwardly rectifying potassium current (Kir) (Stephen and Manchanda 2009). The model also contains two calcium activated potassium channels: the big conductance BK channel and the small conductance SK channel. All equations governing the kinetics of these channels are in Table 6 & Table 7. Intrinsic channel time constants in this model have been temperature corrected with a qfactor of 3 except Kaf and Naf which are adjusted by a qfactor of 1.5 and 2.5 respectively. BK and SK are not in the tables as they are the same as in our previous model (Evans et al. 2012). All channels are present in the soma and in the dendrites; however, the maximal conductances of the Naf, Kaf, and Kas channels were adjusted differentially in the soma and dendrites during model tuning (Table 8). Under the sodium slow inactivation (NaSI) conditions, an additional slow inactivation term is added to the dendritic sodium channels (Ogata and Tatebayashi 1990; Migliore 1996).

**Table 6 Steady state equations.**

Tau values in these tables are not temperature corrected (see methods for temperature correction values). Equations: sigmoid = rate/(1 + (exp ((V- vhalf)/slope))); exp = (rate)\*(exp((V)/slope))

Channel Name	mh form	Steady State	tau	$\alpha$ or $\beta$ equation	Vhalf (mV)	Slope (mV)	Rate
<b>Naf</b>	m <sup>3</sup>	sigmoid	<i>see table 2</i>	-	-25	-10	1
	h	sigmoid	<i>see table 2</i>	-	-60	6	1
<b>Kir</b>	m	$\alpha/(\alpha+\beta)$	$(1e^{-3}/(\alpha+\beta))*2$	$\alpha$ (exp)	-	-11	1e-5
				$\beta$ (sigmoid)	30	-50	1.2
<b>Kaf</b>	m <sup>2</sup>	$\alpha/(\alpha+\beta)$	$1e^{-3}/(\alpha+\beta)$	$\alpha$ (sigmoid)	-18	-13	1.8
				$\beta$ (sigmoid)	2	11	0.45
	h	$\alpha/(\alpha+\beta)$	$1e^{-3}/(\alpha+\beta)$	$\alpha$ (sigmoid)	-121	22	0.105
				$\beta$ (sigmoid)	-55	-11	0.065
<b>Kas</b>	m <sup>2</sup>	$\alpha/(\alpha+\beta)$	$1/(\alpha+\beta)$	$\alpha$ (sigmoid)	54	-22	0.25
				$\beta$ (sigmoid)	-100	35	0.05
	h	$0.8+(\alpha/(\alpha+\beta))*0.2$	$1/(\alpha+\beta)$	$\alpha$ (sigmoid)	-95	16	2.5
				$\beta$ (sigmoid)	50	-70	2
<b>Krp</b>	m <sup>2</sup>	$\alpha/(\alpha+\beta)$	$1/(\alpha+\beta)$	$\alpha$ (exp)	-	24	16
				$\beta$ (exp)	-	-45	2.4
	h	$0.87+(\alpha/(\alpha+\beta))*0.13$	$1/(\alpha+\beta)$	$\alpha$ (exp)	-	-100	0.01
				$\beta$ (exp)	-	18	0.4
<b>CaL1.2</b>	m	sigmoid	<i>see table 2</i>	-	-8.9	-6.7	1
	h	$0.17+(\text{sigmoid})*0.83$	44.3ms	-	-55	8	1
<b>CaL1.3</b>	m	sigmoid	<i>see table 2</i>	-	-40	-5	1
	h	sigmoid	44.3ms	-	-37	5	1
<b>CaN</b>	m <sup>2</sup>	sigmoid	<i>see table 2</i>	-	-3	-8	1
	h	$0.21+(\text{sigmoid})*0.79$	70ms	-	-74.8	6.5	1
<b>CaR</b>	m <sup>3</sup>	sigmoid	5.1ms	-	-29	-9.6	1
	h	sigmoid	<i>see table 2</i>	-	-33.3	17	1
<b>CaT</b>	m <sup>3</sup>	sigmoid	<i>see table 2</i>	-	-63	-8	1
	h	sigmoid	<i>see table 2</i>	-	-84	5	1

**Table 7 Tau equations for inward currents.**

Tau values in this table have not been temperature corrected (see methods for temperature correction values).

Equations: Eqn1 =  $0.1 + (\text{rate}/(1 + (\exp((V - \text{vhalf})/\text{slope}))))^2$ ; Eqn2 =  $0.2754 + (\text{rate}/(1 + (\exp((V - \text{vhalf})/\text{slope}))))$ ; linoid :  $(\text{rate}*(V+\text{vhalf})/((\exp(V+\text{vhalf})/\text{slope})-1))$ ; exp:  $(\text{rate}*\exp(V/\text{slope}))$ . \*Rate units are ms<sup>-1</sup> for linoid and exp, and ms for eqn 1 and 2. § Channels undergoing CDI with the equation:  $(0.0005^3/(0.0005^3+[Ca^{2+}]^3))^{100}$  and a time constant of 47.3ms, only when CDI is turned on.

Channel Name	mh form	tau	$\alpha$ or $\beta$ equation	Rate*	Slope (mV)	Vhalf (mV)
--------------	---------	-----	------------------------------	-------	------------	------------

<b>Naf</b>	m <sup>3</sup>	Eqn1	-	1.45	8	-62
	h	Eqn2	-	1.2	3	-42
<b>CaL1.2</b> <sup>§</sup>	m	1/( $\alpha+\beta$ )	$\alpha$ (linoid)	39.8e3	8.124e-3	9.005
			$\beta$ (exp)	0.99e3	31.4e-3	-
<b>CaL1.3</b> <sup>§</sup>	m	1/( $\alpha+\beta$ )	$\alpha$ (linoid)	39.8e3	67.24e-3	15.005
			$\beta$ (exp)	3.5e3	31.4e-3	-
<b>CaN</b> <sup>§</sup>	m <sup>2</sup>	1/( $\alpha+\beta$ )	$\alpha$ (linoid)	39.8e3	17.19e-3	15.22
			$\beta$ (exp)	384.2	23.82e-3	-
<b>CaR</b> <sup>§</sup>	h	(1/( $\alpha+\beta$ ))+20	$\alpha$ (linoid)	10e6	94.5e-3	5.12
			$\beta$ (exp)	84.2	13e-3	-
<b>CaT</b>	m <sup>3</sup>	(1/( $\alpha+\beta$ ))+2.2	$\alpha$ (linoid)	14.552e3	84.5e-3	7.12
			$\beta$ (exp)	4.9842e3	13e-3	-
	h	(1/( $\alpha+\beta$ ))+100	$\alpha$ (linoid)	2.652e3	94.5e-3	5.12
			$\beta$ (exp)	684.2	13e-3	-

**Table 8 Maximal conductance and permeability for ionic channels.**

Gbar=maximal conductance S/M<sup>2</sup>=Siemens per meter squared; Pbar = maximal calcium permeability cm/s=centimeters per second. Prox dend = proximal dendrites (up to 42 $\mu$ m from the soma); mid dend = middle dendrites (42 $\mu$ m-60 $\mu$ m from soma); dist dend = distal dendrites (60 $\mu$ m -224 $\mu$ m from soma).

<b>Gbar (S/M<sup>2</sup>)</b>	<b>soma</b>	<b>prox dend</b>	<b>mid dend</b>	<b>dist dend</b>
<b>NaF</b>	50,000	6,000	6,000	2,000
<b>Kir</b>	11	11	11	11
<b>KaF</b>	300	550	550	550
<b>KaS</b>	200	22	22	22
<b>Krp</b>	14	14	14	14
<b>SK</b>	1	1	1	1
<b>BK</b>	10	10	10	10
<b>Pbar (cm/s)</b>				
<b>CaL1.2</b>	6e-7	1e-7	1e-7	1e-7
<b>CaL1.3</b>	3e-7	0.5e-8	0.5e-8	0.5e-8
<b>CaN</b>	12e-7	0	0	0
<b>CaR</b>	8e-7	10e-7	10e-7	10e-7
<b>CaT</b>	0	0	8e-8	8e-8

**Calcium channels.**

Five voltage gated calcium channels (VGCCs) are included in this model. High voltage activated channels include CaR (Foehring et al. 2000; Brevi et al. 2001), CaN (Cav2.2) (Bargas et al. 1994; Kasai and Neher 1992; McNaughton and Randall 1997), and CaL1.2 (Cav1.2) (Bargas et al. 1994; Kasai and Neher 1992; Tuckwell 2012; Wolf et al. 2005). Low voltage activated channels include CaT (Cav3.3,  $\alpha 1G$ ) (McRory et al. 2001) and CaL1.3 (Cav1.3) (Tuckwell 2012; Wolf et al. 2005). Calcium channel kinetics and equations are in Table 6 & Table 7. For each calcium channel, the Goldman-Hodgkin-Katz (GHK) formula is applied to accurately compute the driving potential for these channels. Under the calcium dependent inactivation (CDI) conditions, an additional calcium-dependent inactivation term is added to the R-type, N-type, and both L-type calcium channels (Liang et al. 2003). The maximal permeabilities of these VGCCs were adjusted in the soma to produce calcium elevations comparable in size and shape to published experiments (Kerr and Plenz 2002). Similarly, calcium permeabilities in the dendrites were adjusted to match their contributions during back-propagating action potentials (Carter and Sabatini 2004) (Figure 13). Permeabilities are shown in Table 8.

**Calcium diffusion, buffers, and pumps.**

Calcium dynamics were implemented using the calcium *difshell* object in GENESIS, which integrates changes to calcium concentration produced by calcium influx, buffers, pumps and diffusion. A thin (0.1 $\mu\text{m}$ ) submembrane shell was created as the outermost shell and concentric shells progressively doubling in thickness were added within the compartment (Figure 13A). One dimensional calcium diffusion between shells occurred at a rate of 200 $\mu\text{m}^2/\text{sec}$  (Allbritton et al. 1992). Calcium extrusion was achieved

by the addition of a Michaelis-Menten pump with  $k_m=0.3e-3mM$ , and  $K_{cat}=85pmol/(cm^2/s)$  in the soma and  $12pmol/(cm^2/s)$  in the dendrites. The endogenous calcium buffers calbindin and calmodulin (both N and C terminal binding site) were included with concentrations and kinetics taken from published models (Kim et al. 2010; Oliveira et al. 2012) (Table 9).

**Table 9 Calcium buffer parameters.**

CaMN= calmodulin N terminal binding site, CaMC= calmodulin C terminal binding site. Conc: concentration; Diff: diffusion constant.

	<b>Conc (<math>\mu M</math>)</b>	<b>Kf (<math>/\mu M/s</math>)</b>	<b>Kb (/s)</b>	<b>Diff (<math>(m^2)/s</math>)</b>
<b>CaMN</b>	15	100	1000	11e-12
<b>CaMC</b>	15	6	9.1	11e-12
<b>Calbindin</b>	80	28	19.6	0

### **Synaptic channels.**

AMPA, NMDA, and GABA receptors are distributed along the dendrites. For simplicity, there is one excitatory synapse (containing AMPA and NMDA) and one inhibitory (GABA) synapse per isopotential compartment. The maximal conductances and time constants are summarized in Table 10.

**Table 10 conductances and time constants for synaptic channels.**

Gbar is maximal conductance. Time constants have already been temperature corrected by a qfactor of 2.  $\tau_1$ = activation time constant;  $\tau_2$ =inactivation time constant.

	<b>Gbar (pS)</b>	<b><math>\tau_1</math> (ms)</b>	<b><math>\tau_2</math> (ms)</b>
<b>NMDA</b>	470	2.2312	25
<b>AMPA</b>	171	1.1	5.75
<b>GABA</b>	900	0.25	3.75

All synaptic channels use the *facsynchan* object in GENESIS, which uses the equation below to calculate the conductance of the channel from the activation and inactivation time constants ( $\tau_1$  and  $\tau_2$  respectively), time  $t$  relative to the action potential, and the maximal conductance ( $g_{\max}$ ).  $K$  is a normalization constant which is calculated from the time constants and allows  $G_{\text{syn}}$  to reach a peak value of  $g_{\max}$ .

$$G_{\text{syn}}(t) = (K * wt * g_{\max} / (\tau_1 - \tau_2))(e^{-\frac{t}{\tau_1}} - e^{-\frac{t}{\tau_2}})$$

$wt$  = synaptic weight which depends on short term facilitation or depression of these synapses.

$$wt = wt_0 * \frac{1}{1 + depr}$$

where  $wt_0 = 1$ . For NMDA and GABA channels,  $depr=0$ . AMPA receptor desensitization, known to occur in the striatum (Akopian and Walsh 2007; Carter et al.

2007), is simulated with a time dependent *depr* value. Each time an AMPA synapse is activated *depr* is incremented by 1.0, and the value of *depr* decays with a time constant of 100ms. NMDA receptors are modulated by the addition of a magnesium block object, where B=99 and A=18.

$$\frac{A}{A + [Mg^{2+}] * \exp(-Vm * B)}$$

Extracellular magnesium concentration is set to 1.4 mM (Kerr and Plenz 2002; 2004). These parameters closely match, but slightly accentuate the magnesium sensitivity seen in (Monyer et al. 1994). Excitatory inputs activate both an NMDA and an AMPA component with an NMDA/AMPA ratio of 2.75/1 (Ding et al. 2008), except in the ‘no NMDA’ condition where the NMDA channel was removed. The fraction of the NMDA receptor current carried by calcium was set to 10% (Wolf et al. 2005), and the AMPA receptors were not calcium permeable. A GHK object was employed to calculate the driving potential of the calcium current through the NMDA receptor independently of the driving potential of the total NMDA current. An empirically determined multiplicative factor of 35e-9 was needed convert the conductance output of the magnesium block object to the permeability required by the GHK object.

**Synaptic inputs and spike timing.**

Upstates were generated using excitatory and inhibitory Poisson input trains of 300ms duration as input. Inhibitory input frequencies were set to 70Hz and these trains were completely independent of excitatory inputs. A variety of excitatory input patterns were simulated: A flat input of 40Hz and a series of graded inputs at different strengths (see Figure 14 and Table 11). Unless otherwise specified, gradient 'G3' was used for the upstate simulations. APs were evoked at specific times within the upstate by a 5ms 800pA current injection into the soma. AP timing was measured from the beginning of the upstate to the beginning of the 5ms depolarization. The actual peak of the AP varied by <2ms, and our previous work has shown that spike variability on this scale does not affect calcium results (Evans et al. 2012). During the STDP protocols, one segment of dendrite 44um from the soma was given a single input at positive or negative  $\Delta t$  from the AP with no other synaptic inputs.

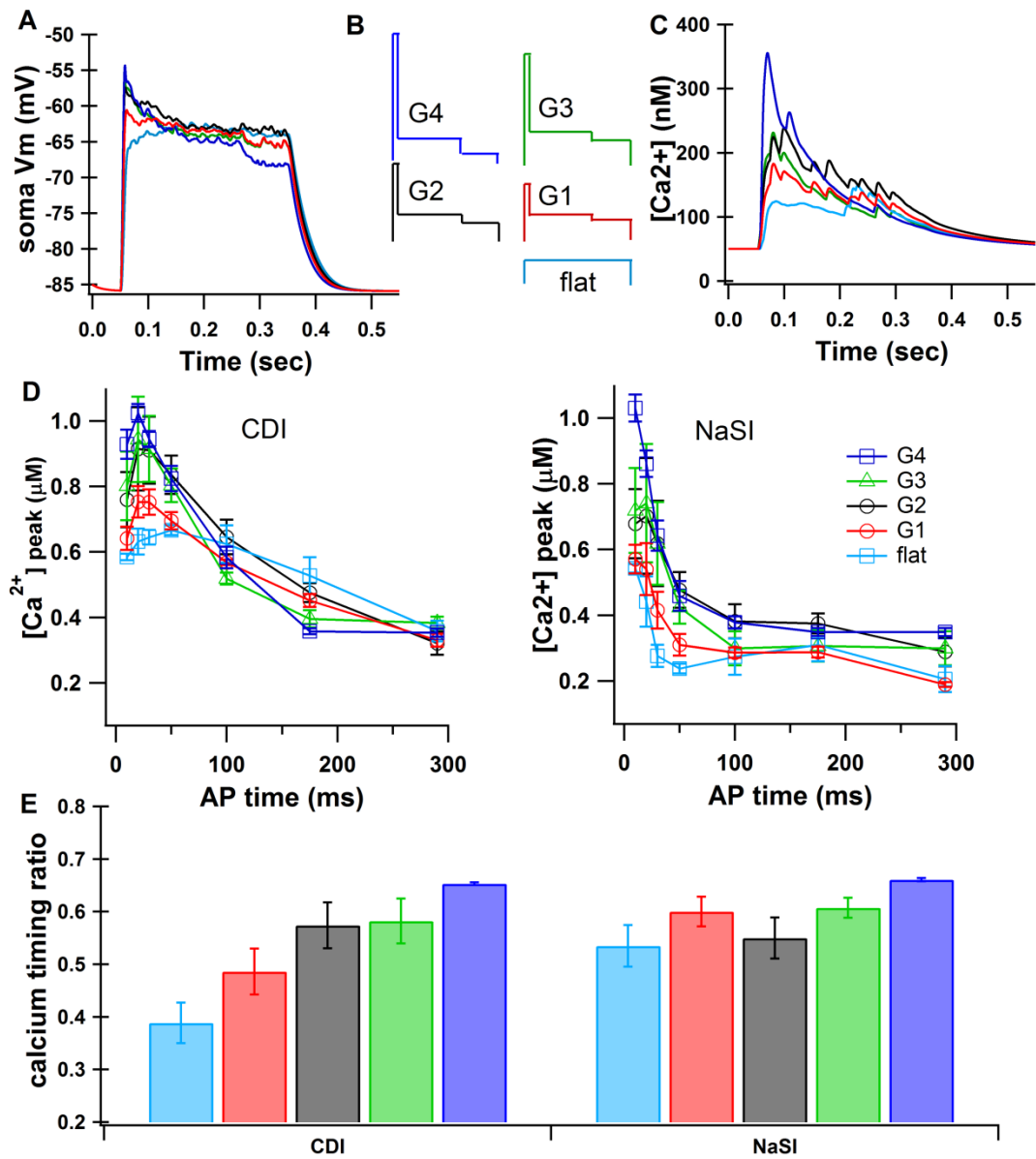


**Figure 14 Input pattern affects calcium dependence on AP timing.**

**A.** Sub-threshold upstates of varying gradient patterns as measured at the soma. **B.** Schematic of input patterns (not to scale, see appendix table 6) **C.** Example traces of calcium in tertiary dendrites during each input pattern (no AP). **D.** Average of 4 tertiary dendrites as a function of AP timing for each input pattern. **E.** Calcium timing ratio for each input pattern, averaged over 4 tertiary dendrites for one random seed. All error bars  $\pm$ SEM.

**Table 11 Input gradients used to create upstates.**

Input frequencies for different input shapes. Input G3 was used for simulations unless otherwise specified. (see also Figure 14)

<b>Input Name</b>	<b>Frequency for first10ms (Hz)</b>	<b>Frequency for middle 200ms (Hz)</b>	<b>Frequency for last 90ms (Hz)</b>
<b>Flat</b>	40	40	40
<b>Gradient 1 (G1)</b>	200	40	10
<b>Gradient 2 (G2)</b>	400	50	20
<b>Gradient 3 (G3)</b>	500	30	10
<b>Gradient 4 (G4)</b>	600	20	0

### **Voltage clamp of calcium currents.**

All animal handling and procedures were in accordance with the National Institutes of Health animal welfare guidelines and were approved by the George Mason University institutional animal care and use committee (IACUC). C57BL/6 male and female mice (Charles River, p13-21) were anesthetized with isoflurane and euthanized. Every effort was made to minimize anxiety and pain. Brains were extracted and cut 350 $\mu$ m thick using a vibratome (Leica VT 1000S) in ice cold sucrose slicing solution (in mM: KCL 2.8, Dextrose 10, NaHCO<sub>3</sub> 26.2, NaH<sub>2</sub>PO<sub>4</sub> 1.25, CaCl<sub>2</sub> 0.5, Mg<sub>2</sub>SO<sub>4</sub> 7, Sucrose 210). Slices were immediately placed in an incubation chamber containing artificial cerebrospinal fluid (aCSF) (in mM: NaCl 126, NaH<sub>2</sub>PO<sub>4</sub> 1.25, KCl 2.8, CaCl<sub>2</sub>, Mg<sub>2</sub>SO<sub>4</sub> 1, NaHCO<sub>3</sub> 26.2, Dextrose 11) for 30 minutes at 33°C, then removed to room temperature (22-24°C) for at least 90 more minutes before use. Recording aCSF was modified by replacing Mg<sub>2</sub>SO<sub>4</sub> with Mg<sub>2</sub>Cl and including either 2mM Ca<sub>2</sub>Cl or 2mM Ba<sub>2</sub>Cl. TTX (0.5 $\mu$ M) and 4-AP (4mM) were added to block sodium and potassium channels respectively. Slices were individually placed in a submersion chamber (ALA scientific) and cells were visualized using differential interference contrast imaging

(Zeiss Axioskop2 FS plus). Pipettes (3-5M $\Omega$ ) were pulled from borosilicate glass on a laser pipette puller (Sutter P-2000), coated with candle wax (to reduce pipette capacitance), and fire-polished (Narishige MF-830). Pipettes were filled with a cesium based internal solution (in mM Cs-gluconate 85, Cs3-citrate 10, KCl 1, NaCl 10, HEPES 10, EGTA 1.1, CaCl<sub>2</sub> 0.1, MgCl<sub>2</sub> 0.25, TEA-Cl 15, Mg-ATP 3.56, Na-GTP 0.38) pH 7.26 (Rankovic et al. 2011). Voltage clamp recordings were obtained on the HEKA EPC-10 and sampled at 20KHz. Data were acquired in Patchmaster (HEKA Elektronik). Analogue 3-pole (10kHz) and 4-pole (2.9kHz) Bessel filters were applied. Series resistance (4-15M $\Omega$ ) and capacitance were compensated.

### **Simulation and analysis.**

All simulations used a time step of 5  $\mu$ s and were repeated using three random number seeds unless otherwise specified. Four dendrites from each simulation were averaged together to estimate the calcium for a single simulation. For the STDP simulation, calcium from the dendrite receiving only the single timed glutamatergic input was measured from each random number seed. The strength of the dependence of calcium on AP timing (the “calcium timing ratio”) was evaluated by averaging the two latest AP conditions (175ms and 290ms) and normalizing them by the highest calcium elevation of that condition (usually 10, 20 or 30ms). For all these cases graphs report mean and standard deviation across the three random number seeds. Data shown in figures 3-5 are run for one random seed and the data are presented as mean $\pm$ SEM across four measured dendritic segments. Statistical significance was evaluated using the SAS

procedure GLM, and considered significant for  $p < 0.01$ . In the case of multiple comparisons, a Bonferroni correction was applied. This model is available on ModelDB.

## **Results**

### **Part 1: Mechanisms underlying the calcium sensitivity to AP timing during the upstate.**

Here we validate our model against published data and describe two mechanisms that may account for the relationship between calcium and AP timing during cortico-striatal upstates. We confirm that both mechanisms make calcium elevation sensitive to AP timing, and test how these manipulations interact with distance from the soma and the presence of NMDA receptors.

### **Intrinsic physiology and calcium dynamics in the MSN model match published data**

We developed a multi-channel, multi-compartmental biophysical model of a MSN, tuned to match electrophysiological characteristics of whole cell current clamp recordings in slice (Figure 12A&B and see methods), and upstate characteristics (figures Figure 12C&D) such as fast depolarization into the upstate, 200-500 ms plateau, and slower repolarization back to the downstate. To accurately model the calcium dynamics in response to electrical activity, this model included a shell-based representation of calcium pools to simulate diffusion, calcium buffers (Table 9), and submembrane pumps. The intrinsic calcium activity of this MSN was tuned to match published data showing sodium channel-dependent back-propagation of APs into the proximal dendrites (Kerr and Plenz 2002) (Figure 13B) and strong AP decay in distal dendrites (Day et al. 2008) (Figure 13C). Dendritic VGCC channel permeabilities were adjusted to qualitatively match their contribution to dendritic calcium elevations during single back-propagating

APs (Carter and Sabatini 2004) (Figure 13D). Despite the maximal permeabilities being consistent throughout the distal dendrites (Table 8), the contribution of the T-type calcium channels increased with distance from the soma and the contributions of the L and R type calcium channels decreased (Figure 13D). Though the contribution of the T-type calcium channel in our model at 44 $\mu$ m from the soma is not quite as strong as shown in Carter and Sabatini (2004), we consider these results to be a reasonably good match because Carter and Sabatini were sampling a range of distances from the soma. We used this tuned model for all subsequent upstate simulations without any further adjustment to the intrinsic calcium.

### **Two mechanisms can account for the relationship between calcium and AP timing**

Calcium imaging studies have shown that APs evoked early in the upstate correspond to higher dendritic calcium elevations than APs evoked late in the upstate (Kerr and Plenz 2004). We hypothesize that two main mechanisms could cause this relationship between calcium and AP timing. First, if the AP back propagated strongly when it occurred early in the upstate, but weakly when it occurred late in the upstate, the calcium peaks would also be strong early and weak late. Second, even if the AP back propagated with equal strength early and late in the upstate, the calcium response could desensitize during the upstate to show the same strong early, weak late calcium pattern. Because the dendritic voltage during upstates has not been recorded, it is not known if the AP back propagates differently early and late in the upstate. Therefore we test both configurations in the computational model to see how well each matches published data.

We simulated the calcium in response to a range of AP times during an upstate for two model variations. Upstates are simulated in the model MSN using randomly generated Poisson trains of excitatory and inhibitory input. Using the same random seed to generate the pattern of input, the exact same subthreshold upstate could be repeated with several different AP timings. Each upstate was repeated with a somatic current injection evoking an AP delayed 10, 20, 30, 50, 100, 175, or 290 ms from upstate onset.

First, a slow inactivation component, which has been measured in striatal sodium channels (Ogata and Tatebayashi 1990) was added to dendritic sodium channels (Migliore 1996). This NaSI condition indeed caused the AP to back propagate more strongly early in the upstate than late (Figure 15A, top panel), and the corresponding calcium elevations varied with AP timing during the upstate (Figure 15A, bottom panel). Secondly, calcium dependent inactivation (CDI, see Table 7 for equation) of voltage gated calcium channels (VGCCs) (Liang et al. 2003) was added to L, N, and R type calcium channels in our model. When applied to the model, the CDI condition resulted in strong electrical back propagation of the AP both early and late in the upstate (figure 3B, top panel), but the calcium elevation still varied with AP timing (Figure 15B, bottom panel). These two conditions, CDI and NaSI, resulted in APs that were indistinguishable at the soma in size and shape (Figure 15C). If neither manipulation was applied, the relationship between calcium and AP timing was very weak (Figure 15D), and if both were applied simultaneously, the results were not different from the NaSI condition alone (data not shown).

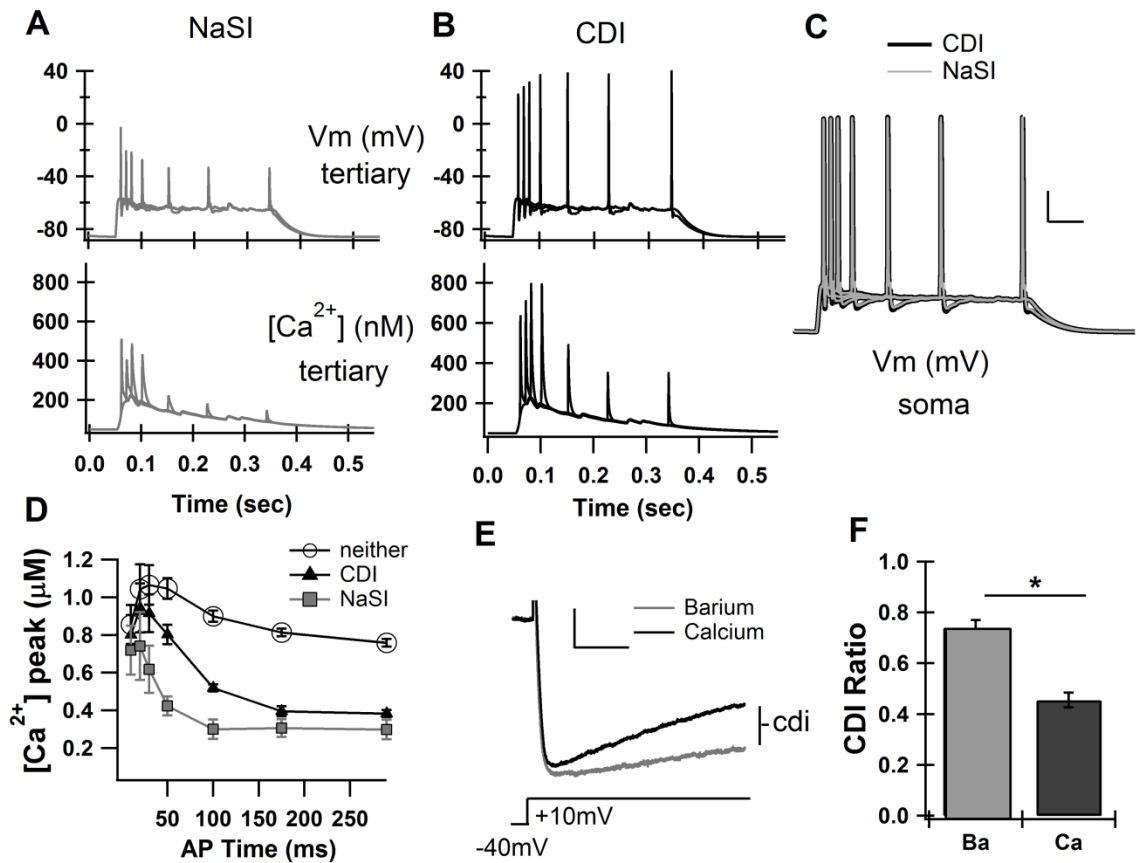


**Figure 15 Two basic mechanisms can account for the relationship between calcium elevation and AP timing during the upstate: reduced AP backpropagation (NaSI) or reduced calcium response (CDI).**

**A.** Reducing the back propagation of the APs through the implementation of NaSI causes a timing dependent reduction in the tertiary dendrite depolarization (top panel) and calcium response (bottom panel). **B.** Reducing the calcium response to depolarization through the implementation of CDI does not cause a reduction in the depolarization of the tertiary dendrite (top panel), but does cause a timing dependent reduction of the calcium response (bottom panel). **C.** APs were elicited at specific times by short (5ms) somatic depolarizations during the synaptically-induced upstate. There was very little difference in the shape of the upstate between the NaSI mechanism (gray) and the CDI mechanism (black). Scale bars vertical: 20mV horizontal: 50ms **D.** Average over 4 tertiary dendrites as a function of AP timing. **E.** Example traces showing CDI in high voltage activated calcium currents from a voltage clamped striatal neuron. Scale bars are vertical: 100pA. horizontal 50ms. **F.** Summary averaged CDI ratio (degree of reduction by end of 200ms) for all cells (n=5). \* =  $p < 0.00001$ , paired T-test.

To confirm that high voltage activated (HVA) channels actually undergo CDI in the striatum, we voltage clamped HVA calcium currents (by holding at -40mV and stepping to +10mV) and repeated measurements using barium (which causes minimal

CDI) and calcium (which causes strong CDI). The ratio of the decayed current (sampled after 180ms) to the peak current (sampled within first 50 ms) was taken as the CDI ratio. In all striatal cells recorded (n=5), the CDI ratio was much stronger in calcium than in barium ( $p < 0.00001$ , paired T-test) (Figure 15E&F).

An additional mechanism could theoretically account for a decrease in calcium elevation late in the upstate. An *increase* in buffer capacity and/or pump capacity during the upstate could increase the rate of calcium removal and thus decrease the free calcium. Changes in buffer capacity due to protein synthesis are unlikely at the temporal scales being investigated. One report of a changes in pump capacity actually demonstrates an activity dependent *decrease* in the sodium calcium exchanger (Scheuss et al. 2006). Because an activity dependent decrease in pump activity would result in *more* calcium late in the upstates, this mechanism is unlikely to contribute to the decrease in calcium elevation observed late in the upstate (Kerr and Plenz 2004). Furthermore, simulations which evaluate the effect of changing pump capacity reveal an insignificant effect on calcium timing ratio for both CDI and NaSI conditions (Figure 16).

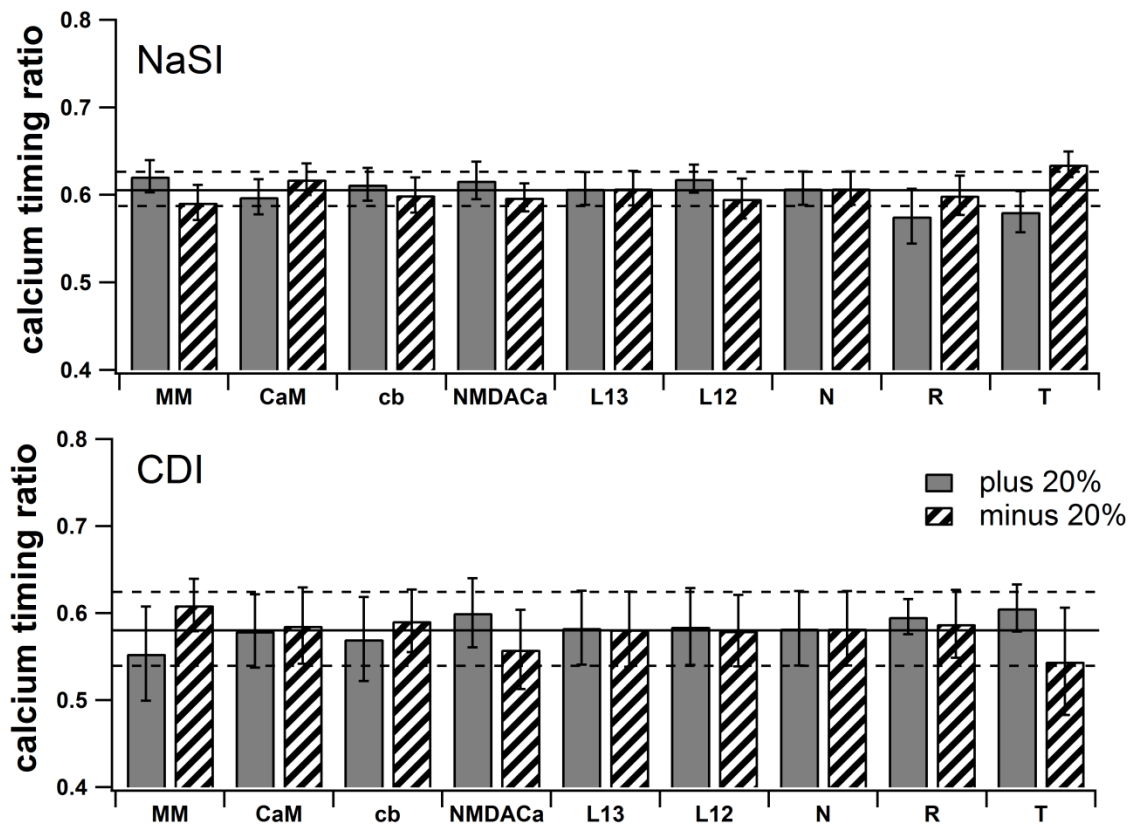


**Figure 16 Robustness tests.**

Changes in calcium parameters  $\pm 20\%$  does not significantly change the main effect of AP timing dependent calcium concentration for either the NaSI condition (top) or the CDI condition (bottom). MM=Michaelis Menten pump (Kcat), CaM= calmodulin (both N and C site), cb=calbindin, NMDACa=fraction of calcium through NMDA receptor, L13=L-type calcium channel Cav1.3, L12=L-type calcium channel Cav1.2, N=N-type calcium channel, R=R type calcium channel, T=T-type calcium channel. All error bars  $\pm$ SEM. Solid black line is mean for control condition and dotted black lines are  $\pm$ SEM for control condition.

In addition to changes in pump capacity, we evaluated the robustness of our computational model to other parameter variations (Figure 16). We systematically varied each parameter directly relating to calcium (buffers, pumps, NMDA calcium and each VGCC) by  $\pm 20\%$  and compared the calcium relationship with AP timing for each condition to the controls. None of these manipulations significantly altered the relationship between calcium and AP timing in either CDI ( $F(18, 75) = 0.15, p > 0.9$ ) or

NaSI ( $F(18, 75) = 0.49, p > 0.9$ ) (averaged over four dendrites for one random seed).

These tests confirm that our main effect is robust to variation in calcium influx, buffering, and pump extrusion.

**The calcium-AP relationship depends on input shape and distance from the soma.**

The strength of the relationship between calcium elevation and AP timing is modulated by the shape of the cortical input creating the upstate. We simulated a range of input gradients, (Figure 14A&B) and the strength of the calcium dependence on AP timing varied with the strength of the gradient (Figure 14D&E). While both the NaSI and CDI conditions showed a dependence on input steepness, the effect was stronger for CDI (calcium timing ratio =  $0.59 \pm 0.0008$  G3,  $0.35 \pm 0.01$  flat;  $p < 0.0001$ ), than for NaSI (calcium timing ratio =  $0.57 \pm 0.04$  G3,  $0.54 \pm 0.07$  flat;  $p > 0.9$ ). This result leaves open the possibility that synaptic input pattern alone is sufficient for AP timing effects on calcium. To test this we repeated simulations using gradient G3 in a model with neither CDI nor NaSI. Without either of these mechanisms, the calcium dependence on AP timing was essentially absent (Figure 15D). Therefore, while the input gradient *contributes* to the calcium dependence on AP timing, it is not sufficient to *generate* it. Because the simulations fit published data more accurately when the synaptic inputs were weighted toward the beginning of the upstate, we used gradient G3 as the upstate-generating input, unless otherwise specified.

Calcium imaging in organotypic co-cultures reveals that the calcium elevation due to the upstate and the relationship between calcium and AP timing increases with distance from the soma (Kerr and Plenz 2004). To test whether both CDI and NaSI show

this increase in the calcium AP timing relationship, the calcium signal is recorded at progressively more distal dendrites during upstate simulations (Figure 17A). Both CDI and NaSI show an increase in the strength of the calcium dependence on AP timing (calcium timing ratio) between primary, secondary, and tertiary branches (Figure 17B&C insets). Therefore, in this case, both conditions equally match the published data.

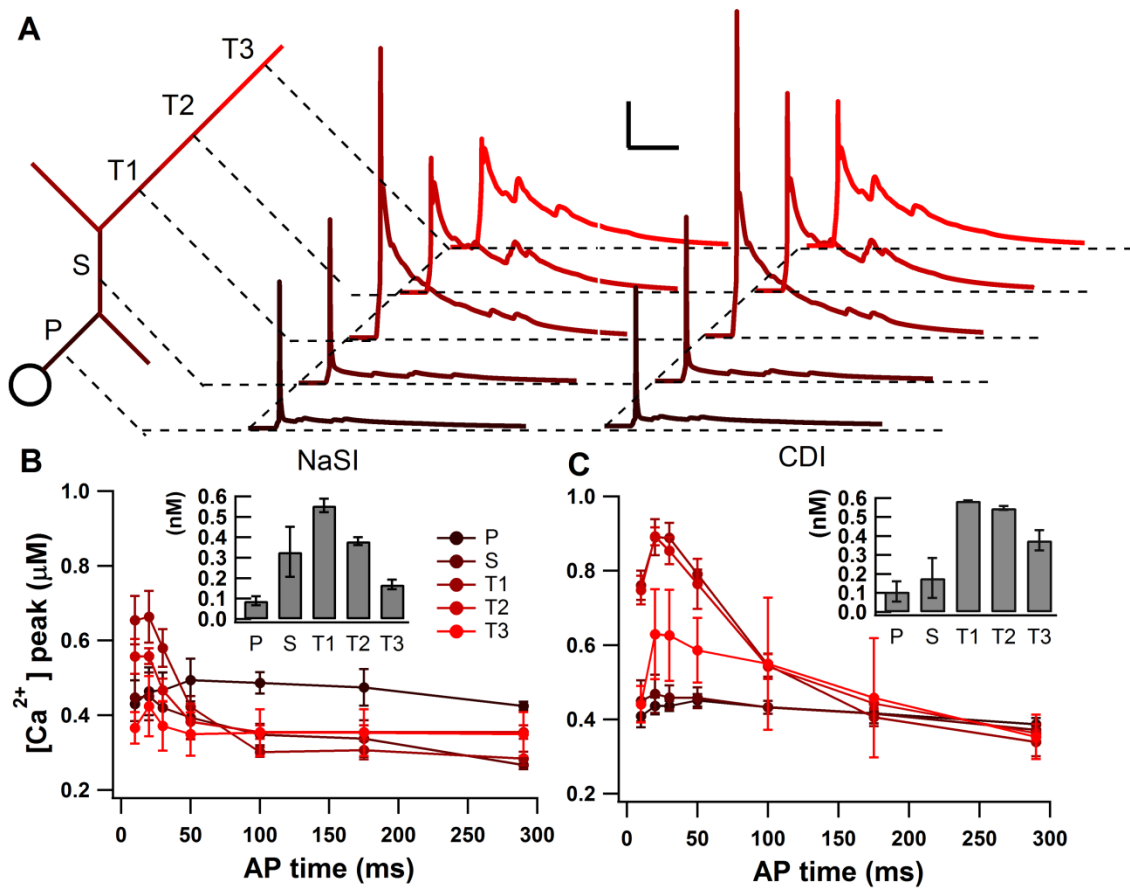


**Figure 17 Distance from soma affects calcium dependence on AP timing.**

A. Morphology (not to scale) of one dendritic branch color-coded dark to light for increasing distance from soma. Example calcium traces for each dendritic segment, primary (P), secondary (S), tertiary1 (T1), tertiary2 (T2), and

tertiary3 (T3) for both NaSI and CDI. Scale bars are vertical: 0.1  $\mu$ M, horizontal: 100ms. **B.** Calcium dependence on AP timing for NaSI condition is most prominent at the proximal tertiary dendritic segment (T1). Inset: bar graph showing the calcium timing ratio between the calcium peak for early (highest point) and late (average of two last points) APs for each dendritic segment. All error bars are  $\pm$  SD. **C.** Same as B, but for CDI condition.

Because the organotypic co-culture study did not record the calcium signals of distal dendrites (Kerr and Plenz 2004), and we have previously shown that the effect of the back-propagating AP on calcium influx is attenuated in distal dendrites (Evans et al. 2012), we tested the relationship between calcium and AP timing distally. Figure 17 shows that distally the relationship between calcium and AP timing *decreases* with distance from the soma. This result implies that there is an optimal distance from the soma where the timing of the AP has the strongest effect on the corresponding calcium signal. More proximal dendrites are larger and have lower impedance, causing a reduced effect of synaptic inputs, and more distal dendrites are subject to the decay of the back-propagating AP causing a weaker relationship between calcium and AP timing. The optimal distance in our model is the first tertiary dendritic segment, 44-62 $\mu$ m from the soma. Interestingly, it is exactly this distance from the soma that has been shown to have the highest density of dendritic spines (Berlanga et al. 2011).

### **CDI replicates the effect of NMDA receptor blockade on the relationship between calcium and AP timing**

Previous work demonstrated that the relationship between calcium influx and AP timing is dependent on the activation of the NMDA receptors (Kerr and Plenz 2004). Therefore, we tested whether our two mechanisms (CDI and NaSI) were each dependent on the NMDA receptor by running upstate simulations with and without the NMDA receptors. Simulations revealed that removing the NMDA receptors greatly reduced the

strength of the relationship between AP timing and calcium influx for the CDI condition (calcium timing ratio =  $0.59 \pm 0.0008$  cntrl,  $0.30 \pm 0.054$  no NMDA;  $p < 0.0001$ ), but did not reduce it for the NaSI condition (Figure 18). In the NaSI condition, calcium elevations corresponding to both the early and the late APs were reduced with NMDA blockade, resulting in essentially the same *relationship* between calcium peak and AP timing (calcium timing ratio =  $0.57 \pm 0.04$  cntrl, =  $0.61 \pm 0.06$  no NMDA;  $p > 0.9$ ; Figure 18A inset). Because the CDI condition matches the dependence of this calcium timing ratio on NMDA receptors and the NaSI condition does not, our model predicts that CDI is more likely to be a mechanism controlling this relationship.

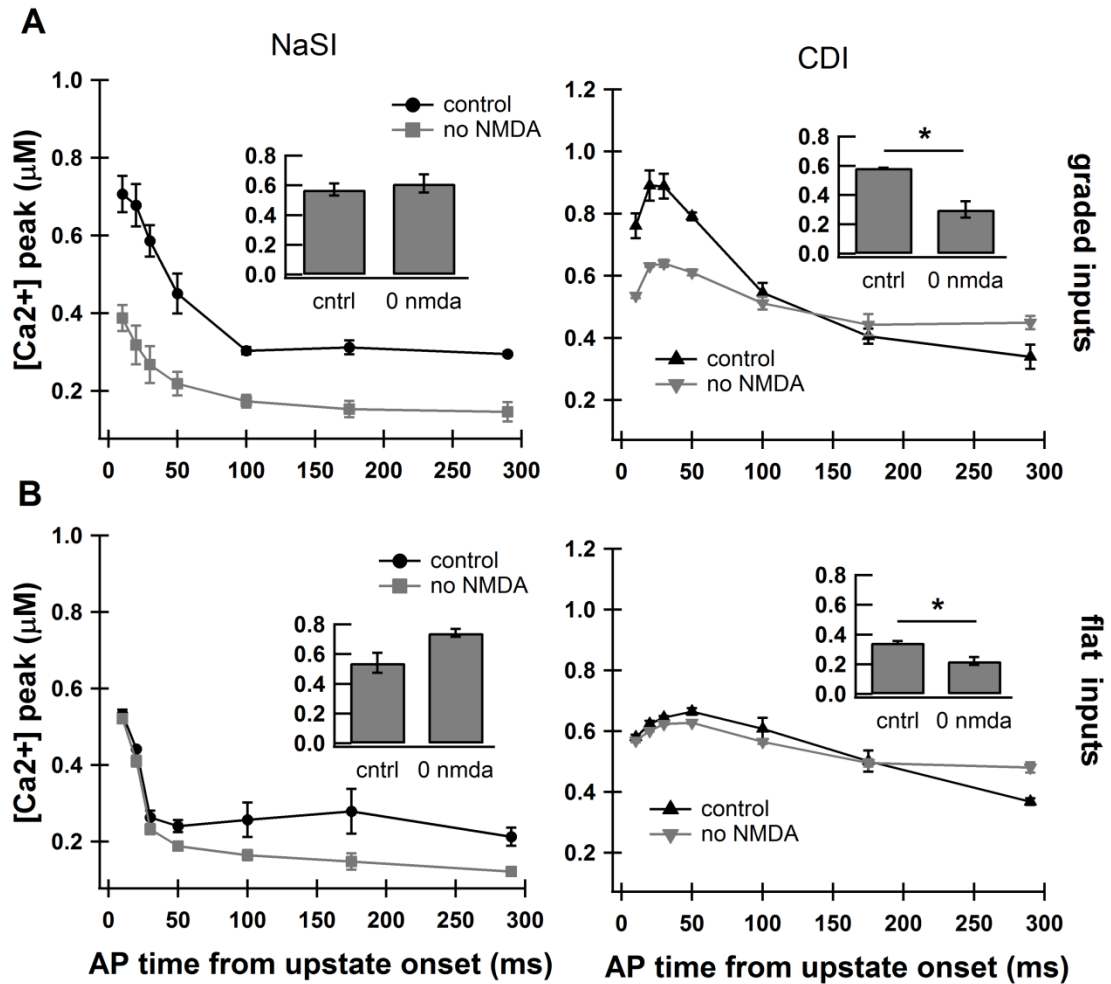


**Figure 18 Dependence on NMDA receptors during flat and graded inputs.**

**A.** Graded inputs result in a strong relationship between calcium signal and AP timing during the upstate. The calcium dependence on AP timing is reduced when the NMDA receptor is blocked only in the CDI condition. Note that the peak calcium elevations, but not the *relationship* between calcium and AP timing (calcium timing ratio, inset), are changed in the NaSI condition. Inset: bar graph showing the calcium timing ratio. All error bars are  $\pm$  SD.

(\*= $p < 0.0001$ ) **B.** When the upstate is elicited by flat input trains, the dependence of calcium peak on AP timing is reduced and the phenomenon is more weakly dependent on NMDA. Again this NMDA-dependence is observed for CDI, but not NaSI. Inset same as A.

Because the input gradient strongly influences the relationship between calcium and AP timing (Figure 14), we repeated the NMDA and no NMDA comparison for the flat input condition. In the CDI condition, removing NMDA receptors during flat inputs

caused a decrease in the calcium timing ratio ( $0.35 \pm 0.01$  flat,  $0.22 \pm 0.03$  flat no NMDA,  $p < 0.01$ ) (Figure 18B), even though the effect of removing NMDA receptors was much stronger for the G3 input gradient (Figure 18A). In the NaSI condition, neither the G3 gradient input nor the flat input resulted in NMDA dependence of the calcium timing ratio. In contrast to the flat CDI condition, the flat NaSI condition showed a surprising enhancing of the relationship between calcium and AP timing due to blocked NMDA receptors (calcium timing ratio =  $0.54 \pm 0.07$  flat,  $0.74 \pm 0.03$  flat no NMDA;  $p < 0.01$ ; Figure 18B inset). This enhancement clearly does not replicate published data (Kerr and Plenz 2004), further supporting CDI as an essential mechanism underlying the relationship between calcium and AP timing.

In conclusion, we find that the CDI model better fits the published data. Specifically, the relationship between calcium and AP timing is dependent on NMDA receptors only in the CDI case. Our voltage clamp experiments support this as a plausible mechanism because they show that CDI does indeed occur in the HVA calcium channels of the striatum. Therefore, all subsequent simulations are run using the CDI condition.

### **Part 2: Effect of neuromodulation and implications for in vivo plasticity.**

Here we use the model to investigate several aspects of plasticity during cortico-striatal upstates. We test how intrinsic and synaptic excitability, which can balance each other in homeostatic plasticity, affect the relationship between calcium and AP timing, and investigate the mechanisms controlling calcium binding to downstream targets which can influence the direction of plasticity at a synapse. Finally, we test whether spike

timing dependent plasticity (STDP) pairings are modulated by their timing within the upstate.

**Modulation of intrinsic, but not synaptic excitability alters calcium relationship with AP timing**

Differences in stimulation patterns or changes in neuromodulator availability can alter MSN intrinsic excitability, which in turn can affect plasticity. The intrinsic excitability of the dendrite depends on the composition of voltage gated potassium and sodium channels as well as the input resistance. Slice experiments have shown that dopamine depletion in the striatum increases intrinsic excitability of MSNs (Fino et al. 2007) and that this excitability increase is due to a two fold increase in the inactivation speed of A-type potassium currents (K<sub>A</sub>) (Azdad et al. 2009). Another potassium channel that can both modify dendritic excitability and be dynamically altered in response to neuromodulation is the inwardly rectifying potassium current (K<sub>ir</sub>). Acetylcholine M1 receptor activation causes a strong (40%) reduction of this current in one class of MSN (Shen et al. 2007).

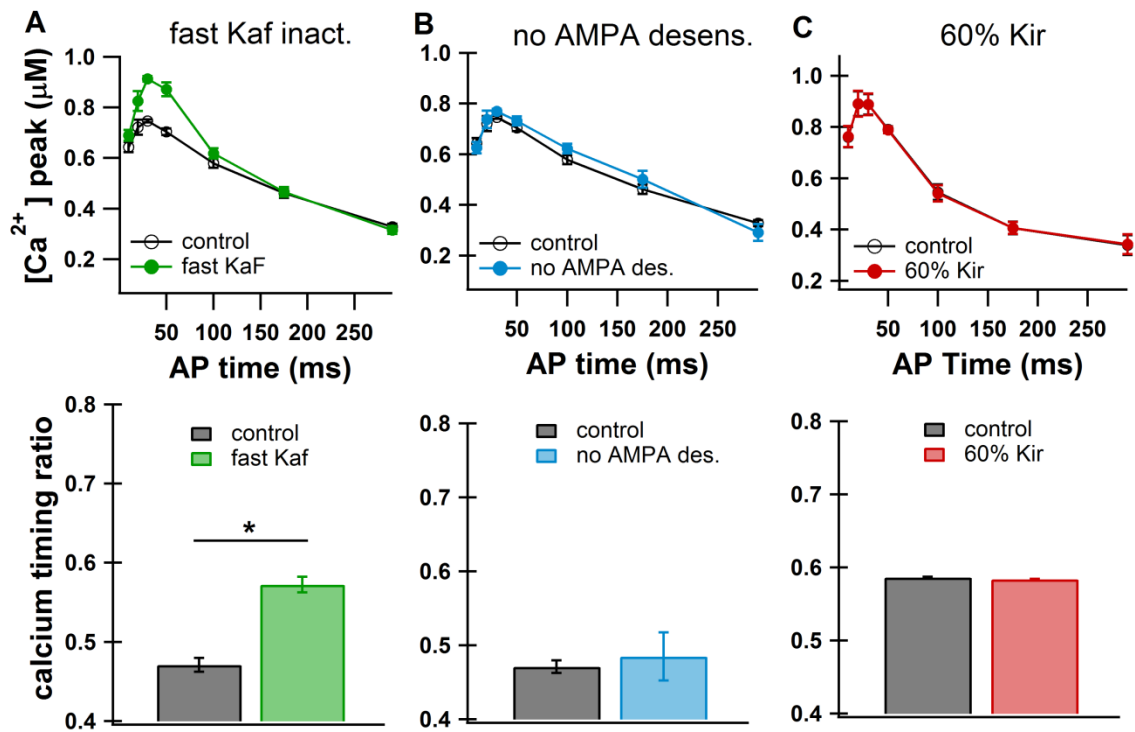


**Figure 19 A change in intrinsic excitability alters calcium relationship with AP timing.**

**A.** Fast Kaf inactivation (green traces) caused an increase in the strength of the calcium relationship with AP timing (\*= $p < 0.005$ ). Synaptic input with gradient G1 (see figure 5) was used to generate upstates to avoid spontaneous APs due to increased excitability. **B.** Removing AMPA receptor desensitization (blue traces) did not affect the calcium relationship with AP timing. Gradient G1 was used to generate upstates. **C.** Reducing Kir by 40% (red traces) did not affect the calcium relationship with AP timing.

To evaluate the effect of excitability on the sensitivity of calcium to AP timing, we repeated simulations with either inactivation of Kaf twice as fast as the control condition or the conductance of the inwardly rectifying Kir channel set to 60% of its control value. Our results show that faster Kaf inactivation makes the calcium elevation corresponding to the upstate more sensitive to AP timing (Figure 19A). Specifically this modification causes a calcium increase in response to APs early in the upstate, but no change in calcium elevation in response to APs late in the upstate (calcium timing ratio =

$0.47 \pm 0.01$  cntrl,  $= 0.57 \pm 0.01$  fast Kaf inact;  $p < 0.005$ ). In contrast to the strong effect seen with Kaf modification, the change in Kir affects neither the absolute calcium nor the relationship between AP timing and calcium elevation (calcium timing ratio =  $0.59 \pm 0.0008$  cntrl,  $0.58 \pm 0.0005$  60% Kir;  $p > 0.9$ ) (Figure 19C).

The increase in intrinsic excitability (via fast Kaf inactivation) may be a homeostatic mechanism deployed by the neuron to compensate for a decrease in synaptic excitability (via reduced AMPA receptor activity) that occurs with dopamine depletion (Azdad et al. 2009). The AMPA receptor plays a strong role in the local depolarization of the dendrite, and has been shown to influence the effect of back-propagating APs on NMDA calcium (Holbro et al. 2010). We therefore hypothesized that increased synaptic excitability implemented by removing AMPA receptor desensitization would reduce calcium sensitivity to AP timing. Surprisingly, when AMPA receptor desensitization was removed, the calcium dependence on AP timing was not altered (calcium timing ratio =  $0.47 \pm 0.009$  cntrl,  $0.48 \pm 0.03$  no AMPA desens;  $p > 0.9$ ) (Figure 19B). These results show that increases in synaptic excitability and increases in intrinsic excitability do not affect calcium during the upstate in the same way. This also suggests that a change in intrinsic excitability cannot fully compensate for a change in synaptic excitability with regards to calcium sensitivity to AP timing and therefore has implications for upstates during dopamine depletion pathologies such as Parkinson's Disease.

### **Fast and slow calcium binding partners are differentially influenced by AP timing and AP number.**

Since calcium is required for plasticity in the striatum (Fino et al. 2010), it has been suggested that the calcium elevations during upstates could cause potentiation or

depression (Kerr and Plenz 2004). However the factors that determine whether calcium causes potentiation or depression are still not clear. Recent studies suggest that the dynamics of calcium influx control preferential binding of calcium to disparate targets (Goldberg et al. 2009; Kubota and Waxham 2010). To test whether the timing of the AP within the upstate would influence not only calcium elevation, but also the binding partners which calcium preferred, we made use of our calmodulin buffer which has a fast binding N site (CaMN) and a slow binding C site (CaMC).

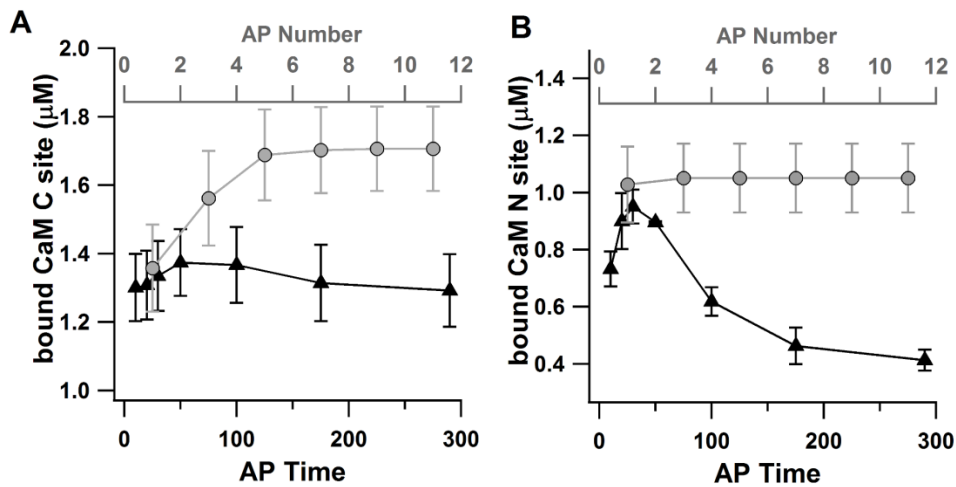


**Figure 20 Preference for calcium binding partners differs with AP timing and AP number.** **A.** Peak bound calmodulin C site (CaMC) is sensitive to AP number (gray) but not AP time (black). **B.** Peak bound calmodulin N site (CaMN) is sensitive to AP time (black), but not AP number (gray). All error bars are ± SEM.

During the upstate simulations, the peak concentration of bound CaMN is more strongly affected by the timing of the AP within the upstate than the peak concentration of bound CaMC (Figure 20A). The slower binding and unbinding of calcium from the

CaMC site smoothes the effect of the AP, making its timing irrelevant, while the fast binding and unbinding of the CaMN site makes it sensitive to AP timing. Figure 20 shows the peak bound CaMC (Figure 20A) and CaMN (Figure 20B) sites as a function of AP timing within the upstate (black symbols). While the peak bound CaMC is always higher than the peak bound CaMN (due to the higher affinity of calcium for the C site than the N site), it is clear that binding to the CaMN site is sensitive to AP timing, but binding to the CaMC site is not.

Another way that information can be conveyed during the upstate is through number of APs, rather than the specific timing of a single AP. To test whether the N and C sites of calmodulin were differentially sensitive to AP number, we ran upstate simulations with 1 to 11 APs. To prevent AP timing from influencing the bound buffer elevation, the timing of the initial AP was kept constant (20ms from upstate onset), and each AP was added 20ms after the most recent one (for a frequency of 50Hz). In contrast to the AP timing condition, the peak bound CaMC site increased with the total number of APs, while the peak bound CaMN remained constant (Figure 20, gray symbols). These results demonstrate that the two lobes of calmodulin are differentially sensitive to either the precise timing of the AP (CaMN) or the total number of APs (CaMC) within the upstate. Because the bound N and bound C sites differentially influence CaM's ability to bind to CaM dependent kinase type 2 (CaMKII), a molecule implicated in synaptic strengthening (Forest et al. 2008), the specific combination of AP timing and AP number during the upstate may determine whether a given synapse will undergo potentiation or depression.

### **AP timing during the upstate interacts with spike timing dependent plasticity protocols**

When APs are paired with precisely timed glutamatergic inputs, a cortico-striatal synapse can undergo spike timing dependent plasticity (STDP) (Fino et al. 2010). However *in vivo* neurons are subject to barrages of synaptic inputs during the upstate; thus a crucial question is whether spike timing influences calcium under *in vivo* like conditions. We have previously shown that the NMDA mediated calcium during STDP protocols correlates with synaptic potentiation (Evans et al. 2012). Here we use similar measurements to test how specifically timed pairings during the upstate would affect NMDA mediated calcium.

Because the spatial constraints of dendritic spines could alter the calcium dynamics, we added a single spine with an NMDA calcium pool to the first tertiary dendritic segment. In order to precisely control the timing of the pre and post-synaptic stimulations, we reserved a single tertiary dendritic segment, 44 $\mu$ m from the soma, and stimulated its spine only one time during the entire upstate. The time of this stimulation was varied ( $\Delta t$ ) around an early (20ms after onset) upstate AP and a late (175ms after onset) upstate AP (Figure 21, inset). The NMDA mediated calcium was recorded for each interval through a separate NMDA calcium pool (Evans et al. 2012). Pairing synaptic input with the AP showed a distinctive STDP-curve both early and late in the upstate (Figure 21). As in our previous model (Evans et al. 2012), the positive intervals showed higher NMDA mediated calcium peaks.

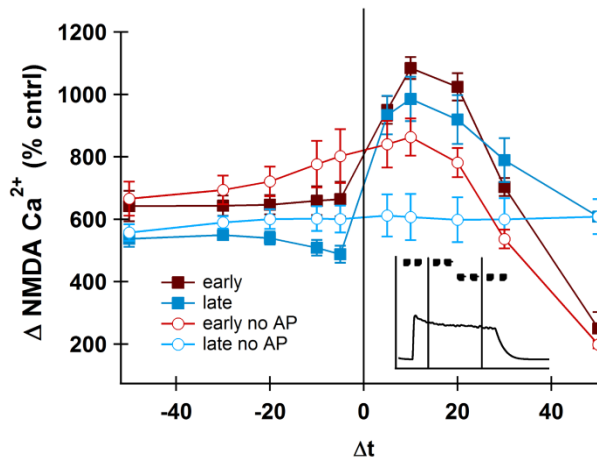


**Figure 21 STDP can occur during an upstate.**

NMDA receptor mediated calcium in the spine head shows an STDP curve shape early and late in the upstate (filled squares), which requires the AP. Cntrl = NMDA stimulation alone. Inset: schematic of early and late AP with stimulation times (not to scale) during the upstate. Vertical lines represent timing of AP; dots represent timing of pre-synaptic stimulation.

The upstate depolarizes the dendrite even without an AP and subthreshold depolarizations have been shown to cause synaptic plasticity in MSNs (Fino et al. 2009). Thus, it is possible that the timing of the synaptic input relative to the subthreshold upstate could produce an STDP-like curve even without an AP. To demonstrate that the timing of the AP is indeed contributing to the shape of the STDP curve, we ran simulations in the absence of an AP (Figure 21, open symbols). The stimulations given late in the upstate have no temporal sensitivity without the AP, while the stimulations early in the upstate demonstrate moderate temporal sensitivity even without the AP. In both the early and late AP cases, however, the AP ‘sharpens’ the curve, lowering the NMDA calcium during negative intervals and increasing NMDA calcium during positive intervals relative to the no AP condition. This ‘sharpening’ effect is much stronger when

the stimulated synapse is on the spine than on the dendritic shaft (data not shown), suggesting that indeed the spatial constraints of the spine head influence the relationship between calcium and the backpropagating AP.

These results suggest that specific pre and post-synaptic pairings could undergo STDP even during an upstate. Because the NMDA mediated calcium is higher early in the upstate than later in the upstate, our model predicts that pairings occurring early in the upstate will have a slight bias toward potentiation when compared to pairings occurring late in the upstate.

## **Discussion**

Upstates in the striatum drive large dendritic calcium transients which may control naturally occurring potentiation and depression of MSN synapses during sleep. The distinct up and downstate pattern is a trademark of the anesthetized or sleeping striatum and is much weaker during wakefulness (Mahon et al. 2006). We have implemented highly realistic calcium dynamics in a biophysical model of a MSN to study the factors governing these calcium elevations during upstates and to investigate the implications of a timing dependent calcium elevation on synaptic plasticity.

### **Is CDI or NaSI more likely?**

We first evaluated two mechanisms that cause the strong relationship between calcium elevation and AP timing within the upstate: NaSI and CDI. Both mechanisms matched the published data regarding the dependence of calcium on AP timing and the effects of distance from the soma on calcium elevation, but they did not both match other published effects such as NMDA dependence. Because CDI matched the published

NMDA dependence of the timing dependent calcium elevations while NaSI did not, our model predicts that CDI is more likely the mechanism producing the effect of AP timing.

It is important to note that these are not the only possible mechanisms that could account for a calcium relationship with AP timing. Pump extrusion, for example, could be altered over the course of the upstate or dependent on number or frequency of action potentials (Scheuss et al. 2006). Further experiments are needed to confirm that CDI is the main mechanism for the calcium relationship with AP timing.

### **Three testable predictions**

First, the simulations fit published data more accurately when the synaptic inputs are weighted toward the beginning of the upstate (Figure 14). Thus, our model predicts that the cortico-striatal upstates are initiated by strong glutamatergic inputs from the cortex. Electrophysiological recordings from organotypic triple co-cultures (Kerr and Plenz 2004) and *in vivo* (Schulz et al. 2009) demonstrate variability in upstate shape. However, the upstates often show steep rise times at initiation rather than slow increases (Figure 12C&D). In addition, recent experimental work has shown that striatal upstates can be sustained hundreds of milliseconds after the glutamatergic barrage has ended (Flores-Barrera et al. 2009; Plotkin et al. 2011) (but see also Kasanetz et al., 2006), indicating that it is indeed possible that naturally occurring upstates could have strong initial inputs that decrease or even disappear over the duration of the upstate. While one study found that distal inputs were able to induce upstates more strongly than proximal (Plotkin et al. 2011), the excitatory and inhibitory inputs in our model are distributed equally throughout the cell and differences based on spatial distribution of inputs were

not explored. Experiments using calcium hotspot imaging (Varga et al. 2011) in organotypic co-cultures could test our model prediction that glutamatergic inputs during the upstate are weighted toward upstate onset. In addition this technique could be used to test the spatial distribution of synaptic inputs during spontaneous upstates.

Second, simulations demonstrate that there is a specific distance from the soma which shows optimal sensitivity to AP timing. In our model it is the first segment of the tertiary dendrite, 44-62 $\mu$ m from the soma. However because each neuron is slightly different, it is likely that the size and location of this optimal distance could be variable. Therefore our simulations predict that for a given neuron there will be an optimal distance that displays a very strong relationship between calcium and AP timing, though it will not necessarily be the exact same distance for every neuron. Synapse and spine counting studies have shown that excitatory synapse density and spine density is highest between 30-60 $\mu$ m from the soma, declining sharply in the proximal direction, and declining more gradually in the distal direction (Berlanga et al. 2011). It is possible that optimal sensitivity to AP timing at this location increases calcium-based plasticity and consequently spine growth and excitatory synapse development. While the changes in sensitivity to AP timing proximal to the soma have already been shown (Kerr and Plenz 2004), experiments imaging calcium on very distal dendrites during striatal upstates could test our model prediction that the sensitivity to AP timing decreases in the distal dendrites.

Third, simulations reveal a means through which MSNs can dynamically alter their sensitivity to AP timing during the upstate by modulating their intrinsic excitability.

Increasing the speed of Kaf inactivation accentuated calcium's dependence on AP timing during the upstate. This doubling of the Kaf inactivation kinetics occurs in the striatum in response to dopamine depletion (Azdad et al. 2009). Azdad et al.(2009) suggest that this excitability change is a form of homeostatic plasticity, increasing *intrinsic* excitability to compensate for a loss in *synaptic* excitability. However, as we have shown, this specific intrinsic excitability change increases the calcium dependence on AP timing, while a synaptic excitability change (the removal of AMPA receptor desensitization) does not alter the relationship. Thus, the balance is not necessarily restored accurately. Such a compensation would result in an increased sensitivity to AP timing which may be too strong for optimal function. Indeed, a change in calcium dependence on AP timing could result in plasticity imbalances and consequently contribute to symptoms of dopamine depletion pathologies such as Parkinson's Disease. Because we did not see an effect of Kir modification, our simulations show that not all changes in potassium-based intrinsic excitability will result in altered calcium dynamics. While we did not model all the effects of dopamine depletion, our model predicts that alterations in Kaf observed during dopamine depletion will increase the dependence of calcium on AP timing. This prediction could be experimentally tested by pharmacologically or genetically manipulating the Kaf channel in organotypic co-cultures to test how changes in kinetics affected the calcium elevation during the upstate. Similarly, application of cyclothiazide to inhibit AMPA desensitization under the same conditions could reveal whether this aspect of synaptic excitability affects the calcium elevation during the upstate.

### **Implications for plasticity**

Calcium elevation is necessary for both the potentiation and depression of corticostriatal synapses (Fino et al. 2007). How calcium can cause these opposing effects is still a question up for debate. Several mechanisms have been postulated, for example, that the total amount of calcium determines the direction of plasticity (Graupner and Brunel 2012), that the channel allowing calcium influx determines plasticity (Fino et al. 2010), or that the binding of calcium to downstream targets makes the difference (Lisman 1989).

It is clear from our results that *if* the total amount of calcium determines the direction of plasticity (high calcium=potentiation; low calcium=depression), upstates that contain early APs will be more likely to potentiate synapses than upstates containing late APs. However, it is not clear that the *amount* of calcium is the only important factor. Therefore, we investigated differences in calcium binding during early and late APs. We found that the fast binding of the CaMN site was sensitive to AP timing, but the slow binding of the CaMC site was not. Previous studies have shown that fast binding partners are more sensitive to the backpropagation of a single AP than slow binding partners (Markram et al. 1998). Our work supports this idea and extends it to an *in vivo*-like context within the upstate. Importantly, we demonstrate that there is a dichotomy in the way that each calmodulin binding site responds to different types of information carried by the upstate. Specifically, the CaMN site is sensitive to AP timing, while the CaMC site is sensitive to AP number. These simulations reveal differential functions of calmodulin lobes without the spatial scale implemented in single spine simulations (Kubota and Waxham 2010). Calcium binding to the CaMN site alone is able to partially activate CaMKII, a molecule strongly implicated in synaptic strengthening (Forest et al. 2008).

The CaMN site's preferential response to APs early in the upstate implies that the APs early in the upstate will more efficiently trigger mechanisms for increasing synaptic strength.

In addition, our results can be extended to other calcium binding partners. Our model predicts that in general fast binding partners will be sensitive to AP timing, while slow binding partners will be sensitive to AP number. This result, in combination with future research revealing the kinetics of plasticity-related calcium binding partners, will shed light on which plasticity mechanisms are sensitive to specific upstate characteristics.

STDP pairings show robust synaptic plasticity in cortico-striatal brain slice and our previous work (Evans et al. 2012) demonstrates that the simulated NMDA calcium under these conditions is an excellent predictor of synaptic potentiation. Here we show that during noisy *in vivo* like conditions, STDP curves can still be established for independent dendritic and spine compartments. This finding suggests that STDP can occur during sleep, when the upstate-downstate pattern is most prominent (Mahon et al. 2006). Plasticity under these conditions may play a role in memory consolidation mediated by replay of cortical activity during sleep (Ribeiro et al. 2004; Lansink et al. 2009)

Our simulations compliment the experimental findings of Fino et al., (2009), which show that subthreshold depolarizations paired with pre-synaptic stimulation can induce synaptic plasticity in MSNs. They show that the curves elicited by pairing pre-synaptic stimulation with subthreshold post-synaptic depolarization are wider and less 'directional' than those elicited by pairing pre-synaptic stimulations with suprathreshold

stimulations containing APs. Similarly, our simulations show that the timing intervals which evoke elevated calcium under the subthreshold (no AP) condition early in the upstate are wider and shallower than the same stimulations paired with an AP.

It has been hypothesized that one population of synapses controls the upstate, but that a separate set of inputs drives the AP (Kasanetz et al. 2006; O'Donnell and Grace 1995). If this is indeed the case, a specific STDP-like pairing could easily occur on a dendritic segment or spine during the upstate. If an input consistently drives an AP during the upstate, it would consistently show a positive  $\Delta t$  and be potentiated. If an input simply drives the upstate, but not the AP, it would be equally likely to fall in a positive or negative  $\Delta t$  relative to the AP and would not be consistently potentiated. In this way the STDP control of calcium influx could control the direction of plasticity for specific synapses despite the calcium influx due to the upstate as a whole. On the other hand, the STDP control of calcium influx is not completely independent of timing during the upstate. We found that the whole STDP curve is shifted slightly upwards, towards higher NMDA calcium, when the AP is early in the upstate compared to when the AP is late. This suggests that even if the plasticity of a synapse is based solely on STDP principles, the pairings that occur early in the upstate will be slightly biased toward potentiation.

### **Conclusion**

Our model is the most advanced biophysical MSN model to date and is a useful tool for studying the calcium dynamics in the striatum. We have used it to investigate the mechanisms which underlie the non-linear calcium dynamics corresponding to AP timing

during striatal upstates, and it could easily be extended to answer other essential questions about striatal function and plasticity.

### **Contributions**

Conceived of project: Rebekah C. Evans, Kim T. Blackwell, Tom Sheehan

Wrote chapter: Rebekah C. Evans, Kim T. Blackwell

Edited chapter: Rebekah C. Evans, Kim T. Blackwell, Wonryull Koh, Sriram Damodaran

Updated model: Rebekah C. Evans, Kim T. Blackwell

Ran simulations: Rebekah C. Evans, Yash Maniar

Made figures: Rebekah C. Evans, Yash Maniar

Analyzed data: Rebekah C. Evans, Kim T. Blackwell

Citation:

Evans, RC, Maniar YM, Blackwell KT. (2013) Dynamic Modulation of Spike Timing

Dependent Calcium Influx During Cortico-striatal Upstates. *J Neurophysiol* 110, 1631-

1645

## **CHAPTER FIVE: REGIONAL AND AGE-DEPENDENT VARIABILITY IN CALCIUM DEPENDENT INACTIVATION OF CALCIUM CHANNELS IN THE STRIATUM**

### **Abstract**

Calcium is essential for striatal function and plasticity. It enters striatal neurons through NMDA receptors and voltage gated calcium channels (VGCCs). Each VGCC allows in different amounts of calcium at different voltages and for different durations. One factor that determines the duration of the calcium influx through these channels is the presence of calcium dependent inactivation (CDI). Some VGCCs undergo strong CDI, inactivating in response to an influx of calcium, while others rely primarily on voltage dependent inactivation (VDI). While calcium currents have been investigated in striatal neurons, the presence of CDI in striatal VGCCs and how it changes during development is not yet clear. Here we use whole cell voltage clamp to isolate calcium currents and characterize CDI over development and across striatal regions. We find that CDI increases at eye opening in the medial striatum, but not the lateral striatum and show that L-type calcium channels partially contribute to this increase. This change in CDI alters the amount and the duration of the calcium influx through VGCCs and thus could modulate striatal plasticity during development.

### **Introduction**

The striatum is a brain structure important for habit and skill learning. Calcium is essential for the neural-rewiring that occurs during such learning and the specific amount

and duration of the calcium influx can affect the underlying plasticity in neurons (Carlson and Giordano 2011; Yang et al. 1999).

Calcium enters striatal neurons through NMDA receptors as well as voltage gated calcium channels (VGCCs). Each type of VGCC (L, N, R, T, and P/Q type) has a specific pattern of activation and inactivation kinetics which determine the amount and duration of the calcium influx. The operation of these channels is not static, but is modulated by molecular events such as phosphorylation. In striatal neurons, the balance of dopamine is critical for triggering the phosphorylation of NMDA receptors and VGCC by PKA. Dopamine depletion alters the composition of VGCCs in these neurons (Martella et al. 2011) indicating that the specific balance of VGCCs is important for striatal function and may be disrupted in pathologies such as Parkinson's Disease.

The amount and duration of the calcium influx through these VGCCs is regulated by both voltage dependent inactivation (VDI) and calcium dependent inactivation (CDI). CDI acts as a self-regulation mechanism: Because calcium itself inactivates the channel, the cell is protected from the adverse effects of too much calcium. Despite its importance in cell function, CDI has barely been investigated in striatal neurons. One study suggests that striatal neurons from aged rats have less CDI than neurons from adult rats (Dunia et al. 1996), and our recent computational model predicts that CDI could play a critical role in determining the calcium influx during cortico-striatal upstates (Evans et al. 2013).

While the striatum does not have clearly defined functional units, many studies have reported regional differences in receptor expression (Chapman et al., 2003; McCaw et al. 2004), afferent inputs (reviewed in Wickens et al., 2007), synaptic plasticity

(Partridge et al. 2000; R. Smith et al. 2001), and learning (Pauli et al. 2012; Yin et al. 2009). Specifically, the dorsomedial (DM) and dorsolateral (DL) regions of the striatum seem to have distinct characteristics which change during development.

Of all the VGCCs, the L type calcium channels are the most well studied. Mutations in L-type calcium channels have been linked to autism, bipolar disorder, and schizophrenia (reviewed in Liao and Soong, 2010) as well as the rare, but devastating disorder Timothy Syndrome (Barrett and Tsien 2008). L type channels have been implicated in striatal plasticity, as blocking them prevents long term depression (LTD) (Fino et al. 2010; Shindou et al. 2011). Previous studies have shown that L type channels have strong CDI (Liang et al. 2003) and make up a large proportion of the VGCC current in young striatal neurons (Martella et al. 2008). Their contribution to total calcium current and CDI has not been tested *in situ* across striatal regions or at pre-eye opening ages.

Here we characterize CDI across striatal regions and at three time points during development, before eye opening (p11-12), after eye opening (p13-15) and after weaning (p22-24). We show that CDI in the DM striatum increases more strongly with age than the CDI in the DL striatum. We also show that the increase in medial CDI which occurs directly after eye opening is impaired when L-type calcium channels are blocked.

## **Methods**

### **Electrophysiology**

All animal handling and procedures were in accordance with the National Institutes of Health animal welfare guidelines and were approved by the George Mason

University institutional animal care and use committee (IACUC). C57BL/6 male and female mice (Charles River) were anesthetized with isoflurane and euthanized. Every effort was made to minimize anxiety and pain. Brains were extracted and cut 350 $\mu$ m thick using a vibratome (Leica VT 1000S) in ice cold sucrose slicing solution (in mM: KCL 2.8, Dextrose 10, NaHCO<sub>3</sub> 26.2, NaH<sub>2</sub>PO<sub>4</sub> 1.25, CaCl<sub>2</sub> 0.5, Mg<sub>2</sub>SO<sub>4</sub> 7, Sucrose 210). Slices were immediately placed in an incubation chamber containing artificial cerebrospinal fluid (aCSF) (in mM: NaCl 126, NaH<sub>2</sub>PO<sub>4</sub> 1.25, KCl 2.8, CaCl<sub>2</sub>, Mg<sub>2</sub>SO<sub>4</sub> 1, NaHCO<sub>3</sub> 26.2, Dextrose 11) for 30 minutes at 33°C, then removed to room temperature (22-24°C) for at least 90 more minutes before use. Recording aCSF was modified by replacing Mg<sub>2</sub>SO<sub>4</sub> with Mg<sub>2</sub>Cl and including either 2mM Ca<sub>2</sub>Cl or 2mM Ba<sub>2</sub>Cl. 4-AP (4mM) was added to block potassium channels. Slices were individually placed in a submersion chamber (ALA scientific) and cells were visualized using differential interference contrast imaging (Zeiss Axioskop2 FS plus). Pipettes (3-5M $\Omega$ ) were pulled from borosilicate glass on a laser pipette puller (Sutter P-2000), coated with candle wax (to reduce pipette capacitance) and fire-polished (Nirshige MF-830). Pipettes were filled with a cesium based internal solution (in mM Cs-gluconate 85, Cs3-citrate 10, KCl 1, NaCl 10, HEPES 10, EGTA 1.1, CaCl<sub>2</sub> 0.1, MgCl<sub>2</sub> 0.25, TEA-Cl 15, Mg-ATP 3.56, Na-GTP 0.38) pH 7.26 (Rankovic et al. 2011). Voltage clamp recordings were obtained on the HEKA EPC-10 and sampled at 20KHz. Data were acquired in Patchmaster (HEKA Elketronik). Analogue 3-pole (10kHz) and 4-pole (2.9kHz) Bessel filters were applied. Series resistance (4-15M $\Omega$ ) was compensated 70-90%. Recordings were made at room temperature (22-24°C).

**Drugs and Drug Application.**

Unless otherwise states salts were from Fisher. Mg-ATP, Na-GTP, Gluconic acid, citric acid, 4-AP, CeOH, TEA-Cl, and Nifedipine were from Sigma. TTX was from Tocris. TTX and Nifedipine were applied via a custom made Y tube local perfusion system (Murase et al.1989). The Y-tube system is well established and validated using dose-response curves (Hevers and Lüddens 2002). Application of TTX (0.5 $\mu$ M) through the Y tube abolished action potentials in less than 1 minute (data not shown). FK506, forskolin, and nifedipine were dissolved in DMSO. Nifedipine was protected from light and made fresh the day of use. Slices were not re-used after either a calcium-barium switch or being exposed to a drug treatment.

**Data Analysis**

CDI was measured during a 200ms depolarizing pulse from -40mV to +10mV (Figure 22A). Steady State (SS) is the mean current at the end of the 200ms depolarization. Peak is the amplitude of the current at its largest point. The ratio of steady state to peak is the measure of inactivation, and the difference between inactivation in barium and inactivation in calcium is the measure of CDI (Ba-Ca DIFF, Figure 22D). When specified, ramp depolarizations from -80 to +50mV were interleaved with the square pulses. In all cases, stimulations were separated by 30 seconds. Only cells requiring less than 200pA to be held at -80mV and that could be compensated between 70-90% with less than 15 M $\Omega$  series resistance were used. Data was collected in Patchmaster, processed with online analysis, and exported to Igor (Wavemetrics). Statistical tests were performed using the general linear model procedure (GLM) in SAS 9.2.

## **Results**

### **Isolating CDI in HVA channels**

Calcium currents were isolated by blocking potassium currents (with TEA, cesium, and 4-AP) and sodium currents (with TTX). High voltage activated (HVA) channels were isolated by voltage clamping striatal neurons at -40mV which inactivates the low voltage activated calcium currents (such as T-type channels). Total inactivation was assessed using the SS/peak ratio in calcium, while voltage dependent inactivation (VDI) was assessed using the SS/peak ration in barium. CDI was assessed using the difference in SS/peak ratio between barium and calcium (Ba-Ca Difference).

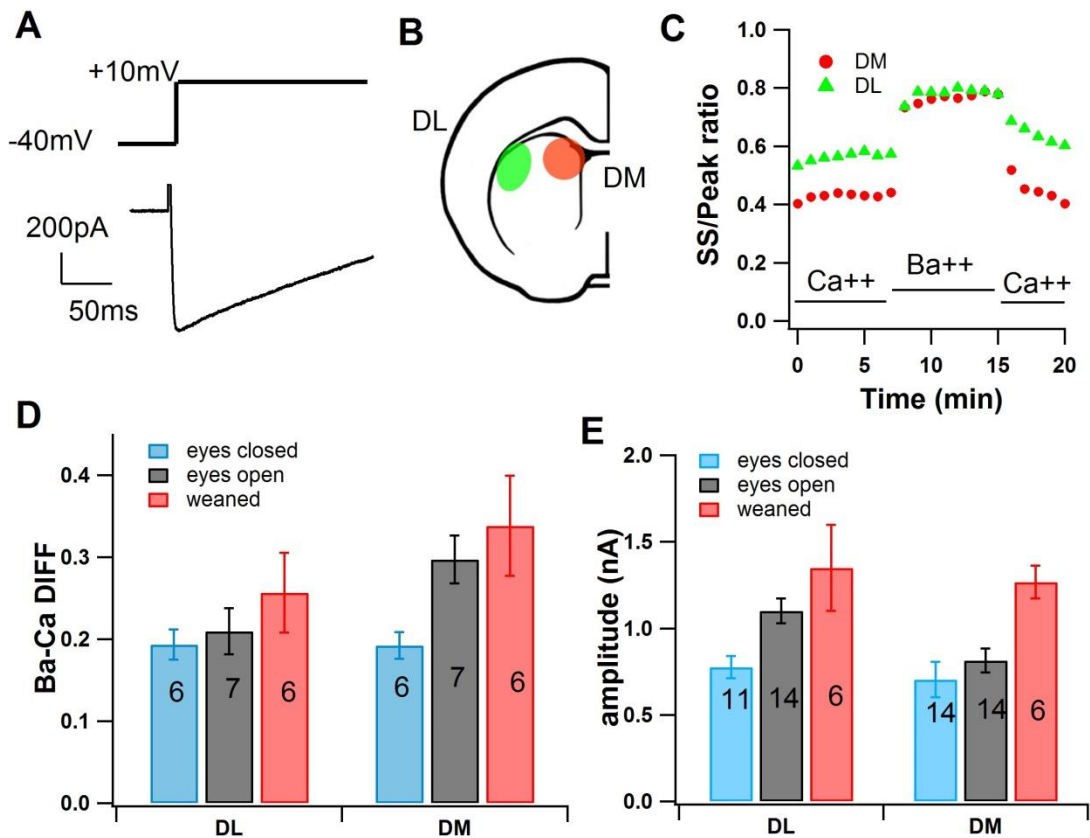


**Figure 22 Striatal CDI depends on age and region.**

A. Schematic showing HVA isolating depolarizing pulse and example trace below. B. Schematic showing medial (DM) and lateral (DL) regions of the striatum where recordings were made. C. Example experiments showing SS/peak ratio in barium and calcium. D. Summary of CDI (Ba-Ca DIFF) for each age group by striatal region (n specified in each bar, error bars are  $\pm$ SEM). E. Summary of total current amplitude in calcium for each age group by striatal region (n specified in each bar, error bars are  $\pm$ SEM).

**CDI increases with age, but is modulated by striatal region.**

CDI measurements in calcium and barium were taken from the dorsomedial (DM) and dorsolateral (DL) striatum (Figure 22B) at three different age groups: p11-12 (before eye opening), p13-15 (after eye opening), and p22-24 (after weaning). Figure 22C shows the SS/Peak ratio over time for one experiment from each region of one mouse (p22). This demonstrates that the measure of CDI is stable over time, and that the SS/Peak ratio

is smaller in calcium than in barium. Figure 22D shows the mean Ba-Ca difference for both dorsal striatal regions at three different age groups and reveals that CDI changes with age (GLM for age\*region  $F=5.51$ ,  $p<0.01$ ). However, the increase in CDI with age was significant medially (slope: 0.01,  $p<0.01$ ), but not laterally (slope: 0.006,  $p=0.07$ ).

The total amplitude of the calcium current also increased with age (GLM age\*region  $F=5.793$ ,  $p<0.01$ ) (Figure 22E). Amplitude was assessed from the peak current in response to the voltage step from -40mV to +10mV. The increase in amplitude with age was significant both medially (slope 0.04,  $p<0.01$ ) and laterally (slope 0.045,  $p<0.01$ ). However, while the increase in CDI due to age was stronger medially, the amplitude increase was most pronounced laterally. This indicates that the CDI increase was not due to a change in total current amplitude.

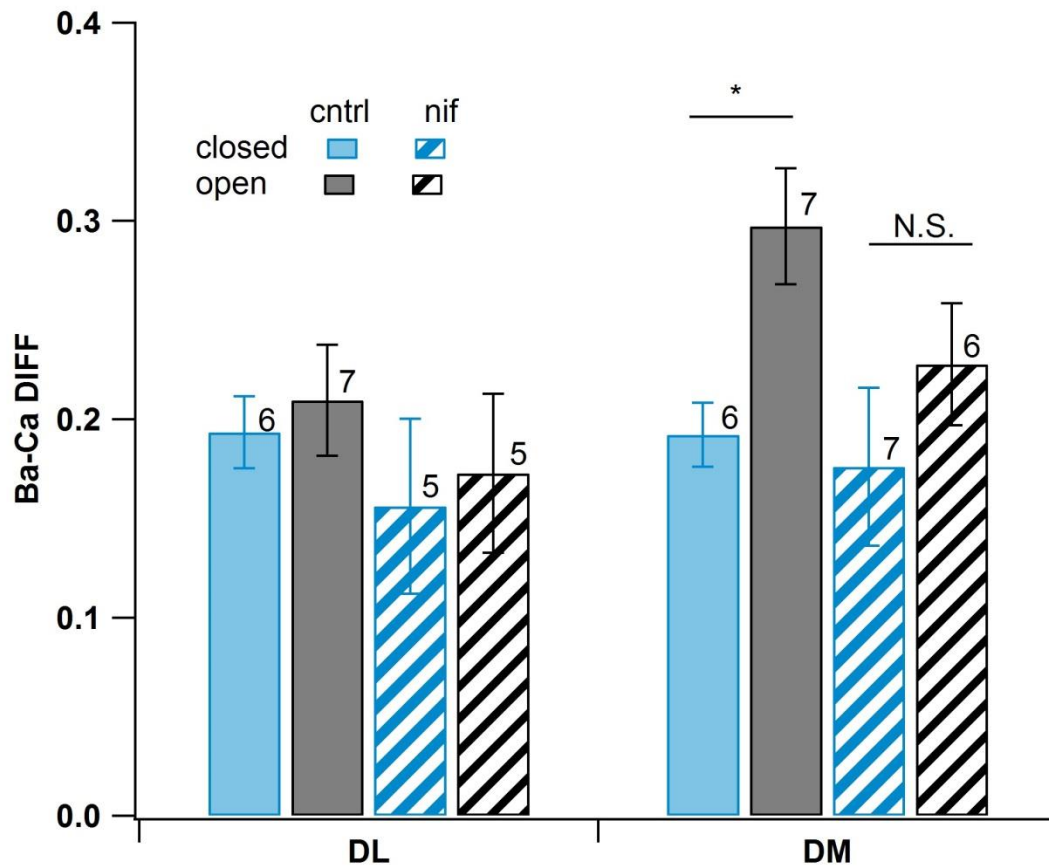


**Figure 23 L type calcium channels contribute to the increase in CDI that occurs at eye opening.** Summary of CDI (Ba-Ca DIFF) before and after eye opening for control (solid bars) and nifedipine (20 $\mu$ M) treated (striped bars). N specified by error bars, error bars are  $\pm$ SEM. \* $p$ <0.05

**L-type calcium channels contribute to the jump in medial CDI that occurs at eye opening.**

Because L-type calcium channels are known to have strong CDI (Liang et al. 2003), and have been shown to contribute significantly to the calcium current in medium spiny neurons (Martella et al. 2008), we tested CDI in DM and DL neurons in the presence of Nifedipine (20 $\mu$ M), a selective L-type calcium channel blocker. Nifedipine inhibited the increase in CDI that occurs at eye opening in the medial striatum (GLM

agegroup\*drug  $F=3.38$ ,  $p=0.037$  for DM) (Figure 23). Post-hoc contrasts confirmed a significant effect of eye opening for control ( $p<0.05$ ), but no significant effect in the presence of nifedipine ( $p=0.25$ ). Laterally there was no effect of age and nifedipine did not alter this (Figure 23) (GLM agegroup\*drug  $F=0.53$ ,  $p=0.67$ ).

These data show that L-type calcium channels contribute to the increase in CDI seen in the medial striatum at eye opening. However, this result does not explain how the L-type channels contribute. There are three explanations for this effect. First, there could be more L-type calcium channels in the DM striatum at eye opening. Second, the L-type calcium channels could undergo more CDI medially at eye opening. Third, it is possible that the influx through L type channels triggers the CDI of other channel types more strongly after eye opening than before. To test the first possibility, we measured the amplitude of ramp depolarizations (Figure 24A) in control conditions and in the presence of nifedipine for each age and region condition. Nifedipine decreased the amplitude of the calcium current by 20-25% for each group, but there was no difference due to age or region (GLM agegroup region  $F=0.71$ ,  $p=0.5$ ). Despite the age-dependent increase in *total* calcium current amplitude (Figure 22E), the proportion of that current carried through L-type calcium channels does not change medially or laterally at eye opening (Figure 24B). Therefore an increase in channel density cannot explain the effect of nifedipine at eye opening.

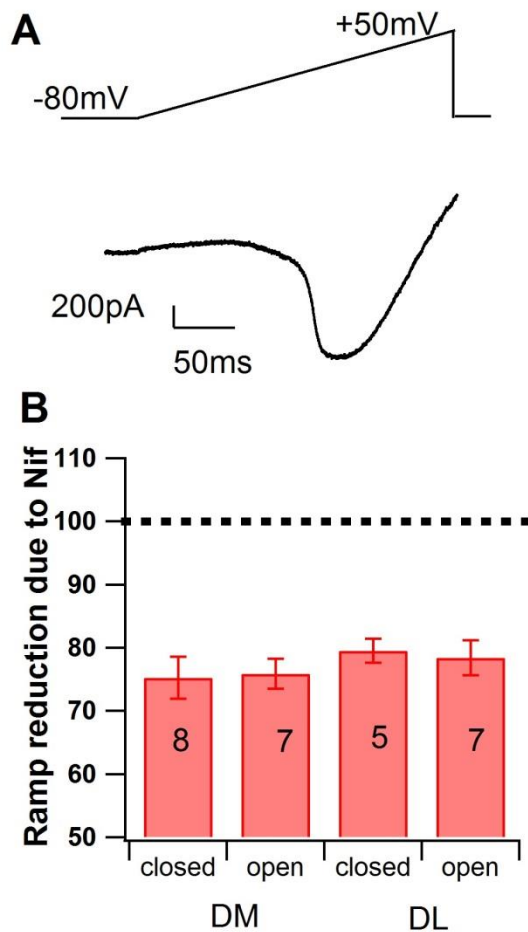


**Figure 24 Proportion of current carried by L-type calcium channels is not altered by region at eye opening.**  
 A. Schematic of ramp depolarization and example current trace. B. Summary of amplitude reduction due to nifedipine (20 $\mu$ M). N specified in each bar, error bars are  $\pm$ SEM.

If it is not because of an increased density of L-type calcium channels, how does the blockade of L-type calcium channels reduce the medial increase in CDI at eye opening? To further investigate the role of L-type channels, we separately analyzed the effect of nifedipine on the inactivation in calcium and the inactivation in barium (Figure 25). The inactivation in calcium is considered the *total inactivation* because it includes both calcium dependent and voltage dependent inactivation. The inactivation in barium

represents the voltage dependent inactivation (VDI) only because barium minimally activates CDI. The difference between the inactivation in barium and the inactivation in calcium is the CDI.

In all groups, the inactivation in barium was stronger in the presence of nifedipine than in control conditions (GLM drug  $F=16.87$ ,  $p<0.0001$ ), indicating an increase in VDI when L-type calcium channels were blocked. This result suggests that the remaining calcium channels (P/Q, N, and R type) undergo more VDI than L-type calcium channels. The effect of nifedipine on VDI was more pronounced laterally ( $p<0.001$ , Figure 25D) than medially ( $p<0.01$ , Figure 25B), suggesting that non-L VGCCs undergo more VDI laterally than medially. There was no effect of age on either lateral ( $p=0.3$ ) or medial ( $p=0.6$ ) VDI. This result shows that eye opening does not alter the effect of nifedipine and therefore an increase in VDI cannot be the mechanism by which nifedipine reduces the increase in CDI medially at eye opening.

The increase in inactivation is also seen when the charge carrier is calcium, indicating that the *total inactivation* is increased when L type channels are blocked with nifedipine. The increase in total inactivation is not as strong as the increase in VDI (GLM drug  $F=4.6$ ,  $P<0.05$ ). This effect is pronounced laterally ( $p<0.01$ , Figure 25C) but not significant medially ( $p=0.6$ , Figure 25A). These results indicate that the other calcium channel types (N, R, and P/Q) also undergo CDI in striatal neurons when no EGTA is present in the internal solution as suggested by (Liang et al. 2003). As in barium, there was no effect of age on lateral ( $p=0.7$ ) or medial ( $p=0.6$ ) total inactivation. Indeed, the total inactivation in the medial striatum at eye opening shows no increase whatsoever

when L-type calcium channels are blocked (Figure 25A open), suggesting that the remaining channels (P/Q, N, and R) undergo the same amount of total inactivation as the L-type channels in that age and region.

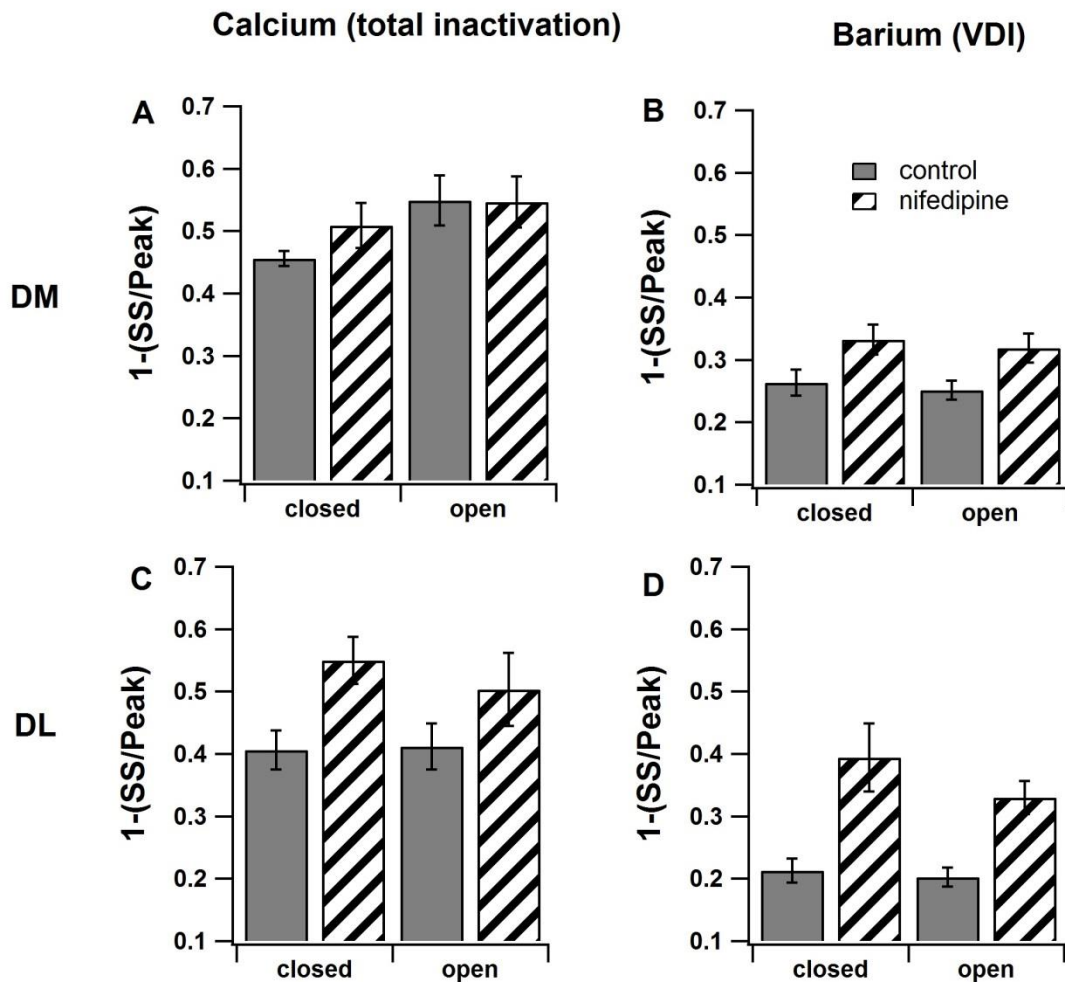


**Figure 25 Blocking L type channels increases VDI.**

A. Total inactivation is unchanged by nifedipine in medial (DM) striatum. Error bars are  $\pm$  SEM for all graphs. B. VDI is increased in the presence of nifedipine in medial striatum. C. Total inactivation is increased by nifedipine in the lateral (DL) striatum. D. VDI is strongly increased in the presence of nifedipine in the lateral striatum.

### **PKA phosphorylation and calcineurin dephosphorylation do not affect total inactivation**

While revealing an increase in VDI, the separation of the data above is not sufficient to explain how L type calcium channels are contributing to the increase in CDI at eye opening in the medial striatum. Because there is no difference in the density of L type channels at eye opening (Figure 24B), it is possible that L type channels undergo more CDI after eye opening than before eye opening. How could this happen? Studies have shown that certain mutations (Barrett and Tsien 2008) and phosphorylation states (Oliveria et al. 2012) can alter the inactivation properties of L type channels. Specifically L type channels are phosphorylated by PKA and dephosphorylated by calcineurin which decreases and increases CDI respectively (Oliveria et al. 2012). To test whether phosphorylation state altered CDI in striatal neurons, we applied FK506 (50 $\mu$ M), a calcineurin antagonist, and forskolin (FSK, 25 $\mu$ M), a PKA activator, to slices medially after eye opening. Figure 26 shows that neither FK506 alone, nor FK506 in conjunction with FSK altered total inactivation. This finding is similar to results seen in hippocampal cultures (Norris et al. 2002), which showed that FK506 reduced the calcium current, but did not affect CDI. This could be because calcineurin selectively acts on the L type calcium channel, leaving the other VGCCs unaltered (Norris et al. 2002). These data seem to suggest that phosphorylation state is not important for CDI in medial striatal neurons after eye opening. However, other studies have shown that PKA phosphorylation enhances L type current amplitude but reduces N and P type current amplitude (Surmeier et al. 1995). Since we have applied these drugs to the entire VGCC current, more studies

are needed to test the role of calcineurin and PKA in isolated L type calcium channels in striatal neurons.

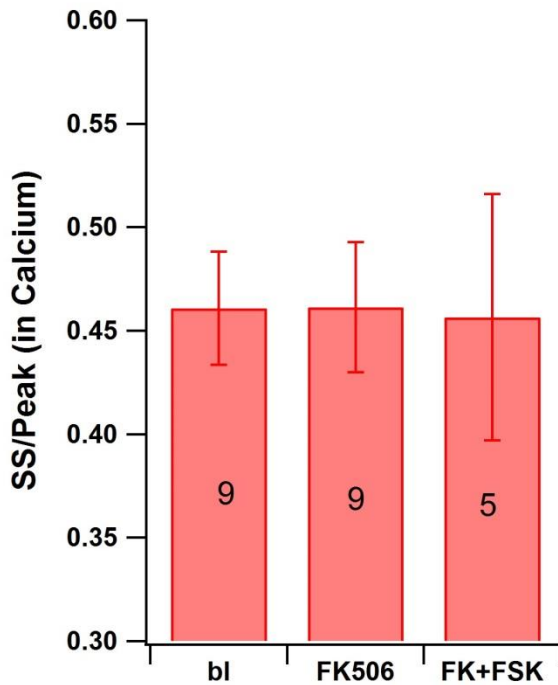


**Figure 26 PKA phosphorylation and calcineurin dephosphorylation do not affect total inactivation medially at eye opening.**  
SS/Peak ratio in calcium is unchanged by FK506 or FK506 (FK) + forskolin (FSK). Bl=baseline. N specified in each bar. Error bars are  $\pm$  SEM.

## Discussion

### Region and age dependent variation in amplitude and CDI

We have shown that HVA current amplitude in striatal neurons increases with age, and that this increase is region dependent. Specifically, we recorded calcium current around two critical events during development: eye-opening and weaning. Previous studies have shown that the amplitude and activation properties of acutely dissociated

striatal HVAs does not change with age (Martella et al. 2008). However, that study did not test pre-eye opening ages and did not discriminate between lateral and medial striatum. Our increase in amplitude with age may be due to slice and culture differences.

We also found that CDI increased in the medial striatum with age. To our knowledge, this is the first study to test CDI in striatal neurons during development. One previous study recorded calcium plateaus from adult and aged rats and found that the calcium plateaus were longer in duration for adult rats than aged, which may suggest more CDI in aged rats (Dunia et al. 1996). Switching between barium and calcium at the charge carrier however revealed that this difference in plateau duration is not due to a difference in CDI. If anything the study demonstrates that the aged rats have *less* CDI than adult rats. Our results show that CDI increases with age during development for the medial striatum, but not the lateral striatum. The functional significance of this finding is not yet clear, but this increase in CDI may alter the excitability of the medial neurons during development and could affect their ability to undergo synaptic plasticity.

### **The significance of eye opening**

Our data show that CDI was increased right after eye opening in only the medial striatum. This finding is particularly interesting in light of new anatomical tracing linking the visual cortex to the medial striatum in rodents and new *in vivo* experiments showing medial striatal neurons responding to visual stimulation (Rieg and Silberberg, 2012). Eye opening corresponds with enhanced synaptogenesis (Blue and Parnavelas 1983) and an increase in synaptic events (Desai et al. 2002) in the visual cortex. These changes would likely be reflected in the cortical output to regions such as the medial striatum.

Eye opening is a critical event during rodent development and may trigger drastic changes in brain areas other than those directly related to vision. Eye opening has been shown to affect hippocampal development, with early eye opening accelerating the maturation of synaptic strength (Dumas 2004). Future *in vivo* studies could reveal whether synaptic connections between the visual cortex and medial striatum are strengthened at eye opening. Morphological analysis of striatal medium spiny neurons could test whether the increase in spine density in visual cortex at p15 (Konur and Yuste 2004) is reflected in the medial striatum. In addition, experimental manipulations such as early eye opening or dark rearing will determine whether visual stimulation is causing this change in CDI rather than simply correlating with it.

### **VGCC types and CDI**

L type calcium channels have long been known to undergo strong CDI, while the other VGCCs particularly N and R type channels have only more recently been shown to also undergo CDI (Liang et al. 2003). L type channels inactivate in response to elevations in small calcium microdomains, while N and R type channels inactivate in response to global calcium. In this study we did not use EGTA or any calcium buffer in our internal solution, allowing for optimal CDI of all channels (Liang et al. 2003; Norris et al. 2002). Because CDI is still present even when L type calcium channels are blocked, our results show that in both medial and lateral striatal neurons, the non-L type channels undergo strong CDI.

We show that right before and right after eye opening the L-type calcium channels make up 20-25% of the total calcium current in both medial and lateral striatal

neurons. A previous study tested the proportion of calcium current carried by each VGCC in dissociated striatal cells at p14 and older (Martella et al. 2008). They showed that L type calcium channels made up about 50% of the total current at p14 and that the proportion of current carried by L types decreased with age. Our results showing a lower contribution of L type calcium channels could be due to a difference in slice preparation, which preserves dendrites and spines, compared to acutely dissociated cells, which only contain soma and proximal dendrites. Another difference that might affect the measurement of L type contribution is that the authors use 5mM barium as the charge carrier, while our measurements were made using 2mM calcium. A study of acutely isolated neurons from the ventral striatum (nucleus accumbens) of mice p5-11 used 5mM calcium as the charge carrier and reported that L type calcium channels account for 18% of the total current (Churchill and Macvicar 1998).

Blocking L type calcium channels with nifedipine increased VDI across all age and region groups. This result is consistent with previous studies suggesting that L type calcium channels only partially inactivate due to voltage (Bell et al. 2001). A partial or slower VDI in L type channels than other VGCCs would explain the increase in VDI when L type channels are blocked.

In our experiments, blockade of L type calcium channels reduced the increase in CDI seen at eye opening in the medial striatum. We found that this effect could not be due to an increase in L type channel density at eye opening because blocking L type channels reduced the total current amplitude by the same percentage at each age group. Therefore it is possible that there is the same proportional L type channel density at eye

opening, but those L type channels may have different inactivation properties. Specifically they might undergo more CDI in the medial striatum right after eye opening. One way that this might happen is through different phosphorylation states of L type channels. A study in the hippocampus showed that L type channels have increased phosphorylation with age (Davare and Hell 2003). Although this study is in the hippocampus and is comparing adult mice to aged mice, it demonstrates that phosphorylation can change with age in neurons. Further studies using immunohistochemistry or *in situ* hybridization could reveal any differences in phosphorylation state of L type channels immediately after eye opening in the medial striatum, and future electrophysiological studies could show whether L-type calcium channel dependent LTD is altered in this region.

### **Conclusion**

This is the first study testing CDI in striatal neurons during development. Our results showing age and region variability in CDI have implications for striatal plasticity and striatal pathologies and is a first step in evaluating the role of CDI in striatal function.

### **Contributions**

Conceived of project: Rebekah C. Evans, Kim T. Blackwell

Wrote chapter: Rebekah C. Evans

Edited chapter: Rebekah C. Evans, Kim T. Blackwell

Performed experiments: Rebekah C. Evans, Greta Ann Herin

Analyzed data: Rebekah C. Evans, Kim T. Blackwell

Publication status: *In preparation*

## **CHAPTER SIX: SPATIAL SPECIFICITY OF INTRACELLULAR SIGNALLING MOLECULES IS CRUCIAL FOR STRIATAL SYNAPTIC PLASTICITY**

### **Abstract**

Striatal synaptic plasticity is the putative mechanism underlying skill and habit learning. Cyclic AMP (cAMP)-dependent protein kinase (PKA) contributes to striatal long term potentiation (LTP) by phosphorylating synaptic glutamate receptors and DARPP-32. Although PKA is known to be necessary for plasticity in the striatum, the role of spatial localization of PKA has not been explored. A-kinase anchoring proteins (AKAPs) anchor PKA close to the source of cAMP that activates it (Efendiev et al. 2010), and close to the glutamate receptors that it phosphorylates (Colledge et al. 2000), suggesting that the location of PKA is important for its proper function. Here we show that PKA must be anchored to AKAPs for striatal LTP to occur. We induce striatal LTP with a high frequency stimulation (HFS) protocol, and this LTP is blocked in the presence of PKA inhibitors. Using the Ht31 peptide, which prevents PKA anchoring to AKAPs, but allows the catalytic subunit to remain active, we found that PKA anchoring to AKAPs is a crucial component of striatal LTP. This study is the first demonstration that PKA must be localized to specific compartments inside the neuron to fulfill its role in striatal synaptic plasticity.

## **Introduction**

Synaptic plasticity is the putative mechanism underlying learning and memory storage. Induction of synaptic plasticity involves calcium or G-protein activation of intracellular signaling cascades in all brain regions. In the striatum, the main input structure of the basal ganglia, disruption of specific signaling cascades impairs synaptic plasticity (Picconi et al. 2005) and normal brain function. For example, depletion of dopamine, an activator of specific signaling cascades, produces Parkinson's Disease-like symptoms and severely impairs memory storage (Calabresi et al. 2007).

Long term potentiation (LTP) of striatal synapses is a form of synaptic plasticity which requires the cAMP-dependent protein kinase (PKA) pathway. The PKA pathway is activated by dopamine in striatal medium spiny neurons (MSNs) containing D1 dopamine receptors, and by adenosine in MSNs containing D2 dopamine receptors (Shen et al. 2008). PKA contributes to striatal LTP by phosphorylating several known plasticity-related targets, including synaptic glutamate receptors (Esteban et al. 2003), Dopamine and cAMP-regulated phosphoprotein of 32 kDa (DARPP-32) (Snyder et al. 2003), and striatally enriched tyrosine phosphatase (STEP) (Paul et al. 2000). Previous work has demonstrated that PKA is necessary for certain types of striatal LTP (Centonze et al. 2003; Spencer and Murphy 2002); however, the spatial and temporal control of PKA activity in the striatum has not been investigated. One mechanism by which signaling pathways are spatially regulated is through the subcellular location of the molecules involved.

In many brain regions including the striatum, scaffolding proteins determine the subcellular location of signaling molecules, organizing them into multi-protein

complexes. A-kinase anchoring proteins (AKAPs) anchor PKA to specific locations within the cell (reviewed in Wong and Scott 2004 and Pidoux and Taskén 2010). AKAPs bind not only PKA, but also other enzymes such as adenylyl cyclase (Dessauer 2009; Efendiev et al. 2010) and phosphodiesterase (Willoughby et al. 2006; Moorthy et al. 2010). These multi-protein complexes participate in the temporal control of PKA activation by co-localizing effectors and inactivators of PKA, and the spatial control of PKA activity by anchoring PKA to specific locations near the cell membrane. Consistent with this role, previous studies have shown that anchoring of PKA to AKAPs is crucial for a PKA-dependent form of hippocampal plasticity (Nie et al. 2007) and for a striatum-dependent learning task (Weisenhaus et al. 2010). Although some AKAPs are highly enriched in the striatum (Ostroveanu et al. 2007), the role of PKA anchoring in striatal synaptic plasticity has not been investigated. Here we show that the specific location of PKA provided by anchoring to AKAPs is essential for striatal LTP.

## **Methods**

### **Brain slice preparation.**

All animal handling and usage procedures were in accordance with the National Institutes of Health animal welfare guidelines and were approved by the George Mason University IACUC committee. C57BL/6 male and female mice (p20-30) were anesthetized with isoflurane and decapitated. Brains were quickly extracted and placed in oxygenated ice cold slicing solution (in mM: KCL 2.8, Dextrose 10, NaHCO<sub>3</sub> 26.2, NaH<sub>2</sub>PO<sub>4</sub> 1.25, CaCl 0.5, Mg<sub>2</sub>SO<sub>4</sub> 7, Sucrose 210). Hemicoronal slices from both hemispheres were cut 350µm thick using a vibratome (Leica VT 1000S). Slices were immediately placed in an incubation chamber containing artificial cerebrospinal fluid

(aCSF) (in mM: NaCl 126, NaH<sub>2</sub>PO<sub>4</sub> 1.25, KCl 2.8, CaCl 2, Mg<sub>2</sub>SO<sub>4</sub> 1, NaHCO<sub>3</sub> 26.2, Dextrose 11) and incubated at 33°C. 30 minutes after the first slice was placed in the incubation chamber, the chamber was removed to room temperature (21-24°C).

**Whole Cell recording.**

A single hemislice was transferred to a submersion recording chamber (ALA science) gravity-perfused with oxygenated aCSF containing 50µM picrotoxin.

Temperature was maintained at 30-32°C (ALA science) and was monitored with an external thermister. Whole cell patch clamp recordings were obtained from neurons under visual guidance using infrared differential interference contrast imaging (Zeiss Axioskop 2 FS plus). Whole cell patch pipettes were pulled from filamented borosilicate glass on a laser pipette puller (Sutter P-2000). Pipettes were fire polished (Narishige MF-830) to a resistance of 3-7 MΩ. Pipettes were filled with a potassium based internal solution (in mM: K-gluconate 132, KCl 10, NaCl 8, HEPES 10, Mg-ATP 3.56, Na-GTP 0.38, Biocytin 0.77) for all recordings. Intracellular signals were collected in bridge mode and filtered at 3kHz using an Axon2B amplifier (Axon instruments), and sampled at 10-20 kHz using an ITC-16 (Instrutech) and Pulse v8.80 (HEKA Elektronik). Series resistance (6-30MΩ) was manually compensated. Experiments in which the compensated series resistance measurement changed >50% or the resting membrane potential changed by >10% were excluded. If these parameters were exceeded briefly (<120 seconds) the outlying sweeps were deleted, but the rest of the experiment was analyzed. Liquid junction potential was calculated (-14.7 mV) and was not compensated.

**White matter stimulation.**

A tungsten bipolar stimulating electrode was placed in the dorsolateral white matter overlying the striatum (Figure 27A). This placement is thought to stimulate cortico-striatal fibers (Centonze et al. 2004). Test pulses (0.05 ms) were applied at a frequency of 0.05Hz through a stimulus isolator (ISOflex, A.M.P.I.). Stimulation amplitude was adjusted (0.03-1.1 mA) to obtain excitatory post-synaptic potentials (EPSPs) with amplitudes between 1.5-6 mV. Because dialysis of cells after patching can cause a rundown of channel activity (Chad et al. 1987), the plasticity induction protocol was always applied shortly after breaking into the cell ( $17 \pm 0.5$ min,  $n=114$ ). A stable baseline was defined as a 5 minute period of EPSPs in which a line fitted to the baseline points did not have a slope more than  $\pm 0.05$  and there were no EPSP failures.

For high frequency stimulation (HFS), 100 pulses given at 100Hz for 1 second were repeated 4 times 10 seconds apart. Stimulation patterns were delivered through a Master-8 stimulation generator and ISOflex (A.M.P.I.). During HFS, stimulation intensity remained the same as the test pulse, but the duration of each pulse was increased to 0.1ms. Neurons were depolarized to spiking threshold via the patch pipette during each 1 second 100Hz stimulation. EPSPs were recorded for at least 20 minutes post-HFS induction protocol.

**Data analysis.**

Data was post-processed using PulseFit (HEKA Elektronik) and Igor pro (Wavemetrics). Statistical tests were performed in SAS (v9.2) using general linear models or the appropriate non-parametric test for non-normally distributed data, using the

average of all points between 20 and 25 minutes post stimulation. Results are expressed at Mean $\pm$ SEM, and all error bars on figures are  $\pm$ SEM.

### **Drug information.**

All basic solution salts were obtained from Fisher Scientific except Na-ATP and Mg-GTP and biocytin which were obtained from Sigma. Picrotoxin and PKI 14-22 were obtained through Tocris scientific. AP5 from Ascent Scientific and H89 from Tocris scientific and Enzo Life Science. Ht31, stHt31, and stHt31P were custom peptides ordered from American Peptide Company. Some stHt31 was obtained as a 10mM solution from Promega. Picrotoxin, and AP5 were dissolved directly into the aCSF. H89 was first dissolved in DMSO, and then added to the aCSF for a final concentration of 0.05% DMSO. stHt31 and stHt31P were dissolved in 50mM trisHCl (pH 7.0) and 0.05% DMSO, and diluted 1000x in aCSF. Drugs added to the pipette (PKI 14-22 and Ht31) were dissolved directly in the patch solution.

## **Results**

### **Medium Spiny Neuron characteristics**

Whole cell patch recordings of Medium Spiny Neurons (MSNs) were obtained in the dorso-lateral striatum (Figure 27A). MSNs were identified visually by their small soma size and their identity was confirmed by their known electrophysiological characteristics (Kawaguchi 1993; Nisenbaum and Wilson 1995; Charpier and Deniau 1997). MSNs displayed hyperpolarized resting membrane potentials ( $-82.05\pm 3.26$ mV,  $\pm$ SD, n=118) and low input resistance ( $53.27\pm 22.3$ M $\Omega$ ,  $\pm$ SD). They also showed inward rectification in their current-voltage relationship (Figure 27B) and a long latency to first action potential with an accompanying rounded shallow afterhyperpolarization (Figure

27C). Cells that did not display these characteristics were rejected, and these characteristics did not differ significantly between experimental groups.

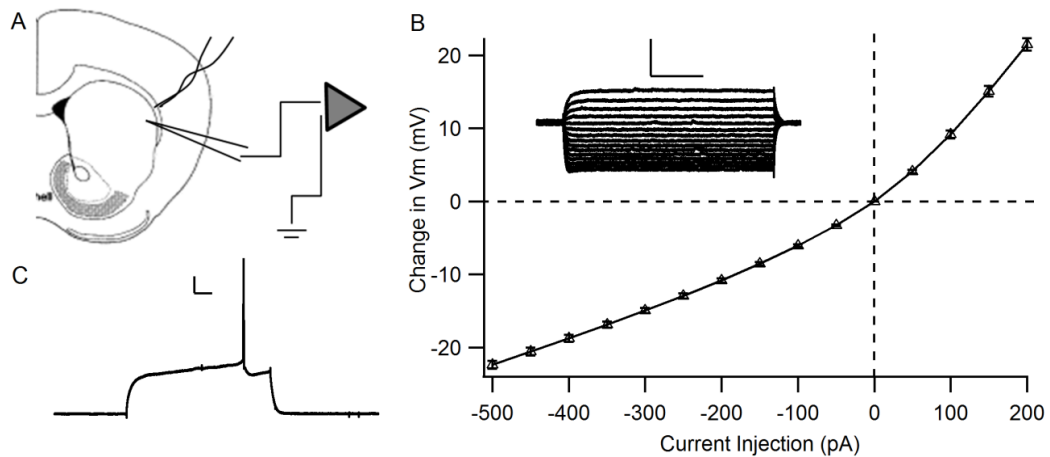


**Figure 27 Characterization of medium spiny neurons.**

**A.** placement of stimulation electrode and whole cell pipette in hemi-coronal slice preparation. **B.** Average current-voltage relationship for all cells used n=114. Inset: example current-voltage traces from a single cell. Scale bars vertical: 10mV, horizontal 100ms. **C.** Recording demonstrating long latency to action potential and shallow rounded afterhyperpolarization from a single cell; scale bar vertical 10mV horizontal 50 ms.

EPSPs (amplitude  $3.17 \pm 0.8 \text{ mV}$ ,  $\pm \text{SD}$ , n=118) were elicited in MSNs using a bipolar stimulating electrode was placed in the white matter overlying the striatum (Figure 27A). To ensure that the recorded EPSPs were glutamatergic,  $50 \mu\text{M}$  picrotoxin was added to the recording aCSF to block GABA<sub>A</sub> receptors. EPSPs were single peaked and occurred roughly 2-7ms after the stimulus artifact (Figure 28B, inset).

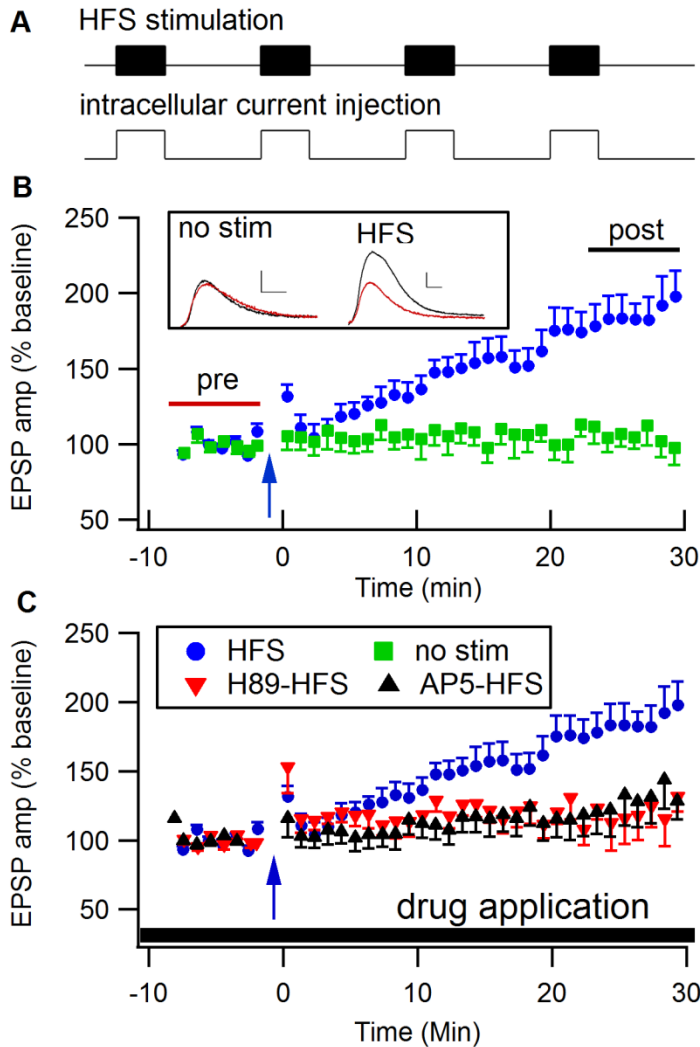


**Figure 28 HFS induces PKA and NMDA dependent LTP in cortico-striatal synapses.**

**A.** Schematic of high frequency stimulation (HFS) protocol used to induce LTP. 4 trains of 1s 100Hz stimulation during which the neuron was depolarized to spiking threshold. **B.** HFS (blue arrow) induces potentiation which lasts at least 30 minutes post-induction. Inset: example traces from ‘HFS’ and control ‘No Stim’ experiments obtained on the same day. Traces represent an average of the 5 minutes before induction (pre, red), and the average between 25 and 30 minutes (post, black). Inset scale bars represent 1mV vertical and 5ms horizontal. **C.** H89 and AP5 prevent LTP development when HFS is applied (blue arrow). Bottom black bar represents duration of either H89 (10 $\mu$ M) or AP5 (50  $\mu$ M) application.

**HFS induced LTP is NMDA and PKA dependent.**

Confirming previous studies (Fino et al. 2005; Kung et al. 2007), we found that 100Hz stimulation (HFS) in a magnesium-containing aCSF can produce LTP in striatal synapses. Medium spiny neuron EPSPs were measured using whole cell current clamp for 5 minutes pre-HFS and were followed for 20-30 minutes post-HFS. Figure 28B shows that HFS induces potentiation ( $180\pm 13\%$ ,  $n=14$ ) lasting at least 30 minutes, while control cells, which received not HFS show no change from baseline ( $105\pm 7\%$   $n=7$ ). This difference was statistically significant ( $p<0.01$ , one-way ANOVA, Dunnett correction for multiple comparisons). As a vehicle control, some samples were collected in 0.05% DMSO (HFS  $n=5$ , control  $n=4$ ). Because there was no difference between the DMSO and non-DMSO conditions for either HFS ( $P=0.38$ ) or control ( $P=0.76$ ), the two conditions were combined.

The NMDA receptor plays an important role in plasticity because of its ability to detect the coincidence of pre-synaptic glutamate release and post-synaptic depolarization. Several forms of LTP in the striatum are dependent on NMDA receptor activation, including spike-timing LTP (Pawlak and Kerr 2008; Fino et al. 2010), magnesium-free LTP (Calabresi et al. 1992; Li et al. 2009) and magnesium-containing LTP (Kung et al. 2007). To demonstrate that in our hands LTP uses the same mechanisms as those previously reported, we applied HFS stimulation in the presence of the NMDA receptor antagonist, AP5 (50  $\mu$ M). Figure 28C shows that AP5 significantly reduced LTP ( $119\pm 15\%$ ,  $n=18$ ) compared to HFS in normal aCSF ( $p<0.01$ , Wilcoxon rank sum).

PKA phosphorylates proteins essential to LTP in the striatum such as DARPP-32 and the GluA1 AMPA subunit (Snyder et al. 2003). Previous studies have shown that

magnesium-free LTP (Centonze et al. 2003) and forskolin induced LTP (Spencer and Murphy 2002) depend on PKA activity. To demonstrate that HFS-induced LTP obtained in the presence of magnesium is dependent on PKA, we applied HFS in the presence of the PKA inhibitor H89 (10  $\mu$ M). As in these previous studies, LTP is prevented by H89 ( $117\pm 9\%$ ,  $n=9$ ) (Figure 28C) and differs significantly from HFS applied in normal aCSF ( $p<0.01$ , Wilcoxon rank sum).

### **Spatial specificity of PKA activity is crucial for striatal LTP**

PKA is not uniformly distributed within the cell; it is anchored in specific places by AKAPs. The location of PKA has been shown to be important in guiding its activity, as it preferentially phosphorylates nearby substrates (Zhang et al. 2001). Therefore, precise localization of PKA within MSNs may be crucial for striatal LTP. Previous studies have used the stHt31 peptide to prevent PKA anchoring in mammalian neurons (Carr et al. 1992; Huang et al. 2006). The stHt31 peptide contains the binding segment of the human thyroid AKAP, and competitively attaches to the PKA regulatory subunits RI and RII. This binding functionally prevents PKA from binding to other AKAPs, but allows it to remain active (Lester et al. 1997; Herberg et al. 2000; Stokka et al. 2006).

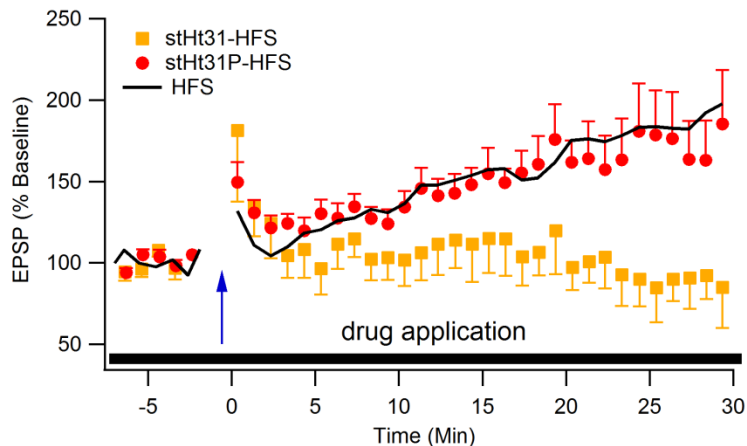


**Figure 29 Blocking PKA from anchoring to AKAPs prevents LTP.**

stHt31 prevents HFS-induced LTP (blue squares), but the inactive form of the peptide, stHt31P, does not prevent LTP (red circles) and is not significantly different from HFS in normal aCSF (thin black line). HFS was applied at the blue arrow. Bottom black bar represents application of either stHt31 (10  $\mu$ M) or stHt31P (10  $\mu$ M).

To test whether the spatial specificity of PKA is essential for striatal LTP, we applied the membrane permeable stHt31 peptide (10 $\mu$ M) to the aCSF during HFS. To control for any non-specific effects of peptide application on plasticity, additional experiments were performed in the presence of the inactive (proline-substituted) form of the peptide, stHt31P (10 $\mu$ M). Figure 29 shows that when the stHt31 peptide is present during HFS, striatal LTP is prevented (96 $\pm$ 14% n=6), whereas LTP developed normally in the presence of stHt31P (168 $\pm$ 23% n=9). Plasticity in the presence of stHt31 is significantly reduced compared to plasticity in the presence of stHt31P (p<0.05, two tailed t-test), confirming that it is the PKA-binding properties of stHt31 that disrupt striatal LTP. These results demonstrate that proper spatial location of PKA is required for striatal LTP.

### **Post-synaptic PKA activity and anchoring is necessary for striatal LTP**

The PKA inhibitor, H89, and the PKA anchoring blocker, stHt31, are both membrane permeable drugs. When applied in the aCSF, these drugs prevent PKA activity or PKA anchoring, respectively, in the entire slice. While PKA phosphorylates well known post-synaptic targets such as DARPP-32 and AMPA GluA1 subunits (Snyder et al. 2003; Esteban et al. 2003), it can also affect pre-synaptic vesicle-release properties (Chavis et al. 1998; Nagy et al. 2004), and plays a pre-synaptic role in forskolin induced LTP in the striatum (Spencer and Murphy 2002). These membrane permeable drugs affect both pre and post synaptic PKA function, thus the previous experiments do not demonstrate whether pre-synaptic or post-synaptic PKA activity and anchoring is necessary for striatal LTP.

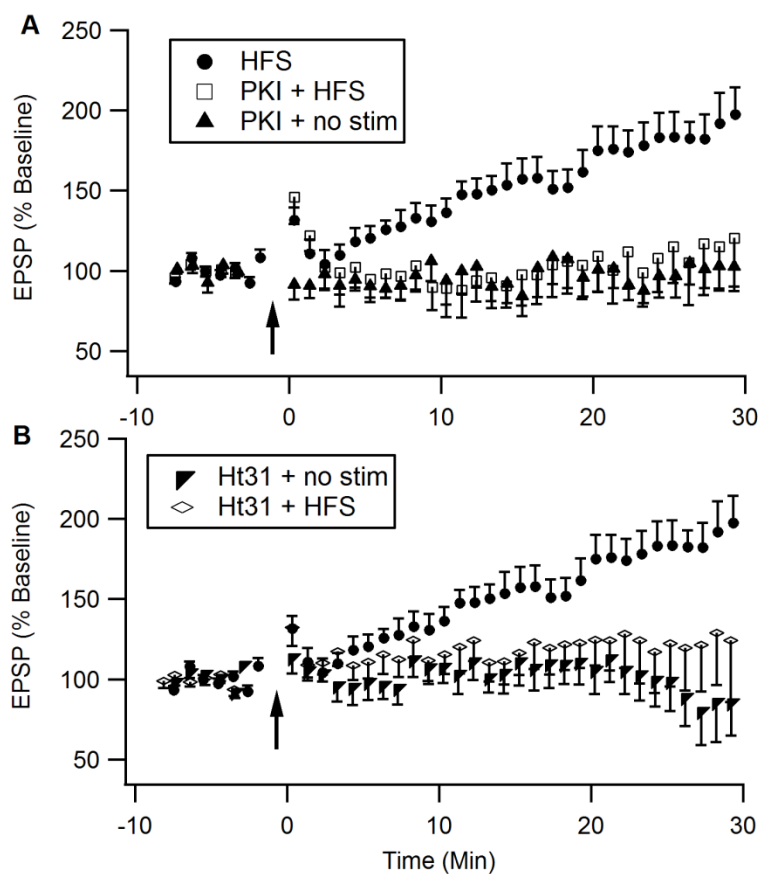


**Figure 30 Post-synaptic PKA activity and PKA anchoring is necessary for striatal LTP.**

A. Intracellular application of the membrane impermeable PKA inhibitor PKI 14-22 (20  $\mu$ M) prevents LTP in response to high frequency stimulation (HFS). Application of PKI 14-22 has no run-down effect on EPSP amplitude when no high frequency stimulation is applied (black arrow). B. Intracellular application of the membrane impermeable anchoring blocker Ht31 (10  $\mu$ M), prevents HFS-induced LTP. Application of Ht31 without high frequency stimulation produces a small amount of rundown in EPSP amplitude that is not significantly different from non-drug control cells.

To test whether post-synaptic PKA activity or PKA anchoring are required for striatal LTP, we applied membrane impermeable drugs via the patch pipette to block either PKA activity (PKI 14-22) or PKA anchoring (non-stearated Ht31). Blocking PKA activity in the post-synaptic MSN with PKI 14-22 (20 $\mu$ M) effectively prevented HFS-

induced striatal LTP ( $106 \pm 19\%$   $n=8$ ) ( $p < 0.05$ , one-way ANOVA, Dunnett correction) (Figure 30A). To test whether the inhibitor causes a rundown of EPSP size on its own, a no stimulation control group was followed for 30 minutes. The no stimulation control group did not show significant rundown due to PKI when compared to normal controls ( $97 \pm 10\%$   $n=7$ ;  $P=0.86$ ) (Figure 30A), confirming that the inhibition of LTP due to PKI is distinct from rundown. Although this experiment does not rule out all possible pre-synaptic changes, these data show that post-synaptic PKA activity is essential for striatal LTP.

Similarly, Ht31 ( $10 \mu\text{M}$ ), the membrane impermeable version of the stHt31 peptide, was applied to the post-synaptic MSN via the patch pipette. The Ht31 peptide prevents PKA from anchoring to AKAPs by competitively binding to its regulatory subunits. The presence of Ht31 in the pipette significantly reduced striatal LTP when HFS was applied ( $124 \pm 17\%$   $n=13$ ) ( $p < 0.05$ , one way ANOVA, Dunnett correction) and did not cause significant rundown of the EPSP in a no stimulation control group ( $101 \pm 14\%$   $n=10$ ;  $P=0.95$ ) (Figure 30B). These results show that specific spatial compartmentalization of PKA by AKAPs in the post-synaptic neuron is essential for striatal LTP.

## **Discussion**

Spatial specificity plays a critical role in intracellular signaling dynamics, allowing one molecule to perform distinctive functions depending on where it is anchored (Zhang et al. 2001). PKA is one such versatile molecule and is one of the most important molecules mediating striatal LTP. Here we have shown that PKA activity is necessary for

striatal LTP, but that its activity alone is not sufficient. In addition to being active, PKA must be anchored to specific locations within the post-synaptic cell for striatal LTP to occur. Determining that a molecule is necessary for plasticity is an important step, but understanding the spatial factors that influence the molecule is crucial for constructing a complete picture of the underlying signaling pathway. The field of plasticity research is shifting from a focus on specific signaling molecules to a broader view of spatial aspects of signaling networks. Investigations into the impact of spatial dynamics on molecular interactions within these networks are already transforming our understanding of plasticity mechanisms (Dell'Acqua et al. 2006).

PKA is necessary for LTP, in part, because it phosphorylates post-synaptic DARPP-32, inhibiting protein phosphatase 1, and the GluA1 AMPA subunit, facilitating incorporation of AMPA receptors into the membrane. When this process is prevented by a mutation of the PKA phosphorylation site on GluA1 (Ser845), hippocampal LTP is prevented (Esteban et al. 2003). Consistent with this post-synaptic role for PKA, we have found that blocking PKA activity exclusively in the post-synaptic MSN prevents striatal LTP. Computational models of signaling pathways underlying PKA dependent plasticity also show a role for post-synaptic PKA activity and demonstrate that PKA anchoring is required to place the PKA close to adenylyl cyclase, the source of cAMP (Kim et al. 2010; Oliveira et al. 2012). The model predicts that disruption of post-synaptic anchoring would decrease PKA phosphorylation of GluA1 and DARPP-32 thereby preventing LTP. Supporting this prediction, we have demonstrated that post-synaptic PKA anchoring, just like post-synaptic PKA activity, is essential for striatal LTP.

We have found that, similar to certain forms of LTP in the hippocampus (Nie et al. 2007), PKA anchoring to AKAPs is essential for LTP in the striatum. However, there is an important difference between the role of PKA anchoring in the striatum and in the hippocampus. In the hippocampus, PKA activity and PKA anchoring are only necessary for the late phase of LTP (lasting longer than 2 hours) in the hippocampus. In the hippocampus, the early phase of LTP that can be measured 20-30 minutes post-induction does not depend on PKA (Huang et al. 2006). Here we show that in the striatum, unlike the hippocampus, the LTP measured 20-30 minutes after induction is sensitive to the inhibition of PKA activity and the prevention of PKA anchoring.

There are many ways that PKA can be localized close to its wide range of target substrates (Wong and Scott 2004; Pidoux and Taskén 2010). Our results show that PKA needs to be anchored to AKAPs in general to function in striatal synaptic plasticity, but future work is required to determine which AKAP is essential to this process. One likely candidate is AKAP5 (AKAP79/150), which anchors PKA to the post-synaptic density, enhancing its proximity to glutamate receptors. AKAP5 is also more highly concentrated in the striatum than in any other brain structure (Ostroveanu et al. 2007) and was recently shown to play an essential role in a striatum-dependent learning task (Weisenhaus et al. 2010). A recent study shows that AKAP5 is essential for hippocampal LTD (Jurado, et al. 2010). Another, less well studied AKAP, AKAP 12 (gravin) is also highly concentrated in the striatum (Ted Abel, *personal communication*), and may play a role in striatal plasticity by anchoring PKA near another set of substrates. Further experiments are

needed to determine where within the post-synaptic MSN PKA must be localized, and which AKAPs are essential for striatal LTP.

### **Contributions**

Conceived of project: Rebekah C. Evans, Kim T. Blackwell

Wrote chapter: Rebekah C. Evans, Kim T. Blackwell

Edited chapter: Rebekah C. Evans, Kim T. Blackwell, Ted Abel, Robbert Havekes

Performed experiments: Rebekah C. Evans

Analyzed data: Rebekah C. Evans, Kim T. Blackwell

Publication status: *unpublished*

## CHAPTER SEVEN: SUMMARY AND EXTENDED APPLICATIONS

### **Introduction**

This dissertation presents a computational and experimental investigation into the role of calcium in striatal plasticity. It is presented in three parts: background and context, computational approaches, and experimental approaches.

### **Background and context**

It is clear that calcium is necessary for many forms of plasticity, and has been implicated in both LTP and LTD. The first chapter presents a review of the three current hypotheses for how calcium could control both potentiation and depression of synaptic strength. These hypotheses are that the calcium *amplitude, duration, or location* determines whether calcium triggers LTP or LTD pathways. This chapter reviews the experimental evidence supporting each hypothesis and the computational models based on each hypothesis. It also addresses problems and unanswered questions for each of these hypotheses.

Most of the computational models and experiments reviewed in chapter one address calcium and plasticity in cortical and hippocampal neurons. However, electrical activity and plasticity is different for the medium spiny neurons of the striatum. A separate overview of several computational models of medium spiny neurons and other striatal cells is presented in chapter two, which is an invited encyclopedia article. This

brief, focused review helps to put the computational portion of this dissertation in context.

### **Computational approaches**

A computational model of a neuron should be considered one in an arsenal of techniques that can provide information on neural function. A computational approach has advantages and disadvantages just as calcium imaging or electrophysiology does. One advantage of computational modeling is that it synthesizes myriad data sources and quantitatively tests conceptual models proposed by experiments. Another advantage is the ability to measure all compartments of a cell at every time point. With this power, one can investigate problems in neuroscience with a temporal and spatial precision beyond that of experiments. Computational models allow a researcher to block ion channels or inhibit molecules more completely and more easily than with experimental preparations.

In chapters three and four I present two versions of a computational model of a medium spiny neuron (MSN). The main difference between the two versions is the method for modeling calcium dynamics. Chapter three uses a simple ‘calcium pool’ model which collects calcium from receptors and channels and decays with a single time constant. The calcium pool model allows for the isolation of calcium from specific sources (such as the NMDA receptor) and was used to measure the calcium through the NMDA receptor during different STDP induction protocols. Another advantage of this simple calcium concentration model is its computational efficiency, which allows the model to be used in large scale network models. Thus, this model has been put into a computational model of a striatal network by my colleague Sriram Damodaran. He has

used a network of these neurons integrated with a network of fast spiking interneurons (FSIs) to simulate the effects of cortical synchrony and gap junctions between interneurons on network output. Using this network model, he discovered that gap junctions between the FSIs are essential for maintaining the balance in firing between the two different classes of MSN (D1 and D2 MSNs). This work is *in revisions* in the Journal of Neurophysiology.

The second version of the MSN model implements a more physiological model of calcium dynamics. This more sophisticated calcium shell model is more sophisticated than the simple calcium pool model because it explicitly models three different mechanisms for calcium decay. Calcium diffusion, buffering, and pump extrusion all contribute to the decay time of the free calcium in this model. This is an advantage over the single decay time constant of the calcium pool model because the specific calcium decay parameters can be altered and measured. I make specific use of this in Figure 20 by separately measuring the calcium bound to specific buffers. I found that the two lobes of calmodulin (N and C) are differentially sensitive to action potential timing and number. This model was used in chapter four to investigate the calcium elevations underlying the cortico-striatal upstates which are seen in medium spiny neurons *in vivo*. I find that calcium dependent inactivation of voltage gated calcium channels is a likely mechanism for controlling the relationship between calcium and action potential timing during the upstate. Future work using this model could investigate how calcium buffers and pumps contribute to calcium elevations in dendrites and spines, and could test whether calcium

channel kinetics (independent of calcium channel location) could be responsible for their differential activation of the calcium-activated potassium channel (Vilchis et al. 2000).

Both versions of this model MSN are freely available in an online database called ModelDB. Future work could make these models even more physiological by adding a realistic morphology. With a realistic morphology, we could investigate how information is integrated across spines on a single dendritic segment. To this end, I and others in CENlab have been staining medium spiny neurons and digitally reconstructing them for morphological analysis and spine counting. These digital reconstructions made in NeuroLucida can be transferred into the neuron modeling software Genesis and applied to our computational model. Because we have electrophysiology data for each cell that is reconstructed, we could use a combination of computational and experimental approaches to test the influence of morphology and spine density on neuron excitability.

### **Experimental approaches**

Computational models are most effective when used in conjunction with experiments. Experimental data can constrain the model and simulation data can focus the experiments by making specific testable predictions. In this spirit, experimental data is included in both of the computational chapters. In chapter three, I used current clamp recordings to collect IV curves from patched MSNs to constrain the membrane potential characteristics of the MSN model. The STDP plasticity experiments in chapter three were performed in collaborator Laurent Venance's lab in order to test our model predictions. This group was the first to publish STDP experiments in the striatum, and had a reliable slice preparation and protocol to induce timing dependent LTP. Their experiments

confirmed our model prediction that isolating the GluN2A subunit would narrow the timing intervals which allowed timing dependent LTP.

In chapter four, the MSN model was again constrained by my current clamp recordings of IV and IF curves. In addition, I used voltage clamp experiments to test for CDI in striatal neurons. Surprisingly, no one had investigated CDI in striatal neurons and this study is the first to show that the calcium channels in MSNs undergo CDI. This voltage clamp preparation was also used in chapter five to characterize CDI across age and region and identify a mechanism contributing to this change. We showed that the increase in CDI at eye opening in the medial striatum was due in part to the L type calcium channel current, and that this was not due to an increase in L type channel density. One possibility is that the L type calcium channels are differentially phosphorylated by PKA before and after eye opening, causing a different degree of CDI. Work is in progress to investigate this possibility.

Though this dissertation focuses on calcium, striatal LTP requires dopamine which activates PKA through the D1 dopamine receptor. To investigate the role of PKA in frequency dependent striatal LTP, I used whole cell patch clamp and applied high frequency stimulation (HFS) to induce LTP. The results of these experiments are detailed in chapter six. In my hands, HFS yielded a slow rising LTP. My experiments showed that post-synaptic PKA was required for this LTP, and further that PKA binding to AKAPs was necessary. Consequently, I attempted to identify which AKAP was critical for LTP by using the AKAP150 knockout mouse. However, in these experiments, HFS no longer induced LTP even in the wild type littermates (Figure 31).

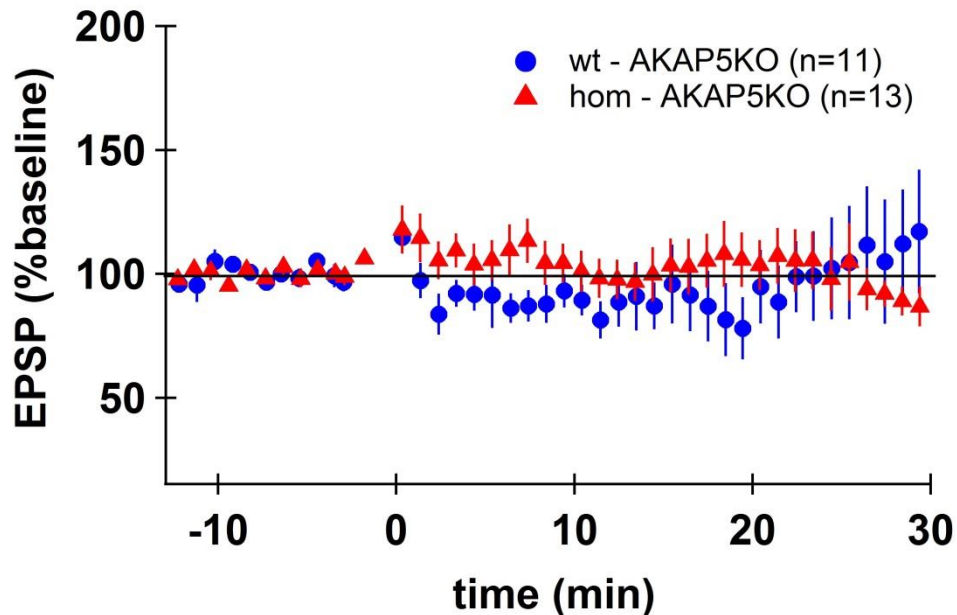


**Figure 31 No plasticity in AKAP 150 knock out strain.**

Neither mutant AKAP 150 (AKAP 5) knock out homozygotes (hom -AKAP5KO) nor their wild type littermates (wt-AKAP5KO) displayed LTP in response to HFS. Error bars  $\pm$ SEM.

Further experiments revealed that even in the C57Bl/6 strain we had previously used, HFS no longer induced LTP. Historically, HFS produces variable plasticity in the striatum with some groups getting LTD (Calabresi et al. 1992), some getting LTP (Fino et al. 2005), and some getting both (Akopian et al. 2000). I manipulated many parameters in the recording set up to try to induce LTP again, but nothing seemed to reproduce my original results. The loss of LTP coincided with our lab and animal facility moving locations, but I still do not know what factors contributed to the occurrence of LTP in the first place or to the loss of it. Chapter six was in revisions at the Journal of

Neurophysiology when we discovered that the results were not reproducible in our hands, so we decided it would be unethical to publish, and withdrew it from submission.

My colleague Sarah Hawes used striatal field recordings to develop a theta-burst induction protocol that produces robust LTP (Hawes et al., 2013). I used her induction protocol in the whole cell current clamp preparation. In whole cell however, theta burst stimulation produced only mild short term potentiation that decayed to baseline by 30 minutes post-induction (Figure 32).

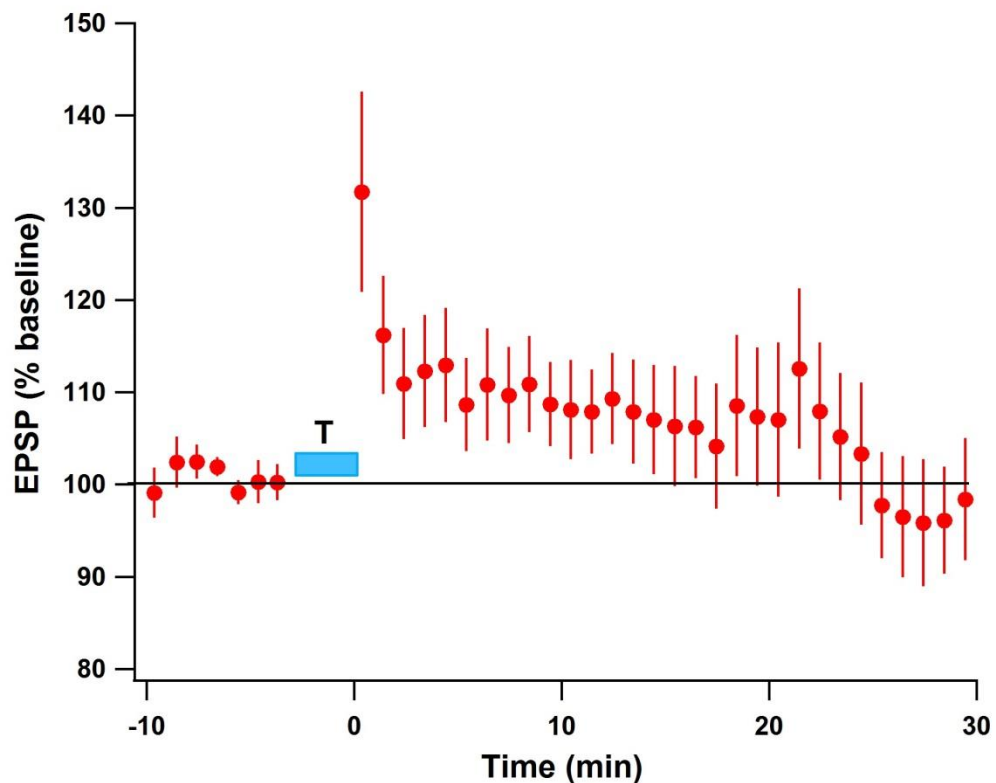


**Figure 32 Theta burst LTP using whole cell preparation**

Theta burst stimulation (T, blue bar) induces mild short term potentiation in medium spiny neurons of the medial striatum  $n=19$ , error bars  $\pm$ SEM.

It is not clear why the whole cell preparation produces weaker LTP than the field preparation, but one possibility is the dialyzation of intracellular molecules during whole cell patch clamp. Perhaps the molecules essential for LTP diffuse out of the cell and into the pipette. Future work could investigate this by using the perforated patch technique which does not dialyze the cell. If theta burst stimulation reliably induces LTP in the perforated patch preparation, the experiments in chapter six could be re-run to demonstrate that PKA anchoring is consistently necessary for striatal LTP. If this is the case, the planned investigations into which AKAP is required for LTP could continue.

## **Conclusion**

This dissertation is a cohesive investigation into the role of calcium in the function of striatal cells. It presents a sophisticated computational model of a medium spiny neuron implementing two different models of calcium dynamics and presents supporting electrophysiological experiments. The simulations and corresponding experiments reveal a role for the NMDA subunit composition in determining the shape of the STDP curve. They predict that CDI is responsible for the relationship between calcium and action potential timing during cortico-striatal upstates. Finally, experiments show that CDI does occur in striatal cells, and that it is altered by age and region.

## REFERENCES

- Aihara, T, Y Abiru, Y Yamazaki, H Watanabe, Y Fukushima, and M Tsukada. 2007. "The Relation between Spike-Timing Dependent Plasticity and Ca<sup>2+</sup> Dynamics in the Hippocampal CA1 Network." *Neuroscience* 145 (1) (March 2): 80–87. doi:10.1016/j.neuroscience.2006.11.025.
- Akopian, G, W Musleh, R Smith, and J P Walsh. 2000. "Functional State of Corticostriatal Synapses Determines Their Expression of Short- and Long-Term Plasticity." *Synapse (New York, N.Y.)* 38 (3) (December 1): 271–280. doi:10.1002/1098-2396(20001201)38:3<271::AID-SYN6>3.0.CO;2-A.
- Akopian, G, and J P Walsh. 2007. "Reliable Long-Lasting Depression Interacts with Variable Short-Term Facilitation to Determine Corticostriatal Paired-Pulse Plasticity in Young Rats." *The Journal of Physiology* 580 (Pt 1) (April 1): 225–240. doi:10.1113/jphysiol.2006.115790.
- Allbritton, N L, T Meyer, and L Stryer. 1992. "Range of Messenger Action of Calcium Ion and Inositol 1,4,5-Trisphosphate." *Science (New York, N.Y.)* 258 (5089) (December 11): 1812–1815.
- Andrews, Steven S, Nathan J Addy, Roger Brent, and Adam P Arkin. 2010. "Detailed Simulations of Cell Biology with Smoldyn 2.1." *PLoS Computational Biology* 6 (3) (March): e1000705. doi:10.1371/journal.pcbi.1000705.
- Artola, A, and W Singer. 1987. "Long-Term Potentiation and NMDA Receptors in Rat Visual Cortex." *Nature* 330 (6149) (December 17): 649–652. doi:10.1038/330649a0.
- . 1993. "Long-Term Depression of Excitatory Synaptic Transmission and Its Relationship to Long-Term Potentiation." *Trends in Neurosciences* 16 (11) (November): 480–487.
- Azdad, Karima, Marcelo Chàvez, Patrick Don Bishop, Pim Wetzelaer, Bart Marescau, Peter Paul De Deyn, David Gall, and Serge N Schiffmann. 2009. "Homeostatic Plasticity of Striatal Neurons Intrinsic Excitability Following Dopamine Depletion." *PLoS One* 4 (9): e6908. doi:10.1371/journal.pone.0006908.

- Banerjee, Abhishek, Rhiannon M Meredith, Antonio Rodríguez-Moreno, Susanna B Mierau, Yves P Auberson, and Ole Paulsen. 2009. "Double Dissociation of Spike Timing-Dependent Potentiation and Depression by Subunit-Preferring NMDA Receptor Antagonists in Mouse Barrel Cortex." *Cerebral Cortex (New York, N.Y.: 1991)* 19 (12) (December): 2959–2969. doi:10.1093/cercor/bhp067.
- Bargas, J, A Howe, J Eberwine, Y Cao, and D J Surmeier. 1994. "Cellular and Molecular Characterization of Ca<sup>2+</sup> Currents in Acutely Isolated, Adult Rat Neostriatal Neurons." *The Journal of Neuroscience: The Official Journal of the Society for Neuroscience* 14 (11 Pt 1) (November): 6667–6686.
- Barrett, Curtis F, and Richard W Tsien. 2008. "The Timothy Syndrome Mutation Differentially Affects Voltage- and Calcium-Dependent Inactivation of CaV1.2 L-Type Calcium Channels." *Proceedings of the National Academy of Sciences of the United States of America* 105 (6) (February 12): 2157–2162. doi:10.1073/pnas.0710501105.
- Bartol, T M, Jr, B R Land, E E Salpeter, and M M Salpeter. 1991. "Monte Carlo Simulation of Miniature Endplate Current Generation in the Vertebrate Neuromuscular Junction." *Biophysical Journal* 59 (6) (June): 1290–1307. doi:10.1016/S0006-3495(91)82344-X.
- Bell, D C, A J Butcher, N S Berrow, K M Page, P F Brust, A Nesterova, K A Stauderman, G R Seabrook, B Nürnberg, and A C Dolphin. 2001. "Biophysical Properties, Pharmacology, and Modulation of Human, Neuronal L-Type (alpha(1D), Ca(V)1.3) Voltage-Dependent Calcium Currents." *Journal of Neurophysiology* 85 (2) (February): 816–827.
- Bender, Vanessa A, Kevin J Bender, Daniel J Brasier, and Daniel E Feldman. 2006. "Two Coincidence Detectors for Spike Timing-Dependent Plasticity in Somatosensory Cortex." *The Journal of Neuroscience: The Official Journal of the Society for Neuroscience* 26 (16) (April 19): 4166–4177. doi:10.1523/JNEUROSCI.0176-06.2006.
- Berkefeld, Henrike, Claudia A Sailer, Wolfgang Bildl, Volker Rohde, Jörg-Oliver Thumfart, Silke Eble, Norbert Klugbauer, et al. 2006. "BKCa-Cav Channel Complexes Mediate Rapid and Localized Ca<sup>2+</sup>-Activated K<sup>+</sup> Signaling." *Science (New York, N.Y.)* 314 (5799) (October 27): 615–620. doi:10.1126/science.1132915.
- Berlanga, M L, D L Price, B S Phung, R Giuly, M Terada, N Yamada, M Cyr, et al. 2011. "Multiscale Imaging Characterization of Dopamine Transporter Knockout Mice Reveals Regional Alterations in Spine Density of Medium Spiny Neurons." *Brain Research* 1390 (May 16): 41–49. doi:10.1016/j.brainres.2011.03.044.

- Bi, G, and M Poo. 2001. "Synaptic Modification by Correlated Activity: Hebb's Postulate Revisited." *Annual Review of Neuroscience* 24: 139–166. doi:10.1146/annurev.neuro.24.1.139.
- Bi, G Q, and M M Poo. 1998. "Synaptic Modifications in Cultured Hippocampal Neurons: Dependence on Spike Timing, Synaptic Strength, and Postsynaptic Cell Type." *The Journal of Neuroscience: The Official Journal of the Society for Neuroscience* 18 (24) (December 15): 10464–10472.
- Blackwell, K T. 2013. "Approaches and Tools for Modeling Signaling Pathways and Calcium Dynamics in Neurons." *Journal of Neuroscience Methods* (June 3). doi:10.1016/j.jneumeth.2013.05.008.
- Bloodgood, Brenda L, and Bernardo L Sabatini. 2007. "Nonlinear Regulation of Unitary Synaptic Signals by CaV(2.3) Voltage-Sensitive Calcium Channels Located in Dendritic Spines." *Neuron* 53 (2) (January 18): 249–260. doi:10.1016/j.neuron.2006.12.017.
- Blue, M E, and J G Parnavelas. 1983. "The Formation and Maturation of Synapses in the Visual Cortex of the Rat. I. Qualitative Analysis." *Journal of Neurocytology* 12 (4) (August): 599–616.
- Brevi, S, M de Curtis, and J Magistretti. 2001. "Pharmacological and Biophysical Characterization of Voltage-Gated Calcium Currents in the Endopiriform Nucleus of the Guinea Pig." *Journal of Neurophysiology* 85 (5) (May): 2076–2087.
- Briggman, Kevin L, Moritz Helmstaedter, and Winfried Denk. 2011. "Wiring Specificity in the Direction-Selectivity Circuit of the Retina." *Nature* 471 (7337) (March 10): 183–188. doi:10.1038/nature09818.
- Bush, Daniel, and Yaochu Jin. 2012. "Calcium Control of Triphasic Hippocampal STDP." *Journal of Computational Neuroscience* (May 19). doi:10.1007/s10827-012-0397-5. <http://www.ncbi.nlm.nih.gov/pubmed/22610510>.
- Byrne, Michael J, M Neal Waxham, and Yoshihisa Kubota. 2010. "Cellular Dynamic Simulator: An Event Driven Molecular Simulation Environment for Cellular Physiology." *Neuroinformatics* 8 (2) (June): 63–82. doi:10.1007/s12021-010-9066-x.
- Calabresi, P, P Gubellini, D Centonze, B Picconi, G Bernardi, K Chergui, P Svenningsson, A A Fienberg, and P Greengard. 2000. "Dopamine and cAMP-Regulated Phosphoprotein 32 kDa Controls Both Striatal Long-Term Depression and Long-Term Potentiation, Opposing Forms of Synaptic Plasticity." *The*

*Journal of Neuroscience: The Official Journal of the Society for Neuroscience* 20 (22) (November 15): 8443–8451.

Calabresi, P, R Maj, A Pisani, N B Mercuri, and G Bernardi. 1992. “Long-Term Synaptic Depression in the Striatum: Physiological and Pharmacological Characterization.” *The Journal of Neuroscience: The Official Journal of the Society for Neuroscience* 12 (11) (November): 4224–4233.

Calabresi, P, N B Mercuri, A Stefani, and G Bernardi. 1990. “Synaptic and Intrinsic Control of Membrane Excitability of Neostriatal Neurons. I. An in Vivo Analysis.” *Journal of Neurophysiology* 63 (4) (April): 651–662.

Calabresi, P., A. Pisani, N. B. Mercuri, and G. Bernardi. 1992. “Long-Term Potentiation in the Striatum Is Unmasked by Removing the Voltage-Dependent Magnesium Block of NMDA Receptor Channels.” *The European Journal of Neuroscience* 4 (10): 929–935.

Calabresi, Paolo, Francesca Galletti, Emanuele Saggese, Veronica Ghiglieri, and Barbara Picconi. 2007. “Neuronal Networks and Synaptic Plasticity in Parkinson’s Disease: Beyond Motor Deficits.” *Parkinsonism & Related Disorders* 13 Suppl 3: S259–262. doi:10.1016/S1353-8020(08)70013-0.

Carlson, Kristofor D, and Nicholas Giordano. 2011. “Interplay of the Magnitude and Time-Course of Postsynaptic Ca<sup>2+</sup> Concentration in Producing Spike Timing-Dependent Plasticity.” *Journal of Computational Neuroscience* 30 (3) (June): 747–758. doi:10.1007/s10827-010-0290-z.

Carr, D W, R E Stofko-Hahn, I D Fraser, R D Cone, and J D Scott. 1992. “Localization of the cAMP-Dependent Protein Kinase to the Postsynaptic Densities by A-Kinase Anchoring Proteins. Characterization of AKAP 79.” *The Journal of Biological Chemistry* 267 (24) (August 25): 16816–16823.

Carter, Adam G, and Bernardo L Sabatini. 2004. “State-Dependent Calcium Signaling in Dendritic Spines of Striatal Medium Spiny Neurons.” *Neuron* 44 (3) (October 28): 483–493. doi:10.1016/j.neuron.2004.10.013.

Carter, Adam G, Gilberto J Soler-Llavina, and Bernardo L Sabatini. 2007. “Timing and Location of Synaptic Inputs Determine Modes of Subthreshold Integration in Striatal Medium Spiny Neurons.” *The Journal of Neuroscience: The Official Journal of the Society for Neuroscience* 27 (33) (August 15): 8967–8977. doi:10.1523/JNEUROSCI.2798-07.2007.

Centonze, Diego, Cristina Grande, Emilia Saulle, Ana B Martin, Paolo Gubellini, Nancy Pavón, Antonio Pisani, Giorgio Bernardi, Rosario Moratalla, and Paolo Calabresi.

2003. “Distinct Roles of D1 and D5 Dopamine Receptors in Motor Activity and Striatal Synaptic Plasticity.” *The Journal of Neuroscience: The Official Journal of the Society for Neuroscience* 23 (24) (September 17): 8506–8512.
- Centonze, Diego, Alessandro Usiello, Cinzia Costa, Barbara Picconi, Eric Erbs, Giorgio Bernardi, Emiliana Borrelli, and Paolo Calabresi. 2004. “Chronic Haloperidol Promotes Corticostriatal Long-Term Potentiation by Targeting Dopamine D2L Receptors.” *The Journal of Neuroscience: The Official Journal of the Society for Neuroscience* 24 (38) (September 22): 8214–8222. doi:10.1523/JNEUROSCI.1274-04.2004.
- Chad, J, D Kalman, and D Armstrong. 1987. “The Role of Cyclic AMP-Dependent Phosphorylation in the Maintenance and Modulation of Voltage-Activated Calcium Channels.” *Society of General Physiologists Series* 42: 167–186.
- Chapman, David E, Kristen A Keefe, and Karen S Wilcox. 2003. “Evidence for Functionally Distinct Synaptic NMDA Receptors in Ventromedial versus Dorsolateral Striatum.” *Journal of Neurophysiology* 89 (1) (January): 69–80. doi:10.1152/jn.00342.2002.
- Charpier, S, and J M Deniau. 1997. “In Vivo Activity-Dependent Plasticity at Cortico-Striatal Connections: Evidence for Physiological Long-Term Potentiation.” *Proceedings of the National Academy of Sciences of the United States of America* 94 (13) (June 24): 7036–7040.
- Chavis, P, P Mollard, J Bockaert, and O Manzoni. 1998. “Visualization of Cyclic AMP-Regulated Presynaptic Activity at Cerebellar Granule Cells.” *Neuron* 20 (4) (April): 773–781.
- Chen, N, T Luo, and L A Raymond. 1999. “Subtype-Dependence of NMDA Receptor Channel Open Probability.” *The Journal of Neuroscience: The Official Journal of the Society for Neuroscience* 19 (16) (August 15): 6844–6854.
- Chen, Tsai-Wen, Trevor J Wardill, Yi Sun, Stefan R Pulver, Sabine L Renninger, Amy Baohan, Eric R Schreier, et al. 2013. “Ultrasensitive Fluorescent Proteins for Imaging Neuronal Activity.” *Nature* 499 (7458) (July 18): 295–300. doi:10.1038/nature12354.
- Chen, Xiaowei, Ulrich Leischner, Zsuzsanna Varga, Hongbo Jia, Diana Deca, Nathalie L Rochefort, and Arthur Konnerth. 2012. “LOTOS-Based Two-Photon Calcium Imaging of Dendritic Spines in Vivo.” *Nature Protocols* 7 (10) (October): 1818–1829. doi:10.1038/nprot.2012.106.

- Cho, K, J P Aggleton, M W Brown, and Z I Bashir. 2001. "An Experimental Test of the Role of Postsynaptic Calcium Levels in Determining Synaptic Strength Using Perirhinal Cortex of Rat." *The Journal of Physiology* 532 (Pt 2) (April 15): 459–466.
- Churchill, D, and B A Macvicar. 1998. "Biophysical and Pharmacological Characterization of Voltage-Dependent Ca<sup>2+</sup> Channels in Neurons Isolated from Rat Nucleus Accumbens." *Journal of Neurophysiology* 79 (2) (February): 635–647.
- Colledge, M, R A Dean, G K Scott, L K Langeberg, R L Huganir, and J D Scott. 2000. "Targeting of PKA to Glutamate Receptors through a MAGUK-AKAP Complex." *Neuron* 27 (1) (July): 107–119.
- Cormier, R J, A C Greenwood, and J A Connor. 2001. "Bidirectional Synaptic Plasticity Correlated with the Magnitude of Dendritic Calcium Transients above a Threshold." *Journal of Neurophysiology* 85 (1) (January): 399–406.
- Cowan, Ann E, Ion I Moraru, James C Schaff, Boris M Slepchenko, and Leslie M Loew. 2012. "Spatial Modeling of Cell Signaling Networks." *Methods in Cell Biology* 110: 195–221. doi:10.1016/B978-0-12-388403-9.00008-4.
- Cummings, J A, R M Mulkey, R A Nicoll, and R C Malenka. 1996. "Ca<sup>2+</sup> Signaling Requirements for Long-Term Depression in the Hippocampus." *Neuron* 16 (4) (April): 825–833.
- Davare, Monika A, and Johannes W Hell. 2003. "Increased Phosphorylation of the Neuronal L-Type Ca(2+) Channel Ca(v)1.2 during Aging." *Proceedings of the National Academy of Sciences of the United States of America* 100 (26) (December 23): 16018–16023. doi:10.1073/pnas.2236970100.
- Day, Michelle, David Wokosin, Joshua L Plotkin, Xinyoung Tian, and D James Surmeier. 2008. "Differential Excitability and Modulation of Striatal Medium Spiny Neuron Dendrites." *The Journal of Neuroscience: The Official Journal of the Society for Neuroscience* 28 (45) (November 5): 11603–11614. doi:10.1523/JNEUROSCI.1840-08.2008.
- Dell'Acqua, Mark L, Karen E Smith, Jessica A Gorski, Eric A Horne, Emily S Gibson, and Lisa L Gomez. 2006. "Regulation of Neuronal PKA Signaling through AKAP Targeting Dynamics." *European Journal of Cell Biology* 85 (7) (July): 627–633. doi:10.1016/j.ejcb.2006.01.010.

- Desai, Niraj S, Robert H Cudmore, Sacha B Nelson, and Gina G Turrigiano. 2002. "Critical Periods for Experience-Dependent Synaptic Scaling in Visual Cortex." *Nature Neuroscience* 5 (8) (August): 783–789. doi:10.1038/nn878.
- Dessauer, Carmen W. 2009. "Adenylyl Cyclase--A-Kinase Anchoring Protein Complexes: The next Dimension in cAMP Signaling." *Molecular Pharmacology* 76 (5) (November): 935–941. doi:10.1124/mol.109.059345.
- Ding, Jun, Jayms D Peterson, and D James Surmeier. 2008. "Corticostriatal and Thalamostriatal Synapses Have Distinctive Properties." *The Journal of Neuroscience: The Official Journal of the Society for Neuroscience* 28 (25) (June 18): 6483–6492. doi:10.1523/JNEUROSCI.0435-08.2008.
- Dumas, Theodore C. 2004. "Early Eyelid Opening Enhances Spontaneous Alternation and Accelerates the Development of Perforant Path Synaptic Strength in the Hippocampus of Juvenile Rats." *Developmental Psychobiology* 45 (1) (July): 1–9. doi:10.1002/dev.20011.
- Dunia, R, G Buckwalter, T Defazio, F D Villar, T H McNeill, and J P Walsh. 1996. "Decreased Duration of Ca(2+)-Mediated Plateau Potentials in Striatal Neurons from Aged Rats." *Journal of Neurophysiology* 76 (4) (October): 2353–2363.
- Efendiev, Riad, Bret K Samelson, Bao T Nguyen, Prasad V Phatarpekar, Faiza Baameur, John D Scott, and Carmen W Dessauer. 2010. "AKAP79 Interacts with Multiple Adenylyl Cyclase (AC) Isoforms and Scaffolds AC5 and -6 to Alpha-Amino-3-Hydroxyl-5-Methyl-4-Isoxazole-Propionate (AMPA) Receptors." *The Journal of Biological Chemistry* 285 (19) (May 7): 14450–14458. doi:10.1074/jbc.M110.109769.
- Esteban, José A, Song-Hai Shi, Christopher Wilson, Mutsuo Nuriya, Richard L Huganir, and Roberto Malinow. 2003. "PKA Phosphorylation of AMPA Receptor Subunits Controls Synaptic Trafficking Underlying Plasticity." *Nature Neuroscience* 6 (2) (February): 136–143. doi:10.1038/nn997.
- Evans, Rebekah C, Yash M Maniar, and Kim T Blackwell. 2013. "Dynamic Modulation of Spike Timing Dependent Calcium Influx during Cortico-Striatal Upstates." *Journal of Neurophysiology* (July 10). doi:10.1152/jn.00232.2013.
- Evans, Rebekah C, Teresa Morera-Herreras, Yihui Cui, Kai Du, Tom Sheehan, Jeanette Hellgren Kotaleski, Laurent Venance, and Kim T Blackwell. 2012. "The Effects of NMDA Subunit Composition on Calcium Influx and Spike Timing-Dependent Plasticity in Striatal Medium Spiny Neurons." *PLoS Computational Biology* 8 (4) (April): e1002493. doi:10.1371/journal.pcbi.1002493.

- Fino, Elodie, Jean-Michel Deniau, and Laurent Venance. 2009. "Brief Subthreshold Events Can Act as Hebbian Signals for Long-Term Plasticity." *PloS One* 4 (8): e6557. doi:10.1371/journal.pone.0006557.
- Fino, Elodie, Jacques Glowinski, and Laurent Venance. 2005. "Bidirectional Activity-Dependent Plasticity at Corticostriatal Synapses." *The Journal of Neuroscience: The Official Journal of the Society for Neuroscience* 25 (49) (December 7): 11279–11287. doi:10.1523/JNEUROSCI.4476-05.2005.
- . 2007. "Effects of Acute Dopamine Depletion on the Electrophysiological Properties of Striatal Neurons." *Neuroscience Research* 58 (3) (July): 305–316. doi:10.1016/j.neures.2007.04.002.
- Fino, Elodie, Vincent Paille, Yihui Cui, Teresa Morera-Herreras, Jean-Michel Deniau, and Laurent Venance. 2010. "Distinct Coincidence Detectors Govern the Corticostriatal Spike Timing-Dependent Plasticity." *The Journal of Physiology* 588 (Pt 16) (August 15): 3045–3062. doi:10.1113/jphysiol.2010.188466.
- Fino, Elodie, Vincent Paillé, Kai Du, Teresa Morera-Herreras, Jeanette Hellgren Kotaleski, and Laurent Venance. 2011. "GABA Operates as a Hebbian/anti-Hebbian Switch for Spike-Timing-Dependent Plasticity." In Vol. Program No. 348.03. Washington DC: Neuroscience Meeting Planner. online.
- Flores-Barrera, Edén, Antonio Laville, Victor Plata, Dagoberto Tapia, José Bargas, and Elvira Galarraga. 2009. "Inhibitory Contribution to Suprathreshold Corticostriatal Responses: An Experimental and Modeling Study." *Cellular and Molecular Neurobiology* 29 (5) (July): 719–731. doi:10.1007/s10571-009-9394-2.
- Foehring, R C, P G Mermelstein, W J Song, S Ulrich, and D J Surmeier. 2000. "Unique Properties of R-Type Calcium Currents in Neocortical and Neostriatal Neurons." *Journal of Neurophysiology* 84 (5) (November): 2225–2236.
- Forest, Amelie, Matthew T Swulius, Joyce K Y Tse, J Michael Bradshaw, Tara Gaertner, and M Neal Waxham. 2008. "Role of the N- and C-Lobes of Calmodulin in the Activation of Ca(2+)/calmodulin-Dependent Protein Kinase II." *Biochemistry* 47 (40) (October 7): 10587–10599. doi:10.1021/bi8007033.
- Foster, Kelly A, Nathan McLaughlin, Dieter Edbauer, Marnie Phillips, Andrew Bolton, Martha Constantine-Paton, and Morgan Sheng. 2010. "Distinct Roles of NR2A and NR2B Cytoplasmic Tails in Long-Term Potentiation." *The Journal of Neuroscience: The Official Journal of the Society for Neuroscience* 30 (7) (February 17): 2676–2685. doi:10.1523/JNEUROSCI.4022-09.2010.

- Froemke, Robert C, Mu-Ming Poo, and Yang Dan. 2005. "Spike-Timing-Dependent Synaptic Plasticity Depends on Dendritic Location." *Nature* 434 (7030) (March 10): 221–225. doi:10.1038/nature03366.
- Fuenzalida, Marco, David Fernández de Sevilla, Alejandro Couve, and Washington Buño. 2010. "Role of AMPA and NMDA Receptors and Back-Propagating Action Potentials in Spike Timing-Dependent Plasticity." *Journal of Neurophysiology* 103 (1) (January): 47–54. doi:10.1152/jn.00416.2009.
- Gamble, E, and C Koch. 1987. "The Dynamics of Free Calcium in Dendritic Spines in Response to Repetitive Synaptic Input." *Science (New York, N.Y.)* 236 (4806) (June 5): 1311–1315.
- Gardoni, Fabrizio, Barbara Picconi, Veronica Ghiglieri, Federica Polli, Vincenza Bagetta, Giorgio Bernardi, Flaminio Cattabeni, Monica Di Luca, and Paolo Calabresi. 2006. "A Critical Interaction between NR2B and MAGUK in L-DOPA Induced Dyskinesia." *The Journal of Neuroscience: The Official Journal of the Society for Neuroscience* 26 (11) (March 15): 2914–2922. doi:10.1523/JNEUROSCI.5326-05.2006.
- Gertler, Tracy S, C Savio Chan, and D James Surmeier. 2008. "Dichotomous Anatomical Properties of Adult Striatal Medium Spiny Neurons." *The Journal of Neuroscience: The Official Journal of the Society for Neuroscience* 28 (43) (October 22): 10814–10824. doi:10.1523/JNEUROSCI.2660-08.2008.
- Goldberg, Joshua A, Mark A Teagarden, Robert C Foehring, and Charles J Wilson. 2009. "Nonequilibrium Calcium Dynamics Regulate the Autonomous Firing Pattern of Rat Striatal Cholinergic Interneurons." *The Journal of Neuroscience: The Official Journal of the Society for Neuroscience* 29 (26) (July 1): 8396–8407. doi:10.1523/JNEUROSCI.5582-08.2009.
- Götz, T, U Kraushaar, J Geiger, J Lübke, T Berger, and P Jonas. 1997. "Functional Properties of AMPA and NMDA Receptors Expressed in Identified Types of Basal Ganglia Neurons." *The Journal of Neuroscience: The Official Journal of the Society for Neuroscience* 17 (1) (January 1): 204–215.
- Graupner, Michael, and Nicolas Brunel. 2012. "Calcium-Based Plasticity Model Explains Sensitivity of Synaptic Changes to Spike Pattern, Rate, and Dendritic Location." *Proceedings of the National Academy of Sciences of the United States of America* (February 22). doi:10.1073/pnas.1109359109. <http://www.ncbi.nlm.nih.gov/pubmed/22357758>.

- Grover, L M, and T J Teyler. 1990. "Two Components of Long-Term Potentiation Induced by Different Patterns of Afferent Activation." *Nature* 347 (6292) (October 4): 477–479. doi:10.1038/347477a0.
- Gruber, Aaron J, Sara A Solla, D James Surmeier, and James C Houk. 2003. "Modulation of Striatal Single Units by Expected Reward: A Spiny Neuron Model Displaying Dopamine-Induced Bistability." *Journal of Neurophysiology* 90 (2) (August): 1095–1114. doi:10.1152/jn.00618.2002.
- Halavi, Maryam, Sridevi Polavaram, Duncan E Donohue, Gail Hamilton, Jeffrey Hoyt, Kenneth P Smith, and Giorgio A Ascoli. 2008. "NeuroMorpho.Org Implementation of Digital Neuroscience: Dense Coverage and Integration with the NIF." *Neuroinformatics* 6 (3) (September): 241–252. doi:10.1007/s12021-008-9030-1.
- Hallett, Penelope J, and David G Standaert. 2004. "Rationale for and Use of NMDA Receptor Antagonists in Parkinson's Disease." *Pharmacology & Therapeutics* 102 (2) (May): 155–174. doi:10.1016/j.pharmthera.2004.04.001.
- Hansel, C, A Artola, and W Singer. 1996. "Different Threshold Levels of Postsynaptic [Ca<sup>2+</sup>]<sub>i</sub> Have to Be Reached to Induce LTP and LTD in Neocortical Pyramidal Cells." *Journal of Physiology, Paris* 90 (5-6): 317–319.
- Hardingham, Giles E, and Hilmar Bading. 2010. "Synaptic versus Extrasynaptic NMDA Receptor Signalling: Implications for Neurodegenerative Disorders." *Nature Reviews. Neuroscience* 11 (10) (October): 682–696. doi:10.1038/nrn2911.
- Hatton, Christopher J, and Pierre Paoletti. 2005. "Modulation of Triheteromeric NMDA Receptors by N-Terminal Domain Ligands." *Neuron* 46 (2) (April 21): 261–274. doi:10.1016/j.neuron.2005.03.005.
- Hawes, Sarah Louise, Fawad Gillani, Rebekah Coleman Evans, Elizabeth A Benkert, and Kim T Blackwell. 2013. "Sensitivity to Theta-Burst Timing Permits LTP in Dorsal Striatal Adult Brain Slice." *Journal of Neurophysiology* (August 7). doi:10.1152/jn.00115.2013.
- Herberg, F W, A Maleszka, T Eide, L Vossebein, and K Tasken. 2000. "Analysis of A-Kinase Anchoring Protein (AKAP) Interaction with Protein Kinase A (PKA) Regulatory Subunits: PKA Isoform Specificity in AKAP Binding." *Journal of Molecular Biology* 298 (2) (April 28): 329–339. doi:10.1006/jmbi.2000.3662.
- Hevers, W, and H Lüddens. 2002. "Pharmacological Heterogeneity of Gamma-Aminobutyric Acid Receptors during Development Suggests Distinct Classes of

- Rat Cerebellar Granule Cells in Situ.” *Neuropharmacology* 42 (1) (January): 34–47.
- Higley, Michael J, and Bernardo L Sabatini. 2010. “Competitive Regulation of Synaptic Ca<sup>2+</sup> Influx by D2 Dopamine and A2A Adenosine Receptors.” *Nature Neuroscience* 13 (8) (August): 958–966. doi:10.1038/nn.2592.
- Hires, Samuel Andrew, Yongling Zhu, and Roger Y Tsien. 2008. “Optical Measurement of Synaptic Glutamate Spillover and Reuptake by Linker Optimized Glutamate-Sensitive Fluorescent Reporters.” *Proceedings of the National Academy of Sciences of the United States of America* 105 (11) (March 18): 4411–4416. doi:10.1073/pnas.0712008105.
- Hjorth, Johannes, Kim T Blackwell, and Jeanette Hellgren Kotaleski. 2009. “Gap Junctions between Striatal Fast-Spiking Interneurons Regulate Spiking Activity and Synchronization as a Function of Cortical Activity.” *The Journal of Neuroscience: The Official Journal of the Society for Neuroscience* 29 (16) (April 22): 5276–5286. doi:10.1523/JNEUROSCI.6031-08.2009.
- Holbro, Niklaus, Asa Grunditz, J Simon Wiegert, and Thomas G Oertner. 2010. “AMPA Receptors Gate Spine Ca<sup>2+</sup> Transients and Spike-Timing-Dependent Potentiation.” *Proceedings of the National Academy of Sciences of the United States of America* 107 (36) (September 7): 15975–15980. doi:10.1073/pnas.1004562107.
- Hopf, F Woodward, Taban Seif, Maysha L Mohamedi, Billy T Chen, and Antonello Bonci. 2010. “The Small-Conductance Calcium-Activated Potassium Channel Is a Key Modulator of Firing and Long-Term Depression in the Dorsal Striatum.” *The European Journal of Neuroscience* 31 (11) (June): 1946–1959. doi:10.1111/j.1460-9568.2010.07231.x.
- Huang, Ted, Conor B McDonough, and Ted Abel. 2006. “Compartmentalized PKA Signaling Events Are Required for Synaptic Tagging and Capture during Hippocampal Late-Phase Long-Term Potentiation.” *European Journal of Cell Biology* 85 (7) (July): 635–642. doi:10.1016/j.ejcb.2006.02.005.
- Isaacson, J S, and G J Murphy. 2001. “Glutamate-Mediated Extrasynaptic Inhibition: Direct Coupling of NMDA Receptors to Ca<sup>2+</sup>-Activated K<sup>+</sup> Channels.” *Neuron* 31 (6) (September 27): 1027–1034.
- Jurado, Sandra, Virginie Biou, and Robert C Malenka. 2010. “A calcineurin/AKAP Complex Is Required for NMDA Receptor-Dependent Long-Term Depression.” *Nature Neuroscience* 13 (9) (September): 1053–1055. doi:10.1038/nn.2613.

- Kasai, H, and E Neher. 1992. "Dihydropyridine-Sensitive and Omega-Conotoxin-Sensitive Calcium Channels in a Mammalian Neuroblastoma-Glioma Cell Line." *The Journal of Physiology* 448 (March): 161–188.
- Kasanetz, Fernando, Luis A Riquelme, Patricio O'Donnell, and M Gustavo Murer. 2006. "Turning off Cortical Ensembles Stops Striatal Up States and Elicits Phase Perturbations in Cortical and Striatal Slow Oscillations in Rat in Vivo." *The Journal of Physiology* 577 (Pt 1) (November 15): 97–113. doi:10.1113/jphysiol.2006.113050.
- Kawaguchi, Y. 1993. "Physiological, Morphological, and Histochemical Characterization of Three Classes of Interneurons in Rat Neostriatum." *The Journal of Neuroscience: The Official Journal of the Society for Neuroscience* 13 (11) (November): 4908–4923.
- Keller, Daniel X, Kevin M Franks, Thomas M Bartol Jr, and Terrence J Sejnowski. 2008. "Calmodulin Activation by Calcium Transients in the Postsynaptic Density of Dendritic Spines." *PloS One* 3 (4): e2045. doi:10.1371/journal.pone.0002045.
- Kerr, Jason N D, and Dietmar Plenz. 2002. "Dendritic Calcium Encodes Striatal Neuron Output during up-States." *The Journal of Neuroscience: The Official Journal of the Society for Neuroscience* 22 (5) (March 1): 1499–1512.
- . 2004. "Action Potential Timing Determines Dendritic Calcium during Striatal up-States." *The Journal of Neuroscience: The Official Journal of the Society for Neuroscience* 24 (4) (January 28): 877–885. doi:10.1523/JNEUROSCI.4475-03.2004.
- Kim, MyungSook, Ted Huang, Ted Abel, and Kim T Blackwell. 2010. "Temporal Sensitivity of Protein Kinase a Activation in Late-Phase Long Term Potentiation." *PLoS Computational Biology* 6 (2) (February): e1000691. doi:10.1371/journal.pcbi.1000691.
- Koester, H J, and B Sakmann. 1998. "Calcium Dynamics in Single Spines during Coincident Pre- and Postsynaptic Activity Depend on Relative Timing of Back-Propagating Action Potentials and Subthreshold Excitatory Postsynaptic Potentials." *Proceedings of the National Academy of Sciences of the United States of America* 95 (16) (August 4): 9596–9601.
- Konur, Sila, and Rafael Yuste. 2004. "Developmental Regulation of Spine and Filopodial Motility in Primary Visual Cortex: Reduced Effects of Activity and Sensory Deprivation." *Journal of Neurobiology* 59 (2) (May): 236–246. doi:10.1002/neu.10306.

- Koos, Tibor, James M Tepper, and Charles J Wilson. 2004. "Comparison of IPSCs Evoked by Spiny and Fast-Spiking Neurons in the Neostriatum." *The Journal of Neuroscience: The Official Journal of the Society for Neuroscience* 24 (36) (September 8): 7916–7922. doi:10.1523/JNEUROSCI.2163-04.2004.
- Kotaleski, J Hellgren, D Plenz, and K T Blackwell. 2006. "Using Potassium Currents to Solve Signal-to-Noise Problems in Inhibitory Feedforward Networks of the Striatum." *Journal of Neurophysiology* 95 (1) (January): 331–341. doi:10.1152/jn.00063.2005.
- Kotaleski, Jeanette Hellgren, and Kim T Blackwell. 2010. "Modelling the Molecular Mechanisms of Synaptic Plasticity Using Systems Biology Approaches." *Nature Reviews. Neuroscience* 11 (4) (April): 239–251. doi:10.1038/nrn2807.
- Kubota, Yoshihisa, and M Neal Waxham. 2010. "Lobe Specific Ca<sup>2+</sup>-Calmodulin Nano-Domain in Neuronal Spines: A Single Molecule Level Analysis." *PLoS Computational Biology* 6 (11): e1000987. doi:10.1371/journal.pcbi.1000987.
- Kung, V W S, R Hassam, A J Morton, and S Jones. 2007. "Dopamine-Dependent Long Term Potentiation in the Dorsal Striatum Is Reduced in the R6/2 Mouse Model of Huntington's Disease." *Neuroscience* 146 (4) (June 8): 1571–1580. doi:10.1016/j.neuroscience.2007.03.036.
- Lansink, Carien S, Pieter M Goltstein, Jan V Lankelma, Bruce L McNaughton, and Cyriel M A Pennartz. 2009. "Hippocampus Leads Ventral Striatum in Replay of Place-Reward Information." *PLoS Biology* 7 (8) (August): e1000173. doi:10.1371/journal.pbio.1000173.
- Laurie, D J, and P H Seeburg. 1994. "Ligand Affinities at Recombinant N-Methyl-D-Aspartate Receptors Depend on Subunit Composition." *European Journal of Pharmacology* 268 (3) (August 16): 335–345.
- Lester, Linda B., Lorene K. Langeberg, and John D. Scott. 1997. "Anchoring of Protein Kinase A Facilitates Hormone-Mediated Insulin Secretion." *Proceedings of the National Academy of Sciences of the United States of America* 94 (26) (December 23): 14942–14947.
- Li, Lijun, Mannie Fan, Carolyn D Icton, Nansheng Chen, Blair R Leavitt, Michael R Hayden, Tim H Murphy, and Lynn A Raymond. 2003. "Role of NR2B-Type NMDA Receptors in Selective Neurodegeneration in Huntington Disease." *Neurobiology of Aging* 24 (8) (December): 1113–1121.
- Li, Lijun, Timothy H Murphy, Michael R Hayden, and Lynn A Raymond. 2004. "Enhanced Striatal NR2B-Containing N-Methyl-D-Aspartate Receptor-Mediated

- Synaptic Currents in a Mouse Model of Huntington Disease.” *Journal of Neurophysiology* 92 (5) (November): 2738–2746. doi:10.1152/jn.00308.2004.
- Li, Lu, Melanie I Stefan, and Nicolas Le Novère. 2012. “Calcium Input Frequency, Duration and Amplitude Differentially Modulate the Relative Activation of Calcineurin and CaMKII.” *PloS One* 7 (9): e43810. doi:10.1371/journal.pone.0043810.
- Li, Ping, Yan-Hai Li, and Tai-Zhen Han. 2009. “NR2A-Containing NMDA Receptors Are Required for LTP Induction in Rat Dorsolateral Striatum in Vitro.” *Brain Research* 1274 (June 5): 40–46. doi:10.1016/j.brainres.2009.04.016.
- Liang, Haoya, Carla D DeMaria, Michael G Erickson, Masayuki X Mori, Badr A Alseikhan, and David T Yue. 2003a. “Unified Mechanisms of Ca<sup>2+</sup> Regulation across the Ca<sup>2+</sup> Channel Family.” *Neuron* 39 (6) (September 11): 951–960.
- . 2003b. “Unified Mechanisms of Ca<sup>2+</sup> Regulation across the Ca<sup>2+</sup> Channel Family.” *Neuron* 39 (6) (September 11): 951–960.
- Liao, Ping, and Tuck Wah Soong. 2010. “CaV1.2 Channelopathies: From Arrhythmias to Autism, Bipolar Disorder, and Immunodeficiency.” *Pflügers Archiv: European Journal of Physiology* 460 (2) (July): 353–359. doi:10.1007/s00424-009-0753-0.
- Lin, Yi-Wen, Ming-Yuan Min, Tsai-Hsien Chiu, and Hsiu-Wen Yang. 2003. “Enhancement of Associative Long-Term Potentiation by Activation of Beta-Adrenergic Receptors at CA1 Synapses in Rat Hippocampal Slices.” *The Journal of Neuroscience: The Official Journal of the Society for Neuroscience* 23 (10) (May 15): 4173–4181.
- Lisman, J. 1989. “A Mechanism for the Hebb and the Anti-Hebb Processes Underlying Learning and Memory.” *Proceedings of the National Academy of Sciences of the United States of America* 86 (23) (December): 9574–9578.
- Liu, Dan-dan, Qian Yang, and Sheng-tian Li. 2013. “Activation of Extrasynaptic NMDA Receptors Induces LTD in Rat Hippocampal CA1 Neurons.” *Brain Research Bulletin* 93 (April): 10–16. doi:10.1016/j.brainresbull.2012.12.003.
- Logan, Stephen M, John G Partridge, Jose A Matta, Andres Buonanno, and Stefano Vicini. 2007. “Long-Lasting NMDA Receptor-Mediated EPSCs in Mouse Striatal Medium Spiny Neurons.” *Journal of Neurophysiology* 98 (5) (November): 2693–2704. doi:10.1152/jn.00462.2007.
- Mahon, Séverine, Nicolas Vautrelle, Laurent Pezard, Seán J Slaght, Jean-Michel Deniau, Guy Chouvet, and Stéphane Charpier. 2006. “Distinct Patterns of Striatal Medium

- Spiny Neuron Activity during the Natural Sleep-Wake Cycle.” *The Journal of Neuroscience: The Official Journal of the Society for Neuroscience* 26 (48) (November 29): 12587–12595. doi:10.1523/JNEUROSCI.3987-06.2006.
- Markram, H, A Roth, and F Helmchen. 1998. “Competitive Calcium Binding: Implications for Dendritic Calcium Signaling.” *Journal of Computational Neuroscience* 5 (3) (July): 331–348.
- Martella, G, G Madeo, T Schirinzi, A Tassone, G Sciamanna, F Spadoni, A Stefani, J Shen, A Pisani, and P Bonsi. 2011. “Altered Profile and D2-Dopamine Receptor Modulation of High Voltage-Activated Calcium Current in Striatal Medium Spiny Neurons from Animal Models of Parkinson’s Disease.” *Neuroscience* 177 (March 17): 240–251. doi:10.1016/j.neuroscience.2010.12.057.
- Martella, G., F. Spadoni, G. Sciamanna, A. Tassone, G. Bernardi, A. Pisani, and P. Bonsi. 2008. “Age-Related Functional Changes of High-Voltage-Activated Calcium Channels in Different Neuronal Subtypes of Mouse Striatum.” *Neuroscience* 152 (2) (March 18): 469–476. doi:10.1016/j.neuroscience.2007.12.040.
- Maylie, James, Chris T Bond, Paco S Herson, Wei-Sheng Lee, and John P Adelman. 2004. “Small Conductance Ca<sup>2+</sup>-Activated K<sup>+</sup> Channels and Calmodulin.” *The Journal of Physiology* 554 (Pt 2) (January 15): 255–261. doi:10.1113/jphysiol.2003.049072.
- McCaw, Elizabeth A, Haibei Hu, Geraldine T Gomez, Andrea L O Hebb, Melanie E M Kelly, and Eileen M Denovan-Wright. 2004. “Structure, Expression and Regulation of the Cannabinoid Receptor Gene (CB1) in Huntington’s Disease Transgenic Mice.” *European Journal of Biochemistry / FEBS* 271 (23-24) (December): 4909–4920. doi:10.1111/j.1432-1033.2004.04460.x.
- McNaughton, N C, and A D Randall. 1997. “Electrophysiological Properties of the Human N-Type Ca<sup>2+</sup> Channel: I. Channel Gating in Ca<sup>2+</sup>, Ba<sup>2+</sup> and Sr<sup>2+</sup> Containing Solutions.” *Neuropharmacology* 36 (7) (July): 895–915.
- McRory, J E, C M Santi, K S Hamming, J Mezeyova, K G Sutton, D L Baillie, A Stea, and T P Snutch. 2001. “Molecular and Functional Characterization of a Family of Rat Brain T-Type Calcium Channels.” *The Journal of Biological Chemistry* 276 (6) (February 9): 3999–4011. doi:10.1074/jbc.M008215200.
- Micheva, Kristina D, Brad Busse, Nicholas C Weiler, Nancy O’Rourke, and Stephen J Smith. 2010. “Single-Synapse Analysis of a Diverse Synapse Population: Proteomic Imaging Methods and Markers.” *Neuron* 68 (4) (November 18): 639–653. doi:10.1016/j.neuron.2010.09.024.

- Migliore, M. 1996. "Modeling the Attenuation and Failure of Action Potentials in the Dendrites of Hippocampal Neurons." *Biophysical Journal* 71 (5) (November): 2394–2403. doi:10.1016/S0006-3495(96)79433-X.
- Migliore, M, D A Hoffman, J C Magee, and D Johnston. 1999. "Role of an A-Type K<sup>+</sup> Conductance in the Back-Propagation of Action Potentials in the Dendrites of Hippocampal Pyramidal Neurons." *Journal of Computational Neuroscience* 7 (1) (August): 5–15.
- Mihalas, Stefan. 2011. "Calcium Messenger Heterogeneity: A Possible Signal for Spike Timing-Dependent Plasticity." *Frontiers in Computational Neuroscience* 4: 158. doi:10.3389/fncom.2010.00158.
- Milnerwood, Austen J, Clare M Gladding, Mahmoud A Pouladi, Alexandra M Kaufman, Rochelle M Hines, Jamie D Boyd, Rebecca W Y Ko, et al. 2010. "Early Increase in Extrasynaptic NMDA Receptor Signaling and Expression Contributes to Phenotype Onset in Huntington's Disease Mice." *Neuron* 65 (2) (January 28): 178–190. doi:10.1016/j.neuron.2010.01.008.
- Monyer, H, N Burnashev, D J Laurie, B Sakmann, and P H Seeburg. 1994. "Developmental and Regional Expression in the Rat Brain and Functional Properties of Four NMDA Receptors." *Neuron* 12 (3) (March): 529–540.
- Moorthy, Balakrishnan Shenbaga, Yunfeng Gao, and Ganesh S Anand. 2010. "Phosphodiesterases Catalyze Hydrolysis of cAMP-Bound to Regulatory Subunit of Protein Kinase A and Mediate Signal Termination." *Molecular & Cellular Proteomics: MCP* (October 5). doi:10.1074/mcp.M110.002295. <http://www.ncbi.nlm.nih.gov/pubmed/20923972>.
- Moyer, Jason T, John A Wolf, and Leif H Finkel. 2007. "Effects of Dopaminergic Modulation on the Integrative Properties of the Ventral Striatum Medium Spiny Neuron." *Journal of Neurophysiology* 98 (6) (December): 3731–3748. doi:10.1152/jn.00335.2007.
- Mulkey, R M, and R C Malenka. 1992. "Mechanisms Underlying Induction of Homosynaptic Long-Term Depression in Area CA1 of the Hippocampus." *Neuron* 9 (5) (November): 967–975.
- Murase, K, P D Ryu, and M Randic. 1989. "Excitatory and Inhibitory Amino Acids and Peptide-Induced Responses in Acutely Isolated Rat Spinal Dorsal Horn Neurons." *Neuroscience Letters* 103 (1) (August 14): 56–63.

- Murphy, K P, G P Reid, D R Trentham, and T V Bliss. 1997. "Activation of NMDA Receptors Is Necessary for the Induction of Associative Long-Term Potentiation in Area CA1 of the Rat Hippocampal Slice." *The Journal of Physiology* 504 ( Pt 2) (October 15): 379–385.
- Nagy, Gábor, Kerstin Reim, Ulf Matti, Nils Brose, Thomas Binz, Jens Rettig, Erwin Neher, and Jakob B Sørensen. 2004. "Regulation of Releasable Vesicle Pool Sizes by Protein Kinase A-Dependent Phosphorylation of SNAP-25." *Neuron* 41 (3) (February 5): 417–429.
- Naraghi, M, and E Neher. 1997. "Linearized Buffered Ca<sup>2+</sup> Diffusion in Microdomains and Its Implications for Calculation of [Ca<sup>2+</sup>] at the Mouth of a Calcium Channel." *The Journal of Neuroscience: The Official Journal of the Society for Neuroscience* 17 (18) (September 15): 6961–6973.
- Nash, Joanne E, and Jonathan M Brotchie. 2002. "Characterisation of Striatal NMDA Receptors Involved in the Generation of Parkinsonian Symptoms: Intrastratial Microinjection Studies in the 6-OHDA-Lesioned Rat." *Movement Disorders: Official Journal of the Movement Disorder Society* 17 (3) (May): 455–466. doi:10.1002/mds.10107.
- Neveu, D, and R S Zucker. 1996. "Postsynaptic Levels of [Ca<sup>2+</sup>]<sub>i</sub> Needed to Trigger LTD and LTP." *Neuron* 16 (3) (March): 619–629.
- Nevian, Thomas, and Bert Sakmann. 2006. "Spine Ca<sup>2+</sup> Signaling in Spike-Timing-Dependent Plasticity." *The Journal of Neuroscience: The Official Journal of the Society for Neuroscience* 26 (43) (October 25): 11001–11013. doi:10.1523/JNEUROSCI.1749-06.2006.
- Nie, Ting, Conor B McDonough, Ted Huang, Peter V Nguyen, and Ted Abel. 2007. "Genetic Disruption of Protein Kinase A Anchoring Reveals a Role for Compartmentalized Kinase Signaling in Theta-Burst Long-Term Potentiation and Spatial Memory." *The Journal of Neuroscience: The Official Journal of the Society for Neuroscience* 27 (38) (September 19): 10278–10288. doi:10.1523/JNEUROSCI.1602-07.2007.
- Nisenbaum, E S, and C J Wilson. 1995. "Potassium Currents Responsible for Inward and Outward Rectification in Rat Neostriatal Spiny Projection Neurons." *The Journal of Neuroscience: The Official Journal of the Society for Neuroscience* 15 (6) (June): 4449–4463.
- Norris, C M, E M Blalock, K-C Chen, N M Porter, and P W Landfield. 2002. "Calcineurin Enhances L-Type Ca(2+) Channel Activity in Hippocampal Neurons: Increased Effect with Age in Culture." *Neuroscience* 110 (2): 213–225.

- O'Donnell, P, and A A Grace. 1995. "Synaptic Interactions among Excitatory Afferents to Nucleus Accumbens Neurons: Hippocampal Gating of Prefrontal Cortical Input." *The Journal of Neuroscience: The Official Journal of the Society for Neuroscience* 15 (5 Pt 1) (May): 3622–3639.
- Ogata, N, and H Tatebayashi. 1990. "Sodium Current Kinetics in Freshly Isolated Neostriatal Neurones of the Adult Guinea Pig." *Pflügers Archiv: European Journal of Physiology* 416 (5) (July): 594–603.
- Oliveira, Rodrigo F, Myungsook Kim, and Kim T Blackwell. 2012. "Subcellular Location of PKA Controls Striatal Plasticity: Stochastic Simulations in Spiny Dendrites." *PLoS Computational Biology* 8 (2) (February): e1002383. doi:10.1371/journal.pcbi.1002383.
- Oliveira, Rodrigo F, Anna Terrin, Giulietta Di Benedetto, Robert C Cannon, Wonryull Koh, MyungSook Kim, Manuela Zaccolo, and Kim T Blackwell. 2010. "The Role of Type 4 Phosphodiesterases in Generating Microdomains of cAMP: Large Scale Stochastic Simulations." *PloS One* 5 (7): e11725. doi:10.1371/journal.pone.0011725.
- Oliveria, Seth F, Philip J Dittmer, Dong-ho Youn, Mark L Dell'Acqua, and William A Sather. 2012. "Localized Calcineurin Confers Ca<sup>2+</sup>-Dependent Inactivation on Neuronal L-Type Ca<sup>2+</sup> Channels." *The Journal of Neuroscience: The Official Journal of the Society for Neuroscience* 32 (44) (October 31): 15328–15337. doi:10.1523/JNEUROSCI.2302-12.2012.
- Ostroveanu, Anghelus, Eddy A Van der Zee, Amalia M Dolga, Paul G M Luiten, Ulrich L M Eisel, and Ingrid M Nijholt. 2007. "A-Kinase Anchoring Protein 150 in the Mouse Brain Is Concentrated in Areas Involved in Learning and Memory." *Brain Research* 1145 (May 11): 97–107. doi:10.1016/j.brainres.2007.01.117.
- Paille, Vincent, Elodie Fino, Kai Du, Teresa Morera-Herreras, Sylvie Perez, Jeanette Hellgren Kotaleski, and Laurent Venance. 2013. "GABAergic Circuits Control Spike-Timing-Dependent Plasticity." *The Journal of Neuroscience: The Official Journal of the Society for Neuroscience* 33 (22) (May 29): 9353–9363. doi:10.1523/JNEUROSCI.5796-12.2013.
- Paillé, Vincent, Barbara Picconi, Vincenza Bagetta, Veronica Ghiglieri, Carmelo Sgobio, Massimiliano Di Filippo, Maria T Viscomi, et al. 2010. "Distinct Levels of Dopamine Denervation Differentially Alter Striatal Synaptic Plasticity and NMDA Receptor Subunit Composition." *The Journal of Neuroscience: The Official Journal of the Society for Neuroscience* 30 (42) (October 20): 14182–14193. doi:10.1523/JNEUROSCI.2149-10.2010.

- Paoletti, Pierre. 2011. "Molecular Basis of NMDA Receptor Functional Diversity." *The European Journal of Neuroscience* 33 (8) (April): 1351–1365. doi:10.1111/j.1460-9568.2011.07628.x.
- Partridge, J G, K C Tang, and D M Lovinger. 2000. "Regional and Postnatal Heterogeneity of Activity-Dependent Long-Term Changes in Synaptic Efficacy in the Dorsal Striatum." *Journal of Neurophysiology* 84 (3) (September): 1422–1429.
- Paul, S, G L Snyder, H Yokakura, M R Picciotto, A C Nairn, and P J Lombroso. 2000. "The Dopamine/D1 Receptor Mediates the Phosphorylation and Inactivation of the Protein Tyrosine Phosphatase STEP via a PKA-Dependent Pathway." *The Journal of Neuroscience: The Official Journal of the Society for Neuroscience* 20 (15) (August 1): 5630–5638.
- Pauli, Wolfgang M, Alexandra D Clark, Heidi J Guenther, Randall C O'Reilly, and Jerry W Rudy. 2012. "Inhibiting PKM $\zeta$  Reveals Dorsal Lateral and Dorsal Medial Striatum Store the Different Memories Needed to Support Adaptive Behavior." *Learning & Memory (Cold Spring Harbor, N.Y.)* 19 (7): 307–314. doi:10.1101/lm.025148.111.
- Pawlak, Verena, and Jason N D Kerr. 2008. "Dopamine Receptor Activation Is Required for Corticostriatal Spike-Timing-Dependent Plasticity." *The Journal of Neuroscience: The Official Journal of the Society for Neuroscience* 28 (10) (March 5): 2435–2446. doi:10.1523/JNEUROSCI.4402-07.2008.
- Pi, Hyun Jae, and John E Lisman. 2008. "Coupled Phosphatase and Kinase Switches Produce the Tristability Required for Long-Term Potentiation and Long-Term Depression." *The Journal of Neuroscience: The Official Journal of the Society for Neuroscience* 28 (49) (December 3): 13132–13138. doi:10.1523/JNEUROSCI.2348-08.2008.
- Picconi, Barbara, Antonio Pisani, Ilaria Barone, Paola Bonsi, Diego Centonze, Giorgio Bernardi, and Paolo Calabresi. 2005. "Pathological Synaptic Plasticity in the Striatum: Implications for Parkinson's Disease." *Neurotoxicology* 26 (5) (October): 779–783. doi:10.1016/j.neuro.2005.02.002.
- Pidoux, Guillaume, and Kjetil Taskén. 2010. "Specificity and Spatial Dynamics of Protein Kinase A Signaling Organized by A-Kinase-Anchoring Proteins." *Journal of Molecular Endocrinology* 44 (5) (May): 271–284. doi:10.1677/JME-10-0010.

- Plotkin, Joshua L, Michelle Day, and D James Surmeier. 2011. "Synaptically Driven State Transitions in Distal Dendrites of Striatal Spiny Neurons." *Nature Neuroscience* 14 (7): 881–888. doi:10.1038/nn.2848.
- Rall, W. 1969. "Distributions of Potential in Cylindrical Coordinates and Time Constants for a Membrane Cylinder." *Biophysical Journal* 9 (12) (December): 1509–1541. doi:10.1016/S0006-3495(69)86468-4.
- Rankovic, Vladan, Peter Landgraf, Tatyana Kanyshkova, Petra Ehling, Sven G Meuth, Michael R Kreutz, Thomas Budde, and Thomas Munsch. 2011. "Modulation of Calcium-Dependent Inactivation of L-Type Ca<sup>2+</sup> Channels via B-Adrenergic Signaling in Thalamocortical Relay Neurons." *PloS One* 6 (12): e27474. doi:10.1371/journal.pone.0027474.
- Ribeiro, Sidarta, Damien Gervasoni, Ernesto S Soares, Yi Zhou, Shih-Chieh Lin, Janaina Pantoja, Michael Lavine, and Miguel A L Nicolelis. 2004. "Long-Lasting Novelty-Induced Neuronal Reverberation during Slow-Wave Sleep in Multiple Forebrain Areas." *PLoS Biology* 2 (1) (January): E24. doi:10.1371/journal.pbio.0020024.
- Reig R., Silberberg G. (2012) Bilateral and multisensory integration in striatal microcircuits. Program No. 380.11 Neuroscience meeting planner. New Orleans, LA: Society for Neuroscience. 2012. Online.
- Saudargiene, Ausra, Bernd Porr, and Florentin Wörgötter. 2004. "How the Shape of Pre- and Postsynaptic Signals Can Influence STDP: A Biophysical Model." *Neural Computation* 16 (3) (March): 595–625. doi:10.1162/089976604772744929.
- Scheuss, Volker, Ryohei Yasuda, Aleksander Sobczyk, and Karel Svoboda. 2006. "Nonlinear [Ca<sup>2+</sup>] Signaling in Dendrites and Spines Caused by Activity-Dependent Depression of Ca<sup>2+</sup> Extrusion." *The Journal of Neuroscience: The Official Journal of the Society for Neuroscience* 26 (31) (August 2): 8183–8194. doi:10.1523/JNEUROSCI.1962-06.2006.
- Schulz, Jan M, Peter Redgrave, Carsten Mehring, Ad Aertsen, Koreen M Clements, Jeff R Wickens, and John N J Reynolds. 2009. "Short-Latency Activation of Striatal Spiny Neurons via Subcortical Visual Pathways." *The Journal of Neuroscience: The Official Journal of the Society for Neuroscience* 29 (19) (May 13): 6336–6347. doi:10.1523/JNEUROSCI.4815-08.2009.
- Shen, Weixing, Marc Flajolet, Paul Greengard, and D James Surmeier. 2008. "Dichotomous Dopaminergic Control of Striatal Synaptic Plasticity." *Science (New York, N.Y.)* 321 (5890) (August 8): 848–851. doi:10.1126/science.1160575.

- Shen, Weixing, Salvador Hernandez-Lopez, Tatiana Tkatch, Joshua E Held, and D James Surmeier. 2004. "Kv1.2-Containing K<sup>+</sup> Channels Regulate Subthreshold Excitability of Striatal Medium Spiny Neurons." *Journal of Neurophysiology* 91 (3) (March): 1337–1349. doi:10.1152/jn.00414.2003.
- Shen, Weixing, Xinyong Tian, Michelle Day, Sasha Ulrich, Tatiana Tkatch, Neil M Nathanson, and D James Surmeier. 2007. "Cholinergic Modulation of Kir2 Channels Selectively Elevates Dendritic Excitability in Striatopallidal Neurons." *Nature Neuroscience* 10 (11) (November): 1458–1466. doi:10.1038/nn1972.
- Shindou, Tomomi, Mayumi Ochi-Shindou, and Jeffery R Wickens. 2011. "A Ca<sup>2+</sup> Threshold for Induction of Spike-Timing-Dependent Depression in the Mouse Striatum." *The Journal of Neuroscience: The Official Journal of the Society for Neuroscience* 31 (36) (September 7): 13015–13022. doi:10.1523/JNEUROSCI.3206-11.2011.
- Shouval, Harel Z, Mark F Bear, and Leon N Cooper. 2002. "A Unified Model of NMDA Receptor-Dependent Bidirectional Synaptic Plasticity." *Proceedings of the National Academy of Sciences of the United States of America* 99 (16) (August 6): 10831–10836. doi:10.1073/pnas.152343099.
- Sjöström, Per Jesper, and Michael Häusser. 2006. "A Cooperative Switch Determines the Sign of Synaptic Plasticity in Distal Dendrites of Neocortical Pyramidal Neurons." *Neuron* 51 (2) (July 20): 227–238. doi:10.1016/j.neuron.2006.06.017.
- Skeberdis, V Arvydas, Vivien Chevalleyre, C Geoffrey Lau, Jesse H Goldberg, Diana L Pettit, Sylvia O Suadicani, Ying Lin, et al. 2006. "Protein Kinase A Regulates Calcium Permeability of NMDA Receptors." *Nature Neuroscience* 9 (4) (April): 501–510. doi:10.1038/nn1664.
- Smeal, Roy M, Renee C Gaspar, Kristen A Keefe, and Karen S Wilcox. 2007. "A Rat Brain Slice Preparation for Characterizing Both Thalamostriatal and Corticostriatal Afferents." *Journal of Neuroscience Methods* 159 (2) (January 30): 224–235. doi:10.1016/j.jneumeth.2006.07.007.
- Smeal, Roy M, Kristen A Keefe, and Karen S Wilcox. 2008. "Differences in Excitatory Transmission between Thalamic and Cortical Afferents to Single Spiny Efferent Neurons of Rat Dorsal Striatum." *The European Journal of Neuroscience* 28 (10) (November): 2041–2052. doi:10.1111/j.1460-9568.2008.06505.x.
- Smith, A D, and J P Bolam. 1990. "The Neural Network of the Basal Ganglia as Revealed by the Study of Synaptic Connections of Identified Neurons." *Trends in Neurosciences* 13 (7) (July): 259–265.

- Smith, R, W Musleh, G Akopian, G Buckwalter, and J P Walsh. 2001. "Regional Differences in the Expression of Corticostriatal Synaptic Plasticity." *Neuroscience* 106 (1): 95–101.
- Snyder, Gretchen L, Stacey Galdi, Allen A Fienberg, Patrick Allen, Angus C Nairn, and Paul Greengard. 2003. "Regulation of AMPA Receptor Dephosphorylation by Glutamate Receptor Agonists." *Neuropharmacology* 45 (6) (November): 703–713.
- Spencer, Jonathan P, and Kerry P S J Murphy. 2002. "Activation of Cyclic AMP-Dependent Protein Kinase Is Required for Long-Term Enhancement at Corticostriatal Synapses in Rats." *Neuroscience Letters* 329 (2) (August 30): 217–221.
- Spiga, Saturnino, Alessandra Lintas, Michele Migliore, and Marco Diana. 2010. "Altered Architecture and Functional Consequences of the Mesolimbic Dopamine System in Cannabis Dependence." *Addiction Biology* 15 (3) (July): 266–276. doi:10.1111/j.1369-1600.2010.00218.x.
- Stanton, P K. 1996. "LTD, LTP, and the Sliding Threshold for Long-Term Synaptic Plasticity." *Hippocampus* 6 (1): 35–42. doi:10.1002/(SICI)1098-1063(1996)6:1<35::AID-HIPO7>3.0.CO;2-6.
- Steephen, John Eric, and Rohit Manchanda. 2009. "Differences in Biophysical Properties of Nucleus Accumbens Medium Spiny Neurons Emerging from Inactivation of Inward Rectifying Potassium Currents." *Journal of Computational Neuroscience* 27 (3) (December): 453–470. doi:10.1007/s10827-009-0161-7.
- Sterratt, David C, Martine R Groen, Rhiannon M Meredith, and Arjen van Ooyen. 2012. "Spine Calcium Transients Induced by Synaptically-Evoked Action Potentials Can Predict Synapse Location and Establish Synaptic Democracy." *PLoS Computational Biology* 8 (6): e1002545. doi:10.1371/journal.pcbi.1002545.
- Stoetzner, C R, J R Pettibone, and J D Berke. 2010. "State-Dependent Plasticity of the Corticostriatal Pathway." *Neuroscience* 165 (4) (February 17): 1013–1018. doi:10.1016/j.neuroscience.2009.11.031.
- Stokka, Anne J, Frank Gesellchen, Cathrine R Carlson, John D Scott, Friedrich W Herberg, and Kjetil Taskén. 2006. "Characterization of A-Kinase-Anchoring Disruptors Using a Solution-Based Assay." *The Biochemical Journal* 400 (3) (December 15): 493–499. doi:10.1042/BJ20060962.
- Stoneham, Emily T, Erin M Sanders, Mohima Sanyal, and Theodore C Dumas. 2010. "Rules of Engagement: Factors That Regulate Activity-Dependent Synaptic

- Plasticity during Neural Network Development.” *The Biological Bulletin* 219 (2) (October): 81–99.
- Surmeier, D J, J Bargas, H C Hemmings Jr, A C Nairn, and P Greengard. 1995. “Modulation of Calcium Currents by a D1 Dopaminergic Protein Kinase/phosphatase Cascade in Rat Neostriatal Neurons.” *Neuron* 14 (2) (February): 385–397.
- Takada, M, K Itoh, Y Yasui, T Sugimoto, and N Mizuno. 1985. “Topographical Projections from the Posterior Thalamic Regions to the Striatum in the Cat, with Reference to Possible Tecto-Thalamo-Striatal Connections.” *Experimental Brain Research. Experimentelle Hirnforschung. Expérimentation Cérébrale* 60 (2): 385–396.
- Thomson, A M. 1989. “Glycine Modulation of the NMDA Receptor/channel Complex.” *Trends in Neurosciences* 12 (9) (September): 349–353.
- Tkatch, T, G Baranauskas, and D J Surmeier. 2000. “Kv4.2 mRNA Abundance and A-Type K(+) Current Amplitude Are Linearly Related in Basal Ganglia and Basal Forebrain Neurons.” *The Journal of Neuroscience: The Official Journal of the Society for Neuroscience* 20 (2) (January 15): 579–588.
- Tuckwell, Henry C. 2012. “Quantitative Aspects of L-Type Ca<sup>2+</sup> Currents.” *Progress in Neurobiology* 96 (1) (January): 1–31. doi:10.1016/j.pneurobio.2011.09.010.
- Uchigashima, Motokazu, Madoka Narushima, Masahiro Fukaya, Istvan Katona, Masanobu Kano, and Masahiko Watanabe. 2007. “Subcellular Arrangement of Molecules for 2-Arachidonoyl-Glycerol-Mediated Retrograde Signaling and Its Physiological Contribution to Synaptic Modulation in the Striatum.” *The Journal of Neuroscience: The Official Journal of the Society for Neuroscience* 27 (14) (April 4): 3663–3676. doi:10.1523/JNEUROSCI.0448-07.2007.
- Varga, Zsuzsanna, Hongbo Jia, Bert Sakmann, and Arthur Konnerth. 2011. “Dendritic Coding of Multiple Sensory Inputs in Single Cortical Neurons in Vivo.” *Proceedings of the National Academy of Sciences of the United States of America* 108 (37) (September 13): 15420–15425. doi:10.1073/pnas.1112355108.
- Vicini, S, J F Wang, J H Li, W J Zhu, Y H Wang, J H Luo, B B Wolfe, and D R Grayson. 1998. “Functional and Pharmacological Differences between Recombinant N-Methyl-D-Aspartate Receptors.” *Journal of Neurophysiology* 79 (2) (February): 555–566.

- Vilchis, C, J Bargas, G X Ayala, E Galván, and E Galarraga. 2000. "Ca<sup>2+</sup> Channels That Activate Ca<sup>2+</sup>-Dependent K<sup>+</sup> Currents in Neostriatal Neurons." *Neuroscience* 95 (3): 745–752.
- Weisenhaus, Michael, Margaret L Allen, Linghai Yang, Yuan Lu, C Blake Nichols, Thomas Su, Johannes W Hell, and G Stanley McKnight. 2010. "Mutations in AKAP5 Disrupt Dendritic Signaling Complexes and Lead to Electrophysiological and Behavioral Phenotypes in Mice." *PloS One* 5 (4): e10325. doi:10.1371/journal.pone.0010325.
- Wickens, Jeffery R, Christopher S Budd, Brian I Hyland, and Gordon W Arbuthnott. 2007. "Striatal Contributions to Reward and Decision Making: Making Sense of Regional Variations in a Reiterated Processing Matrix." *Annals of the New York Academy of Sciences* 1104 (May): 192–212. doi:10.1196/annals.1390.016.
- Willoughby, Debbie, Wei Wong, Jerome Schaack, John D Scott, and Dermot M F Cooper. 2006. "An Anchored PKA and PDE4 Complex Regulates Subplasmalemmal cAMP Dynamics." *The EMBO Journal* 25 (10) (May 17): 2051–2061. doi:10.1038/sj.emboj.7601113.
- Wilson, C J, and P M Groves. 1981. "Spontaneous Firing Patterns of Identified Spiny Neurons in the Rat Neostriatum." *Brain Research* 220 (1) (September 7): 67–80.
- Wilson, Charles J. 2005. "The Mechanism of Intrinsic Amplification of Hyperpolarizations and Spontaneous Bursting in Striatal Cholinergic Interneurons." *Neuron* 45 (4) (February 17): 575–585. doi:10.1016/j.neuron.2004.12.053.
- Wilson, Charles J, and Joshua A Goldberg. 2006. "Origin of the Slow Afterhyperpolarization and Slow Rhythmic Bursting in Striatal Cholinergic Interneurons." *Journal of Neurophysiology* 95 (1) (January): 196–204. doi:10.1152/jn.00630.2005.
- Wolf, John A, Jason T Moyer, Maciej T Lazarewicz, Diego Contreras, Marianne Benoit-Marand, Patricio O'Donnell, and Leif H Finkel. 2005. "NMDA/AMPA Ratio Impacts State Transitions and Entrainment to Oscillations in a Computational Model of the Nucleus Accumbens Medium Spiny Projection Neuron." *The Journal of Neuroscience: The Official Journal of the Society for Neuroscience* 25 (40) (October 5): 9080–9095. doi:10.1523/JNEUROSCI.2220-05.2005.
- Wong, Wei, and John D Scott. 2004. "AKAP Signalling Complexes: Focal Points in Space and Time." *Nature Reviews. Molecular Cell Biology* 5 (12) (December): 959–970. doi:10.1038/nrm1527.

- Xu, Ke, Guisheng Zhong, and Xiaowei Zhuang. 2013. "Actin, Spectrin, and Associated Proteins Form a Periodic Cytoskeletal Structure in Axons." *Science (New York, N.Y.)* 339 (6118) (January 25): 452–456. doi:10.1126/science.1232251.
- Yang, S N, Y G Tang, and R S Zucker. 1999. "Selective Induction of LTP and LTD by Postsynaptic [Ca<sup>2+</sup>]<sub>i</sub> Elevation." *Journal of Neurophysiology* 81 (2) (February): 781–787.
- Yashiro, Koji, and Benjamin D Philpot. 2008. "Regulation of NMDA Receptor Subunit Expression and Its Implications for LTD, LTP, and Metaplasticity." *Neuropharmacology* 55 (7) (December): 1081–1094. doi:10.1016/j.neuropharm.2008.07.046.
- Yasuda, Ryohei, Bernardo L Sabatini, and Karel Svoboda. 2003. "Plasticity of Calcium Channels in Dendritic Spines." *Nature Neuroscience* 6 (9) (September): 948–955. doi:10.1038/nn1112.
- Yin, Henry H, Shweta Prasad Mulcare, Monica R F Hilário, Emily Clouse, Terrell Holloway, Margaret I Davis, Anita C Hansson, David M Lovinger, and Rui M Costa. 2009. "Dynamic Reorganization of Striatal Circuits during the Acquisition and Consolidation of a Skill." *Nature Neuroscience* 12 (3) (March): 333–341. doi:10.1038/nn.2261.
- Zhang, J, Y Ma, S S Taylor, and R Y Tsien. 2001. "Genetically Encoded Reporters of Protein Kinase A Activity Reveal Impact of Substrate Tethering." *Proceedings of the National Academy of Sciences of the United States of America* 98 (26) (December 18): 14997–15002. doi:10.1073/pnas.211566798.
- Zhang, Ji-Chuan, Pak-Ming Lau, and Guo-Qiang Bi. 2009. "Gain in Sensitivity and Loss in Temporal Contrast of STDP by Dopaminergic Modulation at Hippocampal Synapses." *Proceedings of the National Academy of Sciences of the United States of America* 106 (31) (August 4): 13028–13033. doi:10.1073/pnas.0900546106.
- Zhang, Li, Kai Meng, Yan-Hai Li, and Tai-Zhen Han. 2009. "NR2A-Containing NMDA Receptors Are Required for L-LTP Induction and Depotentiation in CA1 Region of Hippocampal Slices." *The European Journal of Neuroscience* 29 (11) (June): 2137–2144. doi:10.1111/j.1460-9568.2009.06783.x.
- Zhou, Yu-Dong, Corey D Acker, Theoden I Netoff, Kamal Sen, and John A White. 2005. "Increasing Ca<sup>2+</sup> Transients by Broadening Postsynaptic Action Potentials Enhances Timing-Dependent Synaptic Depression." *Proceedings of the National Academy of Sciences of the United States of America* 102 (52) (December 27): 19121–19125. doi:10.1073/pnas.0509856103.

## BIOGRAPHY

Rebekah Evans graduated from Union High School in Broken Arrow, OK, in 2000. She received her Bachelor of Arts from St. John's College, Annapolis, MD in 2004 with a double major in philosophy and the history of mathematics and science. She was employed as a special education teacher in Prince William County, VA for two years and received her Master's degree in Education from George Mason University in August 2006. She started the Ph.D. program in neuroscience in September 2006 and became a Ph.D. candidate in 2009. She has received several grants and international travel awards including a Presidential Scholarship from GMU, an NRSA F31 pre-doctoral grant from NINDS, a dissertation completion grant from GMU, a SfN travel award to the IBRO conference in Florence, Italy 2011, and an IBAGS travel award to the IBAGS meeting in Eilat, Israel 2013. She maintains a neuroscience outreach blog called The Cellular Scale ([www.cellularscale.blogspot.com](http://www.cellularscale.blogspot.com)) and was an Official Neuroblogger for the 2012 Society for Neuroscience annual meeting in New Orleans, LA.

**Evans RC**, Damodaran S, Blackwell KT (2013) Striatal models: Cellular Detail, *Encyclopedia of Computational Neuroscience*. SpringerReference. Eds. Dieter Jaeger and Ranu Jung. (*invited, in revisions*)

Damodaran S, **Evans RC**, Blackwell KT (2013) Synchronized firing of fast-spiking interneurons is critical for maintaining balance between direct and indirect pathways of striatum. (*in revisions, J. Neurophysiology*)

**Evans RC**, Polavaram S (2013) Growing a Garden of Neurons. *Front. Neuroniform*. 7,17.

**Evans, RC**, Maniar YM, Blackwell KT. (2013) Dynamic Modulation of Spike Timing Dependent Calcium Influx During Cortico-striatal Upstates. *J Neurophysiol* 110, 1631-1645 [[Model Available on ModelDB](#)]

Hawes S, Gillani F, **Evans RC**, Benkert E, Blackwell KT. (2013) Robust dorsal striatal LTP in adult brain slice using Theta-burst stimulation. *J Neurophysiol.* (Aug 7). doi:10.1152/jn.00115.2013

**Evans RC** (2012) On Selling and Over-Selling Science. *Biol. Bull.* Dec 223: 257-258

**Evans RC**, Morera-Herreras T, Cui Y, Du K, Sheehan T, Hellgren Kotaleski J, Venance L, Blackwell, KT. (2012) The Effects of NMDA Subunit Composition on Calcium Influx and Spike Timing-Dependent Plasticity in Striatal Medium Spiny Neurons. *PLoS Comput Biol* 8(4): e1002493 [[Model Available on Model DB](#)]